UNIVERSITÉ D'ORLÉANS

ÉCOLE DOCTORALE ÉNERGIE, MATERIAUX, SCIENCES DE LA TERRE ET DE L'UNIVERS

Institut de Combustion, Aérothermique, Réactivité et Environnement, CNRS, France

Institut de Radioprotection et de Sûreté Nucléaire, France

Forschungszentrum Juelich GmbH, Germany

THÈSE présentée par :

Gabriela SENRA PESSANHA RIOS NOBREGA

soutenue le : **25 octobre 2022**

pour obtenir le grade de: **Docteur de l'Université d'Orléans**

Discipline/ Spécialité: Energétique

Investigation of catalyst deactivation in Passive Autocatalytic Recombiners

THÈSE dirigée par:

Mme CHAUMEIX Nabiha Directrice de recherche, CNRS-ICARE
M. BENTAIB Ahmed Docteur-HDR, IRSN

RAPPORTEURS:

M. FIGUEIRA DA SILVA Luis Fernando Chargé de recherche-HDR, CNRS-PPRIME
M. JIMENEZ Gonzalo Professeur, Universidad Politécnica de Madrid

JURY:

M. FIGUEIRA DA SILVA Luis Fernando	**Chargé de recherche-HDR, CNRS-PPRIME**
M. JIMENEZ Gonzalo	**Professeur, Universidad Politécnica de Madrid**
Mme DOMINGO Pascale	**Directrice de Recherche, CNRS-CORIA**
Mme BATTIN-LECLERC Frédérique	**Directrice de Recherche, CNRS-LRGP, présidente du jury**
Mme CHAUMEIX Nabiha	**Directrice de recherche, CNRS-ICARE**
M. BENTAIB Ahmed	**Docteur-HDR, IRSN**
M. Reinecke Ernst-Arndt	**Docteur, Forschungszentrum Juelich GmbH**
M. Maas Ludovic	**Ingénieur, IRSN, membre invité**

Gabriela SENRA PESSANHA RIOS NOBREGA

Etude de l'empoisonnement des recombineurs auto-catalytiques passifs

En cas d'accident de fusion du cœur, les gaz inflammables (hydrogène et monoxyde de carbone), issus de l'oxydation du cœur et de l'interaction du cœur fondu et le béton, peuvent atteindre des concentrations élevées pouvant provoquer des explosions susceptibles de menacer l'intégrité de l'enceinte de confinement ainsi que les équipements nécessaires pour la gestion de l'accident. Afin d'atténuer le risque lié à l'hydrogène, des recombineurs autocatalytiques passifs ont été installés dans de nombreuses centrales nucléaires. Les recombineurs sont des dispositifs qui visent à recombiner l'hydrogène par une réaction catalytique exothermique. En fonctionnement normal et en cas de scénario accidentel, ces dispositifs peuvent être exposés à divers composés volatils, gaz et aérosols présents dans l'atmosphère de l'enceinte de confinement qui peuvent provoquer une désactivation du catalyseur induisant alors un retard dans le démarrage de la recombinaison et une réduction de l'efficacité du recombineur. Cette thèse a pour objectif de caractériser les conditions de désactivation du catalyseur dans les recombineurs par différents produits. Elle vise également à améliorer les modèles mis en œuvre dans les outils numériques utilisés pour l'analyse de sûreté. Pour mieux comprendre le comportement des RAP et les mécanismes d'empoisonnement, des expériences ont été réalisées dans les installations REKO au Forschungszentrum Juelich, en Allemagne. Les campagnes expérimentales ont été dédiées aux trois produits d'empoisonnement potentiels: le monoxyde de carbone, les produits de combustion des incendies de câbles et l'huile utilisée dans les pompes primaires des centrales nucléaires. Les essais d'empoisonnement au monoxyde de carbone ont été analysés à l'aide du code SPARK, un code CFD dédié aux simulations numériques de recombinateurs catalytiques développé à l'IRSN. L'impact du monoxyde de carbone a été étudié avec des mélanges H2/CO/air. Les résultats montrent que les conditions d'empoisonnement dépendent de la fraction molaire de monoxyde de carbone, de la fraction molaire d'oxygène et de la température du catalyseur. Afin de mieux comprendre comment les produits des feux de câbles affectent le démarrage de la réaction de recombinaison, des expériences ont été réalisées. La campagne expérimentale a permis de conclure que la présence de monoxyde de carbone et le dépôt de particules dû à la pyrolyse des câbles sont les principaux mécanismes d'empoisonnement. Les essais réalisés avec des plaques catalytiques en platine, recouvertes partiellement ou totalement d'huile, montrent que la présence d'un film d'huile bloque les sites actifs du catalyseur, mais que la capacité de recombinaison peut être restaurée par évaporation de l'huile si une réaction de recombinaison est amorcée par une plaque voisine non recouverte d'huile. Les simulations réalisées avec SPARK montrent que le code est capable de prédire la désactivation par le monoxyde de carbone en bon accord avec les résultats expérimentaux. Ces expériences fournissent des données pour l'amélioration des codes numériques dans le cadre du projet AMHYCO.

Mots clés : accidents graves, hydrogène, recombineur auto-catalytique passif, empoisonnement

Investigation of catalyst deactivation in Passive Autocatalytic Recombiners

In case of a core melt accident, flammable gases (hydrogen and carbon monoxide), issued from core oxidation and from molten concrete core interaction, might reach high concentrations inside the containment and lead to explosions that threaten its integrity as well as the equipment used for safety management. In order to mitigate the hydrogen risk, passive autocatalytic recombiners have been installed in many nuclear power plants. Recombiners are devices that aim to recombine hydrogen through an exothermic catalytic reaction. During normal operation and accidental scenario, these devices can be exposed to various volatile compounds, gases and aerosols present in the atmosphere of the containment that may cause catalyst deactivation inducing then delay in recombination start-up and reduction of the efficiency. This thesis aims at characterizing the conditions of deactivation of catalyst in recombiners by different products. It also aims to improve the models implemented in numerical tools used for safety analysis. To better understand the behaviour of PARs and the deactivating mechanisms, experiments were performed at the REKO facilities at Forschungszentrum Juelich, Germany. The experiments focused on three potential deactivating products: carbon monoxide, combustion products from cable fires and oil used in the primary pumps in NPPs. Results were analyzed using the SPARK code, a CFD code dedicated to the numerical simulations of catalytic recombiners developed at IRSN, for CO tests. The impact of carbon monoxide was investigated with H2/CO/air mixtures. The experiments reveal that the poisoning conditions depend on carbon monoxide molar fraction, oxygen molar fraction and the catalyst temperature. The experimental campaign performed to further understand how products of cable fires influence the start of the recombination reaction leads to the conclusion that the presence of carbon monoxide and the particles deposition due to cables pyrolysis are the main mechanisms of deactivation. The tests carried out with platinum catalytic plates, partially or totally covered with oil, show that the presence of a film of oil blocks the active sites of the catalyst, but that the recombination capacity can be restored by evaporation of the oil if a recombination reaction is initiated by a neighboring plate not covered with oil. The simulations performed with SPARK show that the code is able to predict the deactivation by carbon monoxide in a good agreement with the experimental results. These experiments provide data for the further enhancement of numerical codes in the framework of the European AMHYCO project.

Keywords : severe accidents, hydrogen, passive autocatalylic recombiners, catalyst deactivation

IRSN INSTITUT DE RADIOPROTECTION ET DE SÛRETÉ NUCLÉAIRE

Institut de Combustion, Aérothermique, Réactivité et Environnement, CNRS, France

JÜLICH Forschungszentrum

Cette thèse se concentre sur la caractérisation des conditions de désactivation du catalyseur dans les recombineurs par différents produits dont le gaz, les particules et l'huile. Elle vise également à améliorer les modèles mis en œuvre dans les outils numériques utilisés pour l'analyse de la sécurité. Pour mieux comprendre le comportement des RAP installés dans les centrales nucléaires et les mécanismes de désactivation, des expériences ont été réalisées dans les installations REKO de l'Institut de recherche sur l'énergie et le climat (IEK-6) du Forschungszentrum Juelich, en Allemagne. Les expériences se sont concentrées sur trois produits d'empoisonnement potentiels : le monoxyde de carbone, les produits de combustion des incendies de câbles et l'huile utilisée dans les pompes primaires des centrales nucléaires. la définition et l'analyse des essais, ainsi réalisés, ont été réalisés à l'aide du code SPARK (Simulation for Passive Autocatalytic Recombiners' risK), qui est un code CFD développé à l'IRSN et dédié aux simulations numériques de recombineurs catalytiques. Ce code a été utilisé pour l'interprétation des essais d'empoisonnement au monoxyde de carbone. Le premier chapitre du manuscrit présent le contexte et les objectives de la thèse. Le fonctionnement des RAPs et la désactivation du catalyseur sont décrits au chapitre 2. Ensuite, les installations expérimentales utilises sont présentées au chapitre 3 ainsi que les procédures expérimentales et les essais de références. Le chapitre 4 est dédié à la description du code numérique et les simulations de référence. Le résultats expérimentaux et numériques sont traités au chapitre 5. Les résultats expérimentaux sur a l'impact des produits de feux de câbles sur le recombiner sont présentés et discutés au chapitre 6. Le chapitre 7 est consacré à l'effet de l'huile sur le catalyseur.

En situation d'accident grave, une grande quantité de gaz combustibles (hydrogène et monoxyde de carbone) peut être produite et former un mélange explosif dans l'enceinte de confinement du réacteur qui constitue la dernière barrière au relâchement des produits de fission dans l'environnement. Les charges induites par la combustion peuvent menacer l'intégrité de l'enceinte de confinement du réacteur, ainsi que les systèmes importants pour la sûreté. Afin de prévenir ce risque, des recombineurs autocatalytiques passifs ont été installés dans de nombreuses centrales nucléaires, notamment en France et en Allemagne. Les recombineurs sont des dispositifs passifs qui permettent recombiner l'hydrogène par une réaction catalytique exothermique. En fonctionnement normal et en cas de scénario accidentel, ces dispositifs peuvent être exposés à divers composés volatils, gaz et aérosols présents dans l'atmosphère de l'enceinte de confinement. Certains de ces produits peuvent provoquer une désactivation partielle ou totale du catalyseur induisant alors un retard dans le démarrage de la recombinaison et une réduction de l'efficacité du recombineur. En outre et lors de la phase tardive (ex-vessel) de l'accident, du monoxyde de carbone peut être produit lors l'interaction entre le corium et le béton du radier de l'enceinte de confinement. Le monoxyde de carbone, ainsi produit et relâché dans l'enceinte de confinement, peut induire un empoisonnement du catalyseur conduisant à un arrêt de la recombinaison par les RAP.

Aussi, l'impact des produits précités sur les performances des recombineurs est un enjeu de sûreté qu'il convient d'étudier en combinant approche expérimentale et analytique avec l'objectif de caractériser la désactivation du catalyseur ; c'est l'objet des travaux de cette thèse.

Les installations de REKO permettent d'étudier le comportement des recombineurs dans différentes conditions. Le programme expérimental comprend des expériences dans des conditions bien définies d'écoulement forcé et d'écoulement naturel. REKO-1 a été utilisé pour analyser et caractériser l'empoisonnement par le monoxyde de carbone sur des échantillons de catalyseurs individuels, tandis que REKO-3 a été utilisé pour caractériser l'effet d'empoisonnement en utilisant des échantillons de catalyseurs de taille normale. REKO-Fire a permis d'analyser le comportement d'échantillons de catalyseurs individuels lorsqu'ils sont exposés aux produits de combustion de feux de câbles. Enfin, REKO-4 a été utilisé pour étudier l'impact de l'huile sur le démarrage de la recombinaison de l'hydrogène. Les expériences ont été réalisées avec des échantillons de catalyseurs simples Pt, Pd et Pt/Pd de 5x5 cm2. Pour les expériences à grande échelle, les géométries du catalyseur ont été de 15x15 cm2, étant le catalyseur Pt. Les catalyseurs génériques sont similaires aux catalyseurs utilisés dans les recombineurs commerciaux.

Les plateformes expérimentales et les résultats des tests de qualification réalisés avant d'aborder l'étude de l'effet d'empoisonnement ont été présentées au chapitre 3. Tout d'abord, le pyromètre a été calibré pour assurer une bonne mesure de la température du catalyseur. Ensuite, des expériences avec des mélanges gazeux H2/air ont été réalisées pour étudier l'effet de différents paramètres sur le comportement du catalyseur en fonctionnement normal. Des tests ont été réalisés pour des mélanges gazeux à 20°C, 80°C et 150°C afin d'analyser l'impact de la température initiale du gaz. L'impact de la vitesse d'écoulement a été étudié. Pour des vitesses d'écoulement de 0,5 et 1,0 m/s, les résultats expérimentaux révèlent une faible différence dans la température du catalyseur. Les expériences réalisées avec de la vapeur ont été comparées à celles réalisées en conditions sèches et aucune différence significative n'a été observée dans la température du catalyseur. Le comportement du catalyseur a également été analysé dans des conditions de privation d'oxygène. Les données expérimentales montrent que la température du catalyseur diminue avec la teneur en oxygène en dessous d'une certaine valeur, indiquant que le recombineur est moins efficace dans ce cas mais que l'hydrogène est toujours converti en vapeur. Ces résultats servent de référence pour le fonctionnement normal du catalyseur.

Chapitre 4 est dédié au code SPARK. Des calculs ont été effectués pour des mélanges hydrogène-air afin de vérifier que le code SPARK est capable de reproduire les résultats expérimentaux. Des simulations utilisant la géométrie REKO-1 ont été effectuées. Les résultats obtenus dans des conditions normales de fonctionnement sont conformes aux données expérimentales. Cependant, pendant la privation d'oxygène, les résultats indiquent que SPARK prédit les phénomènes légèrement plus tôt que ce qui est observé dans les expériences. La géométrie de REKO-1 étant un cylindre avec un seul échantillon de catalyseur, les simulations 2D réalisées avec SPARK ne sont pas les plus adaptées.

Les simulations utilisant la géométrie de REKO-3 ont également été réalisées en utilisant différents mélanges H2/air. Le comportement du catalyseur dans des conditions où il y a réduction de l'oxygène a également été simulé. L'effet de la vapeur sur la température du catalyseur a également été analysé avec

la présence de monoxyde de carbone et sans restriction d'oxygène. Les résultats numériques sont cohérents avec les résultats expérimentaux pour tous les cas, confirmant que le code SPARK peut prédire la température du catalyseur pour des conditions d'oxygène riche, des conditions de privation d'oxygène et en présence de vapeur.

Afin d'améliorer les connaissances sur l'impact du monoxyde de carbone sur le comportement du catalyseur, des expériences ont été réalisées dans les installations REKO et les résultats obtenus sont présentés et discutés au chapitre 5. Dans une première série de tests d'évaluation, les conditions de désactivation d'un seul échantillon de catalyseur ont été étudiées dans l'installation REKO-1. À cette fin, des échantillons de catalyseurs à base de platine et de palladium ont été exposés à des mélanges d'hydrogène, de monoxyde de carbone, d'air, d'azote et de vapeur à différentes températures et vitesses d'écoulement. Les expériences ont révélé que l'empoisonnement peut être prédit par la fraction de monoxyde de carbone, la fraction d'oxygène et la température du catalyseur. En outre, le catalyseur au palladium est désactivé à des températures plus basses que le catalyseur au platine. Les résultats montrent que la température du catalyseur à laquelle le platine est empoisonné est indépendante de la température du gaz, tandis que pour le catalyseur au palladium, la température du gaz semble influencer la température d'empoisonnement. Dans un deuxième temps, l'installation REKO-3 est utilisée pour étudier l'effet du monoxyde de carbone sur une section d'un recombineur avec quatre plaques catalytiques à échelle réelle disposées verticalement à l'intérieur d'un canal rectangulaire. Ces expériences fournissent des données pour l'amélioration des codes numériques dans le cadre du projet AMHYCO et du code SPARK.

Des simulations SPARK pour des mélanges H2/CO/air ont été réalisées et l'impact de différents paramètres a été analysé. La comparaison des simulations avec les résultats numériques révèle que le code SPARK est capable de reproduire la désactivation du catalyseur par le CO, et notamment de capturer la transition de la désactivation partielle à la désactivation complète. Le code prédit des températures d'empoisonnement plus élevées que celles observées dans les expériences. Bien qu'un nouveau mécanisme de réaction pour H2/CO sur le palladium ait été présenté, les calculs n'ont pas pu être achevés, et davantage de données expérimentales sont nécessaires à la validation. Ce point sera abordé dans les travaux futurs.

Les résultats des essais réalisés pour investiguer l’impact des feux de câbles sur le catalyseur sont présentés au chapitre 6. Trois conditions d'incendie différentes ont été considérées. Dans le cas d'un incendie de câble bien ventilé (well-ventilated regime), ni les produits gazeux (CO2 en quantités relativement importantes et très peu de CO) ni les produits des incendies de câbles particulaires (principalement la suie) ne semblent affecter le début de la conversion catalytique de H2 pour les catalyseurs à base de Pt et de Pd. Dans des conditions d'incendie sous-ventilé (under-ventilated regime), des effets différents sur les deux types de catalyseurs peuvent être observés. Le catalyseur à base de Pt est significativement désactivé, tandis que la seule dégradation du catalyseur à base de Pd est observée à une fraction molaire d'hydrogène aussi faible que 0,5 %. Les niveaux plus élevés de CO par rapport aux

feux de câbles bien ventilés sont soupçonnés d'être la raison des désactivations observées. Pour les produits générés par la pyrolyse oxydative, la désactivation et le retard de démarrage de recombinaison d’hydrogène peuvent se produire pour les deux types de catalyseurs en raison du blocage physique de la surface catalytique. Comme conclusion préliminaire, la présence de monoxyde de carbone dans l'atmosphère ainsi que les dépôts de particules provenant de la pyrolyse des câbles semblent être deux mécanismes pertinents pour la désactivation du catalyseur.

De l'huile a été appliquée sur un catalyseur à base de platine afin d'étudier son impact sur le comportement du recombineur. Les résultats, présentés au chapitre 7, montrent que le catalyseur n'est pas capable de convertir l'hydrogène lorsque la surface est entièrement recouverte d'huile et que la température n'est pas assez élevée pour évaporer et/ou brûler l'huile. Cependant, lorsqu'un seul catalyseur n'était pas recouvert d'huile, la chaleur de la réaction de recombinaison de l'hydrogène sur cet échantillon était suffisante pour évaporer et brûler l'huile de la surface des autres plaques de catalyseur. Une fois que l'huile ne bloquait plus la surface, le catalyseur démarrait immédiatement.

Sur la base de ces résultats, il semble que l'huile ne désactiverait pas de façon permanente les plaques de catalyseur dans les recombineurs. Étant donné que les projections d'huile trouvées dans les RAP couvraient partiellement la surface catalytique, il est probable que les sites actifs sans huile pourraient suffire à démarrer la recombinaison de l'hydrogène, entraînant l’ évaporation de l'huile en raison de la chaleur dégagée par la réaction.

TABLE DES MATIÈRES

FIGURES AND TABLES LISTS

Figures

Table

1. INTRODUCTION

1.1. Context and motivation

Nuclear facilities utilise the nuclear fission process, where a heavy atomic nucleus splits apart in order to form lighter ones, releasing energy. This process also produces neutrons, so a chain reaction can be established wherein each fission event can initiate others. Fission takes place in the nuclear fuel while the rest of the reactor converts the thermal energy produced into electricity.

From a safety perspective, nuclear facilities are designed, constructed and operated to prevent potential radioactive substances release that may lead to human and environmental exposure to radiation. Since in a nuclear power plant, the reactor containment is the last barrier against the release of fission products into the environment, it is important to ensure its integrity. One of the threats to the containment integrity is the risk of hydrogen explosion due to large amount of hydrogen generated by the oxidation of metals present in the reactor core in case of a severe accident.

Nuclear accidents of Three Mile Island in 1979 and more recently Fukushima Daiichi in 2011 reinforced the relevance of investigating SAs and the hydrogen risk. In 1979, the TMI accident showed the possibility of accidents leading to core melting. It also confirmed that the combustion of hydrogen in the reactor building is a potential hazard for the containment integrity. In 2011, the Fukushima Daiichi accident confirmed that a large amount of hydrogen and carbon monoxide might be released and generate an explosion. This accident revived the attention of the nuclear safety community towards hydrogen explosion risk.

Hydrogen risk is defined as the possibility of loss of containment integrity or failure of the reactor backup systems as a result of hydrogen combustion. During severe accidents in a nuclear power plant hydrogen can be produced during two phases. In the in-vessel phase, the exothermal oxidation of the fuel cladding (PWR and BWR) or fuel assembly canisters (BWR) and hot metallic components takes place inside the reactor pressure vessel. During the ex-vessel phase, the molten core-concrete interaction (MCCI) takes place after failure of the reactor pressure vessel and melt relocation to the reactor pit. Carbon monoxide and other gases can also be produced during MCCI in addition to H_2.

After uncovering of the core, since the heat transfer from the fuel to steam is small compared with decay heat production, the fuel temperature increases. The zircaloy in the fuel cladding is exothermically oxidised by steam at high temperatures (above approximately 1300 K). This reaction aggravates the core degradation as it releases thermal power that can become higher than the residual power. During Zr oxidation, hydrogen is produced following the reaction:

$$Zr + 2H_2O \rightarrow ZrO_2 + 2H_2$$

The enthalpy reaction is between -600 and -700 KJ/mole of zirconium, producing 0.0442 kg of hydrogen per kg of zirconium, for temperatures above 1300 K [1].

In the late phase of the core degradation, there may occur injection of the melt into water in the form of a jet and fragmentation of the melt, that would lead to an increase of the oxidation reaction surface and to a generation of steam, which can oxidize the available metal.

In the following table, the amount of hydrogen produced during core degradation phase is provided.

Table 1: Evaluation of the hydrogen mass produced by full Zr oxidation during core degradation for different LWRs.

Reactor type	H_2 (kg)
French PWR 900 MW	900
Konvoi PWR 1300 MW	1,400
BWR-72 1300 MW	4,500

Moreover and In case of a reactor vessel breach when the reactor coolant system is depressurized, a gravitational corium drop occurs and in case of a dry cavity pit, a molten core concrete interaction (MCCI) starts. The Zr and Cr (Chromium coming from the stainless steel internal structures) contained in the corium undergo a fast oxidation when in contact with the steam and CO_2 in the environment. CO_2 comes from the thermal decomposition of the concrete. It is assumed that 100 % of the remaining metallic Zr and Cr will be oxidized by steam generating H_2 and CO within the first hour following the MCCI [3].

Hydrogen and carbon monoxide are then released to the containment and their distribution can be homogeneous or stratified depending on the intensity of the mixing of the containment atmosphere. In case of homogeneous distribution, hydrogen and carbon monoxide significantly contribute to a pressure build-up inside the containment. On the other hand, in case of gas stratification, local concentration of hydrogen and carbon monoxide become a safety concern as the flammability threshold of the gas mixture can be exceeded, leading to combustion. Hydrogen and carbon combustion can happen in a variety of forms: slow deflagration, accelerated flames, deflagration to detonation transition (DDT) and detonation. The combustion mode will be determined by local and global concentrations of hydrogen and carbon monoxide.

The OECD State of the Art Report on *Flame Acceleration and Deflagration-to-Detonation Transition* [10] as well as the IAEA TecDoc [5] addressed the key issue of hydrogen combustion. Additional detailed information are given in the OECD/NEA report [7, 8] related to carbon monoxide combustion. To summarized, two different combustion regimes are shortly characterized here, based on information provided in the reports [27] [25] and [35].

Deflagration

When the flame travels at subsonic speed relative to the unburnt gas, they are called deflagrations. They propagate mostly by heat and mass transfer from the hot burnt gas to the unburnt gas, raising it to a high temperature that allows a rapid exothermic chemical reaction to happen. The characteristic velocities are of the order of several meters per second. The deflagration might be asymmetrical for low hydrogen concentrations. For hydrogen contents between 4.1 and 6.0 vol. %, the propagation initially driven by buoyancy will be upward from ignition source. Hydrogen concentrations between 6.0 and 9.0 vol. % produces upward and horizontal propagation. When the hydrogen content is above 9.0 vol. % the propagation is in all directions, although the upward propagation might be faster than the downward propagation. For higher hydrogen contents and enhanced turbulence, there is no asymmetry.

The hydrogen-air mixtures with low hydrogen content in the range of 4 to 8 vol. % are ignited with a spark and the hydrogen combustion is incomplete. The incomplete combustion of lean hydrogen-air mixtures is significant for reactor safety. Combustion of lean mixtures can be a strategy for decreasing hydrogen risk by consuming the hydrogen without a major increase of containment pressure.

Detonation

A detonation is a combustion wave that propagates at a supersonic speed relative to the unburnt gas in front of it. The speed is about 2000 m/s for stoichiometric hydrogen-air mixtures. During the detonation, the shock waves provoke the compression of the unburnt gas that raises gas temperatures high enough to initiate rapid combustion by auto-ignition. The detonation wave is constituted of a complex front resulting from the coupling between a shock wave and a reaction zone. Understanding the conditions for which hydrogen-air-steam can detonate is of major interest in reactor safety.

Hydrogen-air mixtures near stoichiometric conditions (about 30% hydrogen) are known to be detonable. Mixtures away from stoichiometry are gradually more difficult to detonate. The detonability limits of a mixture are defined as the critical condition that allows the propagation of a self-sustained detonation [5]. The critical conditions designate both the initial and boundary conditions of the explosive mixture. The detonation wave is characterized by a 3D structure due to the existence of transverse waves, and propagates at a detonation speed that varies around an average value: the Chapman-Jouguet detonation speed. The trajectory of the triple points gives the 3D- cellular structure that can be measured experimentally.

The cell size is a characteristic of the detonation and it can be determined experimentally. It is an essential measure of the detonability of the mixture and it shows the relation between the chemical reaction rate and the macroscopic propagation behaviour of detonations. As the auto-ignition increases, the induction length becomes larger leading to a larger detonation cell. If a detonation propagates from a tube into an open space, there is a minimum tube diameter that will allow the detonation to continue propagating. The detonation limits depend on the scale and hence can vary substantially.

Another important phenomenon is the detonation initiation. A very high-energy source is needed to obtain a direct initiation of a detonation. To initiate a stable detonation, a minimum energy of about 4100 J is required around the stoichiometry and increases drastically when away from this composition [3]. That amount of energy is several orders of magnitude greater than it would be generated from an electrical spark and is about eight orders of magnitude greater than the minimum ignition energy required for deflagration initiation. Thus, it is unlikely that a direct initiation in reactor accidents would occur. However, this regime could be achieved if a deflagration accelerates to high speeds and transit to detonation.

Deflagration to detonation transition

Flame acceleration and deflagration to detonation transition influences the maximum load from hydrogen combustion sequences and consequential structural damage in containments. Hence it is of great importance to severe accidents assessment. The main objective in hydrogen hazard mitigation studies is to ensure the containment integrity through the design of countermeasures to avoid flame acceleration and DDT.

For transition to detonation to be possible, the explosive mixture must be within the detonation limits. However, that is not the only condition. The flame acceleration mechanisms must be sufficiently effective to raise the velocity of the turbulent deflagration so a detonation can occur. The flame acceleration process can lead to DDT through shock ignition or amplification mechanisms.

Flame acceleration can be caused by different mechanisms. It can result from turbulence and generated by combustion-induced turbulence over structures present in the flame front, from flame instabilities due to (i) hydrodynamic, (ii) thermo-diffusive, (iii) buoyancy driven effects. When the flame is fast enough from flame generated pressure waves when they interact with the flame after reflection at the confining walls, from the confinement of the gas mixture by the enclosure and from flame-acoustic interactions.

Turbulence can be generated in the combustion-induced flows. Turbulence can increase the local burning rate by increasing the surface area of the flame and the transport of local mass and energy when the flame front advances into the turbulent flow field. A higher burning rate leads to a higher flow velocity in the unburnt gas, resulting in a continuous acceleration of the propagating flame.

The obstacles in the flame path induce velocity gradients in the flow field and the turbulent production. It has been showed that in configurations with repeated obstacles, the turbulent flame propagation regime is self-accelerating due to the feedback mechanism between flame velocity and the level of turbulence in the flame front. Repeated obstacles in the flame path seems to be the most effective flame acceleration mechanism [5].

Flame front instabilities are responsible for the flame surface increase (Hydrodynamic, thermo-diffusive and buoyancy driven) and modify the flame structure itself (thermo-diffusive) leading to an enhancement of the burning rate and a strong increase of the flame speed.

The interaction between the flame propagation and turbulence generation in a flame path is very sensitive to the level of the channel confinement. A decrease of the confinement by venting reduces the flow velocity ahead of the flame and thus reducing the obstacle-induced turbulence. As in the case of flames, detonations are very sensitive to the level of confinement. A sudden venting of confinement at the end of the tube can result in detonation failure.

The Shapiro diagram, shown in Figure 1 can be used to determine if the mixture is flammable. If the containment atmosphere contains diluent gases the lower flammability limit will increase slightly, while the upper limit drops more rapidly [2].

The flammability, deflagration and detonation regions are bounded by curves. The detonation region is within the flammability region and its limits are not an intrinsic characteristic of the gas mixture, it is scale dependent. In a flammable mixture, combustion might be triggered by an energy less than a millijoule. Since more energy is required to initiate a detonation (several kJ), the only mechanism considered leading to detonation is flame acceleration through deflagration to detonation transition.

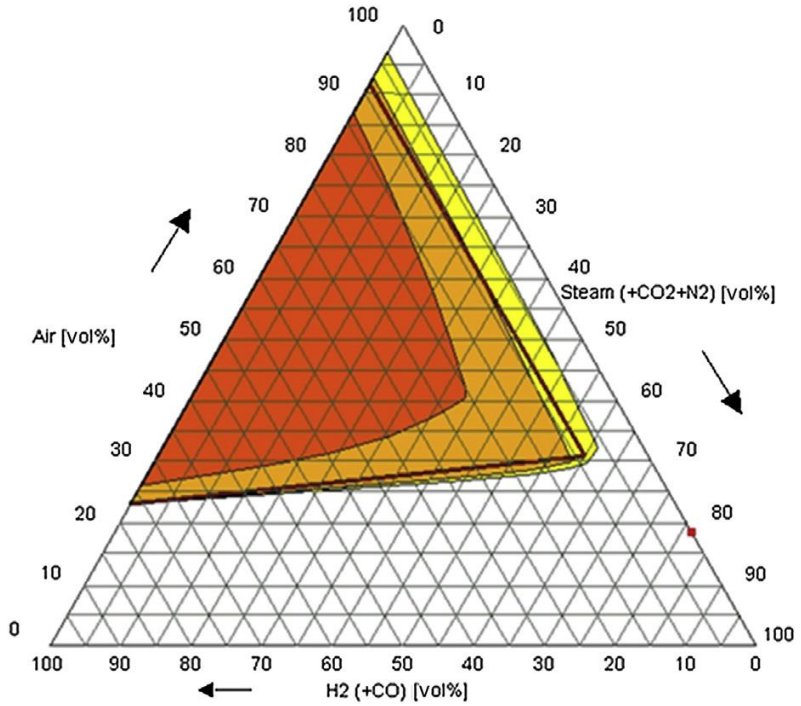

Figure 1: Shapiro diagram.

In case of low hydrogen content below 8%, flame speed is typically slow and deflagration generates a quasi-static pressure loads. When the H2 molar percent is above 9 to 10 vol. %, combustion is complete and it may accelerate leading to higher loads. Above 10 to 11 vol. %,

acceleration might be up to sound speed, as it has been found in many experiments [3] [4]. In an extreme case, flame acceleration, supported by turbulence, can reach detonation conditions, known as Deflagration to Detonation Transition (DDT). Flame acceleration and DDT can be destructive and can damage internal containment structures and safety systems used in severe accident management.

Hydrogen mitigation

An understanding of hydrogen production, distribution and combustion is essential for designing and implementing hydrogen management measures. There are several methods to limit hydrogen concentration in the containment. The strategy consists of the one or a combination of the following measures [6]:

- Deliberate ignition,
- Consumption or recombination of hydrogen by passive autocatalytic recombiners
- Dilution of the hydrogen concentration inside the containment atmosphere by using a large containment volume,
- Injection of an inert gas such as nitrogen in order to limit the relative concentration of oxygen and therefore the risk of combustion.

Several hydrogen hazard mitigation systems have been studied, developed and implemented in nuclear reactors. Some of the mitigation strategies are: thermal recombiners, ignitors, inert systems, mixing systems, hydrogen recombination, hydrogen permutation, metal oxides reduction by hydrogen and controlled combustion of organic matter, a way to remove oxygen [7].

The containment design influences the mitigation measures to be implemented. The strategy chosen for the pressurized water reactors in France is combining the existence of a large containment volume and the installation of passive autocatalytic recombiners.

Catalytic recombiners have been chosen as a mitigation system in most of Europe due to its advantages. A recombiner is a passive system that does not require energy supply to operate and has a large domain of efficiency. It can operate under major accident and design-basis accident conditions. The recombiner starts the recombination reaction at low hydrogen contents, below the hydrogen flammability limit. The catalytic reaction is a well-known

phenomenology. The technology to develop a passive autocatalytic recombiner is simple and does not need complex system. The installation requires only to place the recombiner at appropriate locations in the containment to obtain the desired coverage.

In France, PARs have been installed since 2007. This device converts passively hydrogen into steam by an exothermic catalytic recombination. PARs are assumed to be always fully operational. However, they might be exposed to materials that may damage or block the catalyst leading to its deactivation. The exposure might happen during normal operation, shutdown states (especially with maintenance work), or during accidental conditions. Catalyst deactivation is a safety concern since it can result in start-up delay and in loss of the recombination efficiency, increasing the hydrogen explosion risk [22].

1.2. Objectives

This thesis combines experimental and numerical works in order to expand the knowledge concerning PARs deactivation. The objective is to investigate the effect of potential deactivating products on recombiners performance and to improve models implemented in numerical tools used for safety analysis. For this purpose, experiments were performed on the REKO platform at Jülich, Germany. The experimental facilities permit to study several aspects of catalytic recombiners operation. The experiments aim to investigate and characterize deactivating conditions of recombiners by different products present in the containment during normal operation and in case of an accident. The SPARK code, developed by IRSN and dedicated to catalytic reactor-type operations, have been used to analyze the experimental results. The knowledge gained allows to enhance existing models already implemented.

Thus, the catalyst behavior under the presence of cable fire products was investigated with the REKO-fire facility. The impact of oil on the catalyst has been investigated with the REKO-4. Experiments have been performed with the REKO-1 and REKO-3 facility in order to better understand the deactivation by carbon monoxide. The analysis of the performed experiments was performed using the SPARK code.

Chapter 2 presents the state of the art on PARs. The components and the operation of a recombiner are described, as well as the different existing types of PARs. The catalyst deactivation and its consequences to the recombiner are also outlined in this chapter. Chapter 3 describes the experimental facilities and methods that have been used in the context of the

thesis. Chapter 4 is dedicated to the description of the numerical tool, the SPARK code. The results obtained from the carbon monoxide experiments are discussed in chapter 5, as well as the simulation results. Chapter 6 is dedicated to the findings on the deactivation by cable fire products. Finally, the results from the investigation of oil deposition on the catalyst are presented in 7. The conclusion and perspectives of the thesis are presented in chapter 8.

2. STATE OF THE ART ON PASSIVE AUTOCATALYTIC RECOMBINERS

This chapter gives an overview of the state of the art on PARs. At first, the catalytic reactions are discussed, followed by the principal of PARs and then the catalyst deactivation. Previous experimental programs that have studied the catalyst deactivation are also discussed.

2.1. Catalytic Reaction

In case of homogeneous combustion, the conversion of hydrogen and oxygen to steam requires either flammable mixture with a sufficient ignition source (flame) or high temperatures (auto-ignition). It represents a safety risk since the combustion process is not easily controllable. However, hydrogen can react, exothermically, with oxygen from the containment air on the surface of catalysts even at low contents (< 1 vol. %). The catalytic combustion is the principle used in catalytic recombiners.

A catalyst accelerates a chemical reaction by forming bonds with reactants molecules, allowing these to react and to form a product that then detaches from the catalyst. The catalytic reaction between molecule A and B to product P starts with the bonding of molecules A and B to the catalyst [13]. Then, A and B react, by means of the catalyst, to form product P. Finally, the product P detaches from the catalyst and the reaction cycle starts again. Figure 2 shows how the catalyst accelerates the reaction. In the absence of the catalyst, the reaction proceeds when the reactants collide with sufficient energy to overcome the activation energy. With the catalyst, the activation energy is lowered. The overall catalyst activity and selectivity are determined by the composition and structure of its surface [14].

The catalyst offers an alternative path for the reaction. Although the path is more complex, it is more favourable energetically. The activation energy of the catalytic reaction is smaller than that of the homogeneous gas phase reaction. The overall changes in enthalpy and in free energy is the same for both catalytic and non-catalytic reaction, meaning that the catalyst does not affect the equilibrium constant for the overall reaction of A+B to P. A catalyst changes the kinetics but not the thermodynamics. The total number of active sites on the catalytic surface is a constant. In heterogeneous catalysis, this site density is given by the number of sites per kg

catalyst or per unit of surface area. In homogeneous catalysis, the site density is expressed as the concentration of catalytically active complex molecules [14].

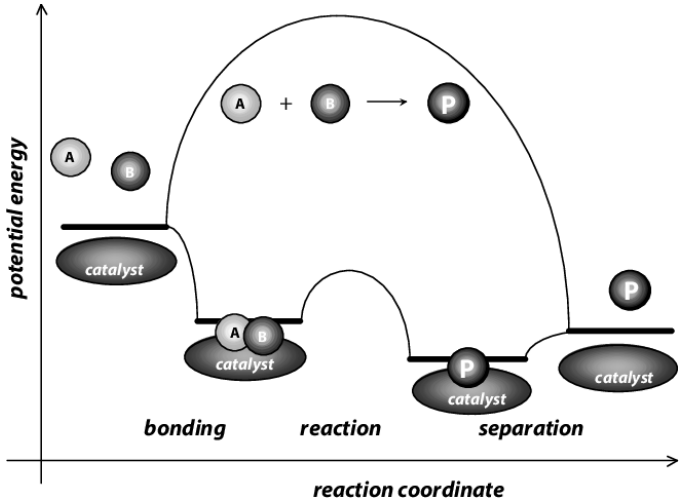

Figure 2: Potential energy diagram of a heterogeneous catalytic reaction, with gaseous reactants and products and a solid catalyst. Note that the uncatalyzed reaction has to overcome a substantial energy barrier, whereas the barriers in the catalytic route are much lower. [13]

A catalyst accelerates the rate of a reaction without being consumed during the process. For the optimum operation of a catalyst, not only the catalyst material but also the surface condition and geometry must be considered.

The adsorption of the molecules and atoms might be direct or indirect. In the direct adsorption process, the particle collides with the surface and stays at the point of impact as an adsorbed species. In the indirect adsorption, the particle first adsorbs in a weakly bond precursor state, moving freely over the surface, until it forms a bond with an adsorption site. Atoms that are already adsorbed may block sites for new incoming atoms. Chemical adsorption (chemisorption) occurs when the adsorbed substance (adsorbate) forms a chemical bond with the adsorption surface (adsorbent) at the so-called adsorption sites. Chemisorbed substances tend to form the highest possible coordination number with the adsorbent surface, so that only a single layer of the molecule is produced on the surface. In contrast, Van der Waals forces are present in physisorption. Chemisorption and physisorption are distinguished by means of the corresponding adsorption heat [15].

Adsorption of reactants on the catalyst's surface is the first step in a heterogeneous catalytic reaction. The relation between the coverage of a particular gas and its partial pressure above the isotherms and they form the basis of the kinetics of catalytic reactions. The first quantitative

theory of gas adsorption on surfaces was the Langmuir adsorption isotherms. The assumptions underlying the Langmuir adsorption isotherm imply an ideal surface and few real systems follows this assumption of ideality [14]. Adsorption equilibrium is assumed to be established at all times. The concentrations of adsorbed species are determined by adsorption equilibrium. If two or more species are present, they compete with each other for adsorption on a fixed number of active sites.

Desorption is the opposite of adsorption. It represents the end of the catalytic cycle. The transition state of a desorbing molecule can be mobile, resembling the precursor state of indirect adsorption or it can be immobile, implying that the molecule only possesses vibrational state.

2.2. General description of Passive Autocatalytic Recombiners

Passive autocatalytic recombiners (PARs) are devices used in nuclear power plants for mitigation of the hydrogen risk. They aim to recombine hydrogen through the exothermic reaction:

$$H_2 + \frac{1}{2}O_2 \rightarrow H_2O \quad \text{with } \Delta H_R = -241.8 \text{ KJ/mole of hydrogen}$$

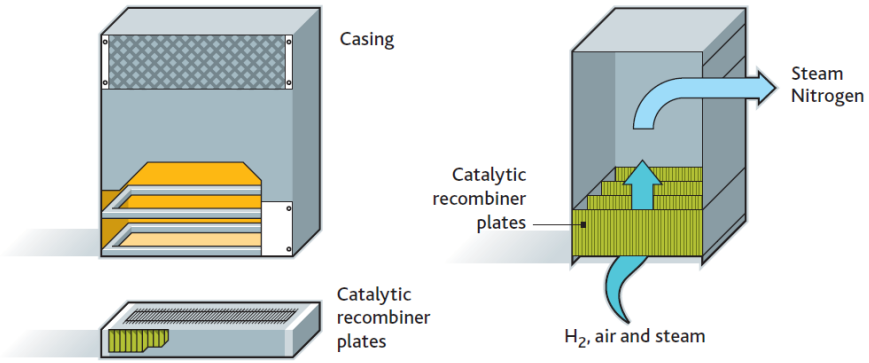

Figure 3: Working principle of a passive autocatalytic recombiner [1].

As shown in figure 2, PARs consist of a rectangular shaped housing containing a set of parallel catalyst sheets in the lower part. In the presence of hydrogen, a catalytic reaction occurs spontaneously at the catalyst surface and the heat of the reaction induces natural convection flow feeding the recombiner with hydrogen.

PARs are defined as passive since they are self-starting, self-feeding and require no external energy. The recombiner starts when the hydrogen content reaches 1-2 vol. % [5].

The chemical reaction only starts after the overcoming the necessary activation energy. Catalytic substances can significantly reduce the activation energy so the reaction starts at lower temperatures by decreasing the bounding of the hydrogen molecules and forming radicals that will react more easily with oxygen.

Catalyst plates have three main components: the substrate, the catalyst carrier and the catalyst active material. Stainless steel is usually used for the catalyst substrate. A ceramic material, as aluminium oxide, is applied to the substrate material to act as structural reinforcement and it will act as catalyst carrier or washcoat due to their thermal stability [8]. Placed on the top of the catalyst carrier is the catalyst itself. The catalyst used is usually platinum (Pt) or palladium. Palladium is known for having a higher reactivity than platinum, however it might lose surface contact with the substrate at higher temperatures.

When in contact with the catalytic plates, hydrogen and oxygen react to produce water vapor. The catalytic recombination follows the reaction mechanism composed of three phases: adsorption, surface reaction and desorption. First, the reactants are adsorbed on the active sites of the catalytic surface. Then, the recombination reaction takes place before desorption of the products and the release from the catalytic active sites. The hydrogen recombination reaction is an exothermic reaction and starts after exceeding the minimum required activation energy.

In presence of catalytic surface, reactive carries are simultaneously produced and consumed from the gas-phase. Reactive radicals disappear at the free stream edge due to gas-phase recombination and at the catalytic surface due to the surface recombination when the boundary layer is fully developed [9]. If there is an increase of the temperature, the production of reactive radicals dominates the consumption, forming a chain propagation to gas-phase ignition. The temperature of the catalytic surface and of the gases can lead to ignition of the gas mixture in the surroundings of the catalyst plates. Ignition of hydrogen on a catalytic recombiner has been subject of several studies [9], [10].

2.3. Types of recombiner

Different types of recombiners have been developed in the industry. There are recombiners that are built on the use of clusters of spherical granulates with palladium as the catalyst and ceramic materials as the carrier. Some catalytic recombiners are based on the use of an entirely metallic catalyst to eliminate the possible spalling hazard constituted by the dust formation. Some recombiners are designed to enhance the reaction heat removal by using passive containment cooling devices. Other designs, such as modular recombiner setup, aimed to limit the local heat production of the exothermal reaction. Diverse recombiners have been commercially provided by PAR manufacturers, such as FRAMATOME (formerly AREVA/Siemens), NUKEM (formerly NIS) and SNC-Lavalin (formerly AECL). FRAMATOME and AECL use plate type catalyst, while NUKEM developed a specialized container with pellet type catalyst [7].

AECL recombiners have been designed for compactness and ease of managing into containment. The recombiner consists of an open-end rectangular box with an attached cover and gratings to ensure the physical protection of the internal elements from sprays. The catalyst plates are arranged parallel to the gas flow direction. The catalysts operate at temperatures up to 1000 K without loss of catalytic activity and are not affected by high radiation exposures. The recombination self-starts at low hydrogen content. FRAMATOME recombiners consist of a metal housing designed to promote natural flow, with the gas inlet arranged at the bottom and gas outlet at the top. Catalytic plates are arranged vertically in the bottom of the housing. The recombiner is protected against direct spraying of water and aerosol deposition by a cover placed at the housing at the top of the recombiner. This allows recombiner operation under spray conditions. The catalyst allows low starting temperatures.

The NUKEM recombiners are available in a variety of sizes. The recombiners contains flat rectangular cartridges filled with porous spherical ceramic pellets, coated with palladium. Between the cartridges, the device has open flow channels to allow for heavier particles or aerosols in the atmosphere to flow through with little plugging of the pellet surface.

In France, PWR of 1300 and 1450 MWe are equipped with recombiners of AECL design while PWR of 900 MWe and EPR are equipped with FRAMATOME type recombiners [11].

Figure 4: Example of an AREVA PAR (FR1-380T) [12].

2.4. Catalyst deactivation

PARs can be exposed to different chemical products or atmospheric pollutants that may lead to the loss over time of catalytic activity and/or selectivity called catalyst deactivation. PARs deactivation is a safety concern since it can result in start-up delay and in loss of the recombination efficiency, increasing the hydrogen explosion risk.

2.4.1. Catalyst deactivation mechanisms

Catalyst deactivation is a complex phenomenon and it is expected for most processes, yet, some of its consequences can be avoided, postponed or reversed. The main mechanisms are poisoning, fouling, thermal degradation, mechanical damage and corrosion/leaching by the reaction mixture. The first two cases are caused by blocking of active catalytic sites but the catalyst might be regenerated. The other mechanisms occur due to loss of active surface and they are considered to be irreversible. Each mechanism is defined in Table 2.

Table 2. Definition of deactivation mechanisms (adapted from [8]).

Mechanism	Type	Definition
Poisoning	Chemical	Blocking of active catalytic sites by strong chemisorption
Fouling	Mechanical	Blocking of active catalytic sites and pores by physisorption
Thermal degradation	Thermal	Thermal induced loss of catalytic surface
Mechanical Damage	Mechanical	Loss of active surface due to mechanical impact
Corrosion/leaching	Chemical	Loss of active surface due to volatile compounds formation

Poisoning

Poisoning is defined as catalyst deactivation by strong chemisorption of impurities on active sites [16]. The adsorption strength, when competing for catalytic sites will determine if a species can act as a poison. Most strongly absorbing components inhibit the adsorption of less strongly adsorbing components. Poisons may not only cause physical blocking of adsorption sites but also induce changes in the electronic or structure of the surface [14]. The poisoning might be temporary, when it can be removed, or permanent. Some poisons might be strong at low temperatures but less harmful at high temperatures. During catalytic combustion, poisoning by traces of sulphur, halogens, phosphorus, arsenic, lead, alkali metals, etc. is less damaging than in catalytic processes at low or medium temperatures (500°C) since these poisons are promptly decomposed and/or are not absorbed on catalytic surface at high temperatures [14]. Catalyst poisons are classified according to their chemical characteristics, selectivity for active sites and types of poisoning reactions. Poisons may affect catalytic activity by different mechanism. The strong chemical bond electronically modifies the nearest neighbour atoms, modifying their abilities to adsorb and/or dissociate reactant molecules.

Fouling

Fouling has been defined as all processes where a deposit covers a surface [16]. The mechanical deposition of species onto the catalyst surface leads to blockage of the active sites and pores and; consequently, leads to activity loss. Its origin might be from species present in the containment, like the deposition of dust, and not always related to processes on the catalyst. However, the catalyst itself might be responsible for fouling by undesired by-products that leads

to deposits. It may cause disintegration of catalyst particles and plugging of the reactor voids, in its advanced stages [14].

Thermal degradation

Thermal degradation comprises physical processes leading to catalyst deactivation due to sintering, evaporation, chemical transformation, etc [14]. Thermal damage can occur during all stages of the catalyst life cycle. Sintering refers to the loss of catalytic surface area due to crystallite growth of the support material or the active phase. The main mechanism for sintering of small particles is the migration of atoms. Sintering processes are kinetically slow and irreversible or difficult to reverse, so it is easier to prevent it than to cure it.

Mechanical degradation

Mechanical damage of catalysts can be presented as crushing of the catalyst during loading, attrition and erosion of the catalyst particles at high fluid velocities [14]. During its life cycle, the catalyst is heated at start-up, leading to thermal expansion of the tube and during cooling the opposite happens.

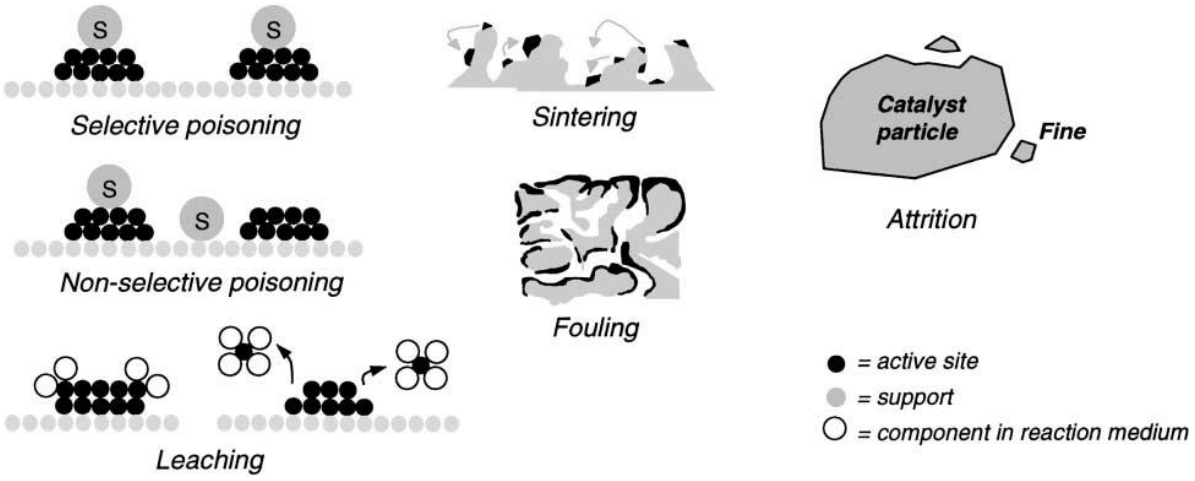

Figure 5. Types of deactivation in heterogeneous catalysis [8].

2.4.2. Deactivation scenarios

Deactivation scenarios can be classified into two types, as the containment conditions differs in normal reactor operation from accidental conditions.

Normal reactor operation

During normal operation, the catalyst plates can be affected by products of maintenance work, impure substances in the containment, the periodic control, the regeneration procedure, etc. Recent controls in French NPPs have for example showed the presence of oil from the primary pumps on the catalyst sheets. Organic (paint fumes) and inorganic (welding aerosols) particles can be released during the maintenance work of the reactor. Those particles are deposited on the catalyst surface by diffusion through the containment atmosphere. It has to be noticed that PARs are supposed to be protected during maintenance work, in order to reduce the risk of pollution. Table 3 shows the classification of different loads in normal operation.

Table 3: Classification of different loads in normal operation that can lead to catalyst deactivation [15]

	Poisoning	**Fouling**	**Thermal Damage**	**Mechanical Damage**	**Corrosion**
Products of maintenance		X			
Atmospheric contaminants		X			
Recurring inspection			X	X	
Regeneration			X		X

Accidental conditions

In case of a severe accident (when there is core melt), several radioactive substances can be released in different states and chemical forms, leading to the contamination of the containment atmosphere and consequently, the catalyst surface. In this situation, all five deactivation mechanisms might happen. During an accident, the deactivation can be caused by the gaseous fission products, water soluble and insoluble aerosols, MCCI products, fire products, thermal loads, hydrogen deflagration and radioactive radiation. In these conditions, the containment temperature can reach 900°C. Table 4 shows the events that might lead to deactivation in case of accident.

Carbon monoxide can be produced during a severe accident, due the MCCI and also in case of fires inside the containment, as it happened in Sweden (Ringhals) in 2011.

Most emissions are released as aerosols, while fission products can be also released in in gaseous form. Radioactive materials are released during an accident by emission of activated cladding material, fission products or nuclear fuel.

The behaviour of aerosol particles is predicted by not only its composition but also by the chemical form of the elements. The aerodynamic radius and the sinking speed determine the behaviour of the particles. Aerosols present low mass and high mobility, which makes them subject to forces that are only observed microscopically. These forces include thermophoresis, photophoresis and diffusiophoresis. They are based on gradients of temperature of the particle and of the ambient and ambient concentrations [15].

An earthquake can also damage a recombiner. It can not only cause external destruction to the housing of the recombiner but also the movement and friction of the catalytic films can cause erosion of catalyst particles and damage to the porous coating, which may induce the detachment of the washcoat from the steel support. To ensure the protection of the recombiner in case of earthquakes, tests are performed on shaker tables with vibrational movement in all three spatial directions. Table 4 shows with deactivation mechanism might affect the loads exposed to the recombiner in case of a severe accident.

Table 4: Classification of different loads that can cause catalyst deactivation in accidental conditions [15].

	Poisoning	**Fouling**	**Thermal Damage**	**Mechanical Damage**	**Corrosion**
Gaseous Fission products	X				
Water soluble aerosols	X	X			X
Water insoluble aerosols	X	X			
Gaseous MCCI products	X				
Containments spray	X	X			X
Fire products	X	X			X
Thermal loads			X		
H2 deflagration			X	X	
Radioactive radiation			X	X	
Earthquake				X	X

2.5. Previous works on PARs and deactivation processes

2.5.1. Hydrogen PAR recombination

The behaviour of recombiners has been subject of several studies performed under different conditions. The deactivation of such devices has been investigated as well. Studies that focus on state-of-the-art on PARs, ignition phenomena and catalyst deactivation will be discussed in this section due to the relevance in the subject.

Bachellerie et al. [16] carried out in 2003 a state-of-the-art on PARs as an objective of the PARSOAR project co-sponsored by the European Commission in the Fifth Euratom Framework Program and the Swiss government and devoted to hydrogen risk in nuclear power plants. Another objective of the project was to elaborate a guide that defines an approach for implementing catalytic recombiners in NPP and also to identify the experimental qualification and computer code developments still required for the research and mitigation of the hydrogen risk in nuclear power plants. This work focussed on the safety criteria that need to be respected when defining/dimensioning the PAR. The project concluded that the selection of an optimal location for the recombiner consists in a well-balancing between expert judgments and computer code simulations. It shows that PARs must be subjected to periodic controls (visual inspections and performance tests).

Payot et al. [17] investigated in 2012 the behaviour of a PAR in realistic containment conditions during a severe Light Water nuclear Reactor (LWR) accident. Catalyst samples have been exposed to an atmosphere representing a core meltdown accident, containing gaseous fission products and aerosols released during degradation of an actual irradiated nuclear fuel. The results from poisoning tests applied to PARs in typical severe accident conditions showed that no serious poisoning effect can be noted under these conditions.

Meynet et al [18] numerically investigated the steady state PAR experiments performed in REKO-3 facility at the German research center of Juelich (JÜLICH). Experiments with 2 and 4 vol. % of hydrogen were used as a basis for the validation and comparison of three numerical codes in order to quantify the importance of main physical phenomena as heat radiation, solid heat conduction and species thermal diffusion. The comparison shows the main influence of radiative heat losses in all calculations and the minor participation of species thermal diffusion while the solid heat conduction is more negligible.

Studies dedicated to the operation of PARs have also been carried out in the frame of the OCDE THAI project, performed in 3 different phases: THAI (2007-2009), THAI-2 (2011-2014) and THAI-3 (2016-2019). The two first phases contributed to hydrogen and fission-product release issues during accident conditions. The later phase investigated the open issues related to the subject in the THAI+ facility. The projects provided an experimental database devoted to the distribution of hydrogen in containment, its removal by PARs and hydrogen combustion processes in accident conditions. Iodine and aerosol interaction with PARS have been investigated as well. The performance of recombiners under different thermal-hydraulic conditions such oxygen starvation and ignition behaviour has also been studied.

The THAI vessel permits operation of medium sized commercial PAR units with free, unrestricted natural convection. The 60m3 facility has 9.2 m height, 3.2 m diameter and it is thermally insulated. Different parameters related to the PAR behaviour have been investigated: onset of recombination, recombination rate, ignition potential and, oxygen starvation [19]. The THAI test program constituted of a total of 30 tests for three different types of commercial recombiners at various conditions of temperature, pressure and gas composition. One of the main objectives of the THAI HR-tests was to investigate the ignition characteristics of commercial PARs.

The THAI tests have showed that the performance of PAR is reduced under the stoichiometric fuel/air ratio. These tests have revealed that a higher O_2/H_2 ratio is required for the PAR operate without loss of recombination.

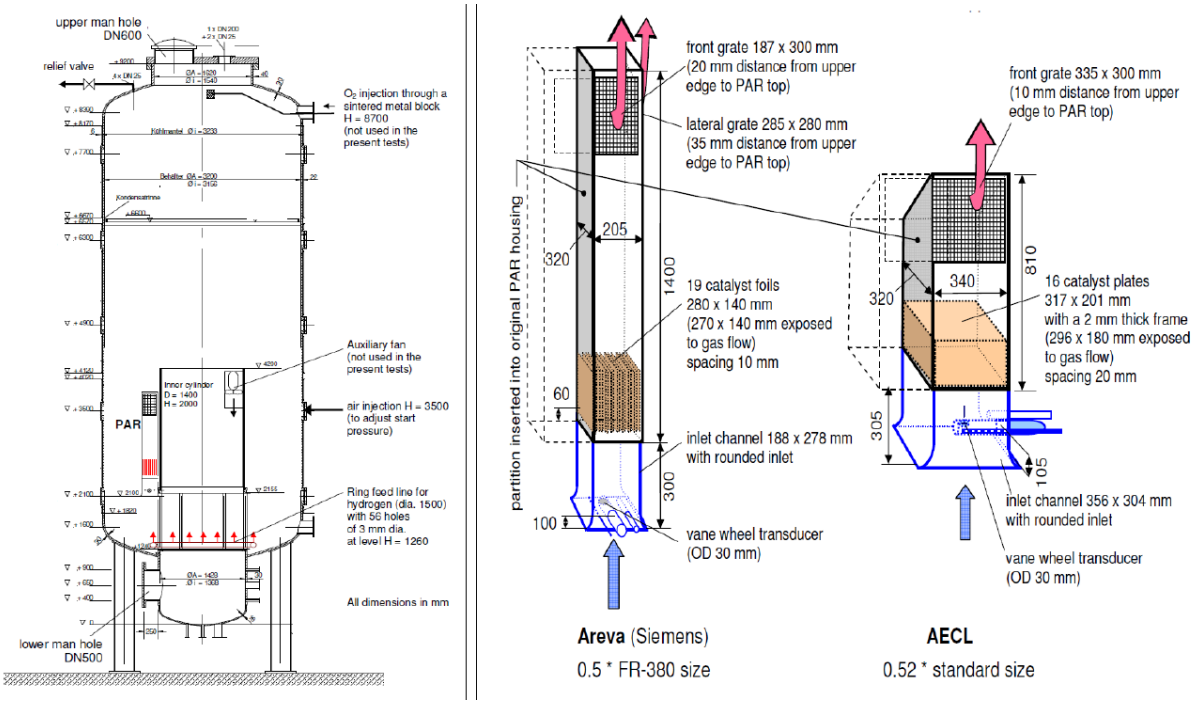

Figure 6: The THAI test vessel configuration and PAR types used in the tests [20].

Many studies have already been performed on recombiners to investigate catalyst deactivation, notably prior their installation in NPPs. Recombiners manufacturers have performed qualification tests on PARS in order to demonstrate their performance during accidental conditions.

2.5.2. Qualification tests

Many qualification tests have been made for PARS by manufacturers, for example the tests performed for the AREVA (now FRAMATOME) qualification program showed in Figure 7.

Germany		
Karlstein	since 1989	Ongoing development and qualification
	1998	Absence of feedback of the PARs: Prevention of sump strainer clogging
	2002	CO_2 tests
	2006	TSP Spray Tests (Tri Sodium Phosphate)
Frankfurt	1991	Performance test in a multi-containment geometry (Battelle Model Containment)
	2008	OECD-THAI Hydrogen Recombiner Deflagration / Ignition test
France		
Cadarache	1995	EDF KALI H_2 tests qualification for 900 MW PWR French accident scenario
	1996 to 1998	– Integrated core melt tests - international PAR qualification testing – Full scale tests simulating inactive core melt conditions - IBSN / EDF H_2 PAR tests
	1998	– Pre-tests simulating inactive core melt conditions with catalysts of different suppliers – EDF/CEA KALI H_2 tests deflagration / degradation
	2004 to 2009	– Final active in-pile core melt test with catalysts of different suppliers (FBT3) – Test performance – Evaluation of results
	2009	– OECD CsI-iodine interaction and high aerosol concentration test (up to 3g/m^3) – OECD-challenging poisoning severe accident atmospheric test – High concentration poisons SnO_2, $LiNO_3$, Iodide
U.S. / France		
Cadarache	1995 to 1996	EPRI/EDF KALI H_2 tests qualification for US-ALWR

Figure 7: AREVA (now FRAMATOME) PAR qualification program [12]

A series of H2-PAR tests were carried out between 1996 and 1998 at the Cadarache Nuclear Centre to investigate the performance of commercially available PARs. Électricité de France (EDF) and Institut de Radioprotection et Sûreté Nucléaire (IRSN) focused their activities on the AREVA NP PAR (now FRAMATOME). The recombiners have been submitted to qualification tests under a wide range of hydrogen concentrations, initial ambient gas temperature and pressures, steam and potential poisons. During this program, the recombiner was exposed to realistic aerosol generated by a molten core. The tests showed the effect of aerosols on the recombination reaction and on catalytic poisoning by fission products in a severe accident atmosphere [21]. The tests indicated no significant reduction in the recombiner performance.

The H2-KALI tests performed by CEA (French Energy Atomic Commission) from 1993 until 1995 aimed at studying the effect of containment spray on the PAR efficiency.

Additional tests were performed to investigate the PAR operation under containment spray conditions with a trisodiumphosphate (TSP), hydrazine, and boric acid solution. The results demonstrated that the PAR efficiency is not significantly influenced by spraying of TSP, boric acid, and hydrazine (in comparison to demineralized water).

The KALI test facility also allowed cable fires tests to investigate the effect of cable combustion fumes on PAR performance. Even though, the catalyst was exposed to cable fire combustion products for several minutes, there was no impact on the efficiency of the recombiner.

Tests carried out at the KALI H2 by the CEA focused on the behavior of the PARs during and after a design basis and severe accident in boiling water reactors and pressurized water reactors. Effect of steam and low hydrogen have been investigated as well as potential poisons as carbon monoxide and cable fire products.

More detailed results and other qualification tests can be found in [21].

2.5.3. Investigation of fouling in recombiners

Recombiners installed in the German NPP Emsland (KKE) are subjected to periodical controls due to their exposition to various airbone substances during normal operation. During this procedure, some of the catalyst sheets installed in the 58 PAR of AREVA design showed a delay in the start of recombination. First analysis indicated a beginning of fouling on the catalytic surface. A study conducted in cooperation between KKE, Forschungszentrum Juelich and RWTH Aachen University aimed at characterizing the composition of the fouling and to correlate it with potential sources within the containment. Sample sheets were selected from the installation and were subjected to a chemical surface analysis in order to identify effects like sintering, poisoning or blocking of the catalytic surface. [22]. Moreover, the samples were subjected to tests that allow the correlation of the chemically quantified deposition on the catalyst with the characteristics of the start-up and the steady-state performance of the recombination. Later, possible sources of the fouling were analysed.

The reports of the periodic inspections were statistically assessed to provide a basis for the selection of appropriate samples. The recombiners were classified according to their location in the compartment and ventilation zones of the containment. PARs installed at staircases, pipe ducts and the four compartments of the circulation fans of the large plant compartment did not show any indication of fouling. However, PARs installed at and above the reactor pool level, especially those near the ventilation fans on the steam generator indicated fouling and the beginning of deactivation. Inspections reports presented the delayed response of these catalyst sheets combined with smoke production from surface reactions.

For the chemical surface analyses the sheets were cut into six stripes and for the performance tests they were cut into one square. New catalyst sheets from the KKE were used as reference for normal operation samples. A set of performance tests was performed in the REKO-3 facility at the Institute for Safety Research and Reactor Technology (IEF-6) at Forschungszentrum Juelich in order to investigate the impact of fouling on the performance of the catalyst sheets so the selected samples for chemical analysis were truly affected by the fouling. The samples were installed inside a vertical rectangular flow channel. The catalyst temperature was measured by means of a pyrometer through an optical access window. The hydrogen and oxygen concentration were measured at different vertical positions by means of gas analysers with continuous gas sampling.

All tested samples showed the formation of smoke and smell and significant delay in the recombination start-up under the specified test conditions. The comparison between the behaviour of a normal condition and a deactivated catalyst sheets is shown in Figure 8. The catalyst temperature was measured at the bottom edge of catalyst plate. The top diagram shows the start-up behaviour of a fresh catalyst sheet in its normal condition while the bottom diagram shows the performance of a deactivated catalyst sample. It is possible to observe that there is a significant delay in the start-up of the deactivated catalyst sheets. At 1 vol. % hydrogen, no start of the catalytic reaction was observed for at least 15 minutes. When the inlet content is increased to 1.5 vol. % a slow continuous decrease in the outlet concentration indicates a gradual start of the recombination reaction. Once the reaction accelerates, the burn-off of the fouling is indicated by a temperature peak accompanied by a visible smoke emission. At higher hydrogen concentrations, the sample recovers to full capacity.

In addition to (organic) fouling that could block the catalytic surface and could cause the smoke production, the damage could be caused by an inorganic poisoning of the catalyst. In order to chemically analyse the catalyst sheet and identify possible sources of poisoning, a semi-quantitative X-ray fluorescence analysis (XRF) was performed at the Central Division for Analytical Chemistry (ZCH). A significant amount of Sulphur was detected, in comparison to the normal operation samples. Since no further catalyst poisons were detected in significant amounts, the possibility of deposition of welding smoke (e.g. titanium oxide, ferrous oxides), aerosols from drilling or grinding work and particles resulting from the maintenance of the reactor was eliminated.

To identify the composition of the fouling, its chemical fingerprint was analysed at the Institute of Chemistry and Dynamics of the Geosphere (ICG-V) by means of pyrolytic gas chromatography with mass spectrometer coupling (Py-GC/MS). The detected chemical patterns of all samples were identical but with different mass distributions of the compounds, which indicates a global source. The fouling mainly consists of single and polycyclic aromatic hydrocarbons. The chemical analysis and the fact that all the impacted PARs were located in areas with air exchange rates and near ventilation fans, made possible to assume that the cause of the fouling was an external carbon and sulphur source transported into the containment in the form of particulate matter by external air supply.

In this case, the organic compounds were completely burned-off, while the sulphur compounds were retained. The catalyst sheets had performed normally and were not affected by the remaining sulphur compounds after its regeneration. The regeneration procedure involves thermal stress on the catalytic coating. Analysis of the surface showed that once the catalyst had been regenerated the structure and performance was not significantly altered.

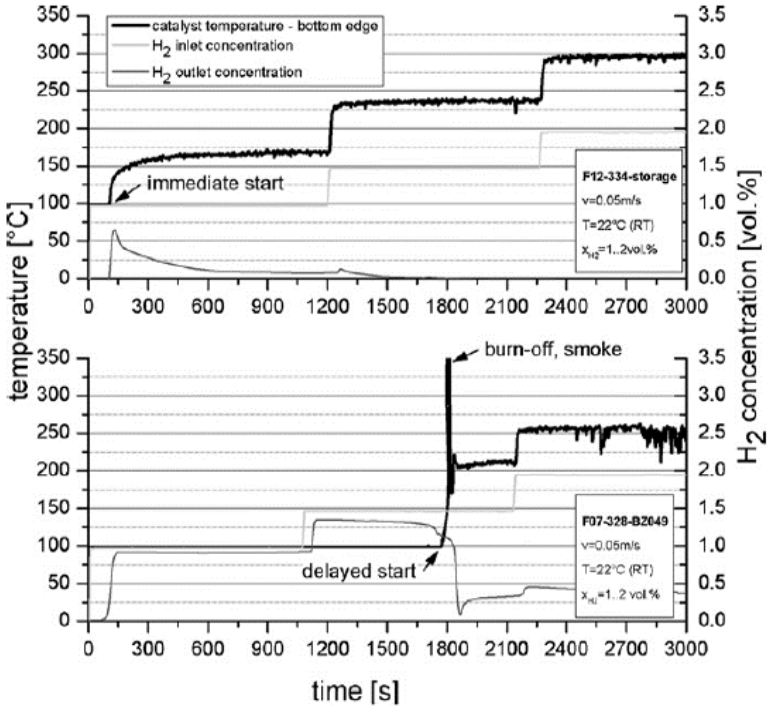

Figure 8: Typical starting behavior of a catalytic plate in normal condition (top) and in poisoning condition (bottom) [22].

2.5.4. Poisoning by iodine

The catalyst might be poisoned by fission products and reactor structure materials under the form of vapours and particulate matter. A study carried out by Morfin et al [23] focused on the poisoning by these chemical substances on catalysts with different compositions. Poisoning of alumina-supported Pt and Pd catalysts were quantifiable in experimental conditions. The study aimed at identifying the effect of poisoning by di-iodine and methyl iodine in the hydrogen recombination in PARs.

A fixed-bed flow reactor was responsible for the catalytic oxidation of hydrogen. The reaction was carried out under high oxygen and low hydrogen partial pressures to ensure a representative atmosphere. To investigate the effect of iodine, a saturator containing iodine flakes, preserved at a required temperature, produced iodine vapour in accordance with vapour pressures versus temperature relation. To study the poisoning by ICH_3, iodine is replaced by a cylinder-fed gas flow containing 1000 ppm of methyl iodine in nitrogen. The CO and CO_2 concentrations are determined by COSMA Beryl-100 infrared analysers.

For each reaction temperature and each catalyst in absence of poisoning, the domain into which the flow of reactants is high enough to avoid reaction rate control by diffusion has to be determined. Pseudo-rates constants showed that platinum is about 400 times more active than palladium. Concerning the Pt-Pd catalyst, their activities are similar being two orders of magnitude higher than that of pure palladium and three times lower than pure platinum.

The activity of the various catalysts has been analysed in the presence of di-iodine vapour and it was shown that palladium and platinum behave differently. The activity of palladium reaches a constant level after an initial decrease during the first 5 minutes. In contrast, a continuous decrease is observed for platinum and the activity becomes insignificant after 3 hours. The reactivity of the Pd-Pt catalyst is less affected by the iodine than platinum and even than pure palladium, as its residual activity was 60% of the initial one. The loss of efficiency due to di-iodine and methyl iodine does not affect significantly the hydrogen recombination. In conclusion, the study reported the resistance of Pd-Pt bimetallic catalyst to di-iodine and methyl iodine poisoning even for concentrations higher than those expected in case of a major accident.

2.5.5. Carbon monoxide effect on PARs

A study carried out in cooperation between Julich, RWTH and IRSN aimed at characterizing the behaviour of a PAR in the presence of hydrogen and carbon monoxide [24]. Klauck et al. performed an experimental test programme to investigate the operation of PARs in the presence of hydrogen and carbon monoxide. The results showed that the under the given conditions the conversion of CO into CO_2 has no negative impact on the simultaneous hydrogen conversion.

The experiments were performed at the REKO-3 facility, at Jülich, to study different aspects of PAR operation under defined conditions. The reaction rates of each species were calculated by determining the gas composition after the catalytic reaction. The removed sample gas was bypassed through a gas analyser with condensate separator including commercial measuring cells for oxygen, hydrogen, carbon monoxide and carbon dioxide. The reaction rates were obtained by balancing the measured outlet concentrations with the inlet gas composition. Temperatures were measured by means of thermocouples.

Initially a mixture of hydrogen and air with hydrogen content up to 5.5 vol. % was fed into the flow channel at different inlet velocities, 0.5 m/s and 1.0 m/s. The fast velocity is assumed to be a realistic flow velocity through an operating full-scale PAR. Hydrogen content was maintained constant while the CO content was stepwise increased. Later, the tests were performed with hydrogen contents of 2.0 and 4.0 vol. % while the CO content was increased until it reached the same one as H_2.

The exothermal reaction on the catalyst surface raises the catalyst temperature, depending on the gas composition. The results showed that the conversion of hydrogen remains constant through the entire test. The addition of carbon monoxide leads to increased temperatures because of the exothermal reaction of converting CO into CO_2. The hydrogen recombination efficiency was approximately 100%, independent from the CO content. The CO conversion increased as the CO content was higher. The CO conversion efficiency remains constant at a lower level than H_2. The main difference between the fast and slow tests is a decrease in the conversion efficiency for both species.

In order to analyse the behaviors observed in the experiments, three different numerical codes were used for the simulation of the recombination in a PAR. The codes REKO-DIREKT (FZJ/RWTH), SPARK (IRSN), and CFX (ANSYS) permit to simulate the behaviour of a recombiner, providing basis for further investigation.

The REKO-DIREKT code was developed to simulate aspects of the operational behaviour of PARs as the start-up, hydrogen conversion under different conditions and ignition. The 2D code calculates not only the conditions at the PAR outlet but also the local catalyst temperature and local gas concentrations along the catalyst surface. It models all relevant heat and mass transfer processes inside the catalyst section. The only input parameters required are the temperatures and gas composition at the recombiner inlet and the absolute pressure. The reaction model of the catalytic reaction is based on mass transfer correlations. The catalyst temperature along the catalyst surface and the outlet H_2/CO concentration values were used in order to compare the experimental data and the calculation results using the code. In general, there was an agreement of measured catalyst temperatures and outlet gas concentration with the simulated results, which confirms the applicability of the model. Figure 9 shows the plot of the calculated outlet concentrations of hydrogen and carbon monoxide against the experimental values. The code underestimates the CO outlet concentration by approximately 10 %.

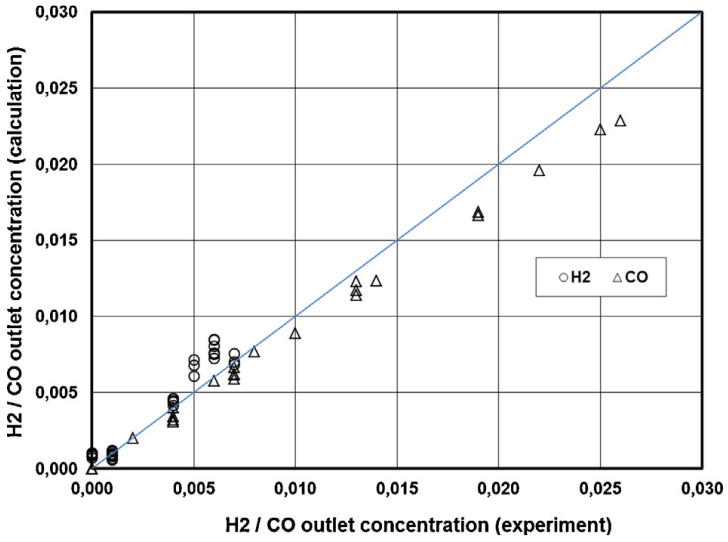

Figure 9: Comparison of calculated (REKO-DIREKT) and measured outlet concentrations of H_2 and CO for the entire test series. [24]

SPARK is a numerical code dedicated to catalytic chemical reactor-type applications developed at IRSN. It solves the 2D steady-state Navier-Stokes equations in the vorticity-velocity formulation by including detailed gas phase and surface chemistry, multicomponent transport and surface heat radiation. More details about the code modelling and applications are given in the chapter 4. The results showed that the calculated catalyst temperatures and conversion rates were in good agreement with the experimental data. Figure 10 shows the calculated and

experimental conversion rates. The conversion rates were slightly underestimated but the code showed that the hydrogen conversion is more efficient compared to carbon monoxide conversion, showing good agreement with the experiments.

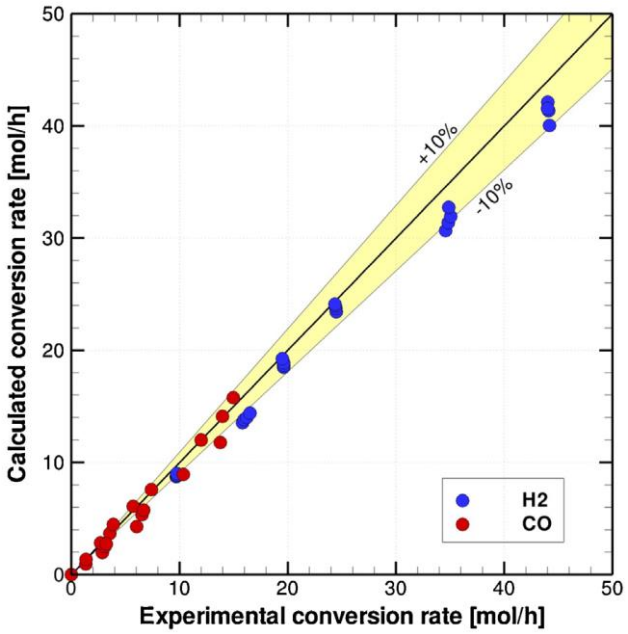

Figure 10: Comparison of calculated (SPARK) and measured recombination rates for H2 and CO for the entire test series [24].

The reaction model was also implemented in the commercial CFD code ANSYS CFX 14 based on the rate determining step of the catalytic recombination. Only the transport of species is considered for simulation of the catalytic process and the outer surface of the catalytic coating is modelled as a wall. The chemical reactions are modelled as single-step reaction. The model predicts the detailed thermal hydraulic and transport phenomena in a catalyst section. The results showed that the flow channel formed between the catalyst sheets is representative for a realistic PAR catalyst section and it can be applied in order to reduce the numerical domain. The temperature level and heat losses at the outer sheets could be simulated in good agreement with the experiment. However, a deviation from experiments was observed for the gradient of the temperature along the catalyst surface that can be attributed to uncertainties in the heat radiation model. Figure 11 presents the comparison between the calculated and the experimental recombination rates for H_2 and CO. The relative discrepancy between simulation and measured conversion rates is below 10 %, showing a good agreement.

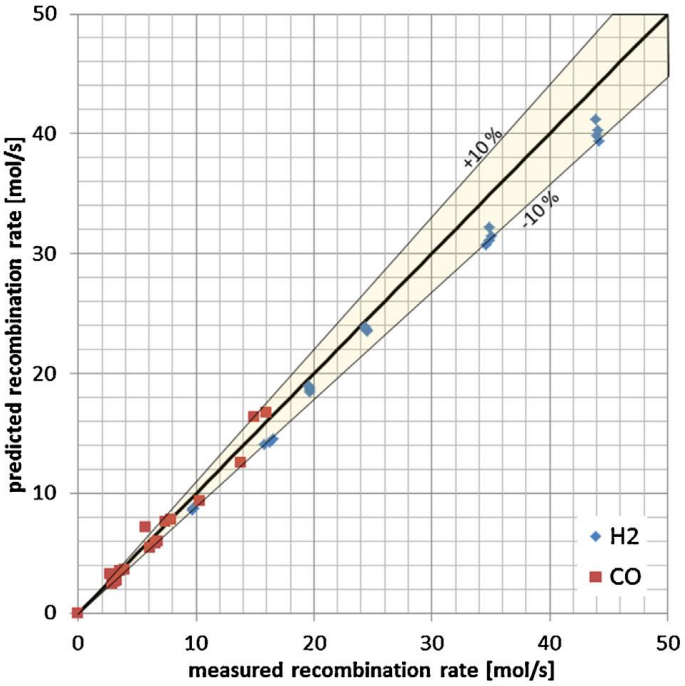

Figure 11: Comparison of calculated (CFX) and measured recombination rates for H_2 and CO for the entire test series [24].

The aforementioned tests were performed under oxygen rich conditions, the reaction kinetics under oxygen starvation still need to be further investigated. The behaviour of CO on a cold catalyst should also be investigated to identify if CO may act as a catalyst poison under these conditions. The experimental study [24] concluded that the CO is converted to CO_2 if the catalyst is at high temperature due to the parallel H2 conversion. The conversion efficiency for CO is significantly lower than for H_2. Under fuel-lean conditions, no visible influence on H_2 conversion was observed in the experiments. The obtained results can be considered as representative of a full size recombiner.

The three different codes used in the study focused on different applications due to their different levels of details. The SPARK code is suited for estimating ignition limits, combustion simulation and reaction on the catalyst surface due to the complex surface and gas chemistry approach. The PAR model based on ANSYS CFX code is applicable for any geometry and different PARs designs since it presents a high level of details. The REKO-DIREKT code is appropriate for the implementation in thermal hydraulic or containment codes. No major discrepancy was identified between the 3 modelling approaches.

2.5.6. Cable fire products effect

Cable material is considered as essential fire material in nuclear power plants. Cables consist of conductors, insulation, filling material and cable sheathing. Cable fire products are physically a mixture of solid, liquid and gaseous components. Released particles can be small drops of condensed organic substances but also carbon-rich agglomerates of many nearly spherical primary particles (soot). The differences in the particle properties result from different formation mechanisms of the fire products in the gas phase or the polymer surface [25].

To investigate the interaction of recombiners with products of cable fires, a set of catalyst samples has been introduced to the atmosphere of cable fires tests performed at IRSN. Later, surface analysis has been performed at Julich, Germany [26].

The cable fire tests were performed at the DIVA facility, a large-scale multi-room facility including four compartments and a corridor. The configuration used for the test consists of two interconnecting rooms with a volume of 120 m^3 each. A set of catalyst sample sheets with a size of 5 x 5 cm^2 has been introduced to both DIVA tests. The catalyst samples were exposed to a maximum temperature of approximately 400°C for a duration of 500 s in CFS-1 and to 280°C for a duration of 800 s in CFS-2. Two reignitions of unburnt gases (e.g. pyrolysis gases accumulated under the ceiling) were observed that led to short-term significantly higher thermal loads.

The surface analysis performed were: Scanning Electron Microscopy (SEM) for identification of catalyst damages; X-ray Fluorescence Spectroscopy (XRF) for semi-quantitative element screening and Ion Chromatography (IC) and Inductively Coupled Plasma Atomic Emission Spectroscopy (ICP-AES) for quantification of inorganic deposition. Catalyst samples showed significant higher amount of chlorine (Cl, constituent of PVC), and zinc (Zn) as well as a new amount of antimony (Sb, flame retardant) and significant carbon signal.

A performance test was also carried out at the REKO-1 platform to identify possible impact of the soot deposition on the start-up behaviour and conversion efficiency of the catalyst samples. A delay time on the start-up was identified due to the impact of the soot contamination. However, all catalyst sheets achieved very similar steady-state conversion efficiencies. For illustration, Figure 12 shows the measurement of the hydrogen content after the catalytic reaction is initiated.

The results demonstrated the adverse effect of cable fire products on the efficiency of hydrogen conversion in a PAR. The study concluded that all catalyst samples from the cable fire tests start with significant delay. The influence of cable fires products was not subject of this research and it still needs to be investigated since humidity due to its possible corrosive impact on the catalyst and since humidity is likely to play an important role for the nature of the soot deposition due to blockage effects.

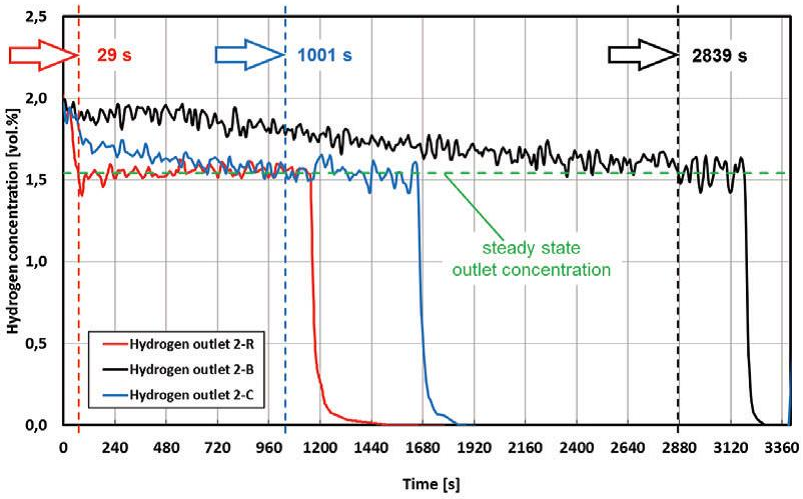

Figure 12: Hydrogen content measurements after start of the catalytic reaction (t=0 s) for type 2 samples from cable fire test CFS-1 [26].

2.5.7. Outcomes and remaining open issues

Even though catalyst poisoning has already been investigated by manufacturers and R&D organizations, there are still open issues regarding the subject.

It is known that carbon monoxide can lead to catalyst poisoning. The deactivation by carbon monoxide has already been investigated. However, some conditions still need to be further analysed, such as the recombiner operation when there is CO at lower temperatures and also O_2 starvation. Also, CO might react differently in Pt and Pd catalyst. The comparison between the two types of catalyst still needs to be performed.

Cable fire products might be a threat to the operation of the recombiner. The substances formed by the cables burning might block the catalyst surface and lead to the deactivation. There is not enough research available on this subject and it needs to be further investigated in order to determine the effect of cable fires in recombiners.

Oil projections have been found on catalyst surface on recombiners in French NPPs. It is important to determine if the presence of oil on the catalyst might lead to the deactivation and how it can impact the behaviour of recombiners.

Poisoning by fission products and aerosols might lead to catalyst deactivation as well. Deposition of aerosol on catalytic plates might take place during exposure to iodine, thus blocking active catalytic surface. It has been found that palladium and platinum behave differently when in presence of iodine.

3. EXPERIMENTAL MATERIALS AND METHODS

This chapter gives an overview of the facilities of the REKO platform at Forschungszentrum Jülich, Germany which were used in order to achieve the thesis objectives. The methodology used to obtain the results is also described.

The REKO facilities allow to study the behaviour of recombiners under different conditions. The experimental program includes experiments under well-defined forced flow conditions and natural flow conditions. REKO-1 has been used to analyse and characterize the poisoning by carbon monoxide on single catalyst samples, while REKO-3 has been used to characterize the poisoning effect using full size catalyst samples. REKO-Fire allowed to analyse the behaviour of single catalyst samples when exposed to combustion products of cable fires. Finally, REKO-4 was used to investigate the impact of oil on the start-up of the hydrogen recombination. Experiments have been performed with single Pt, Pd and Pt/Pd catalyst samples with 5x5 cm^2, as shown in Figure 13. For full scale experiments, the catalyst geometries have been 15x15 cm^2, being Pt catalyst. The generic catalysts are similar to the catalysts used in commercial recombiners. They which have been manufactured by company Chemical Consulting Dornseiffer. The supporting material is a thin sheet of stainless steel with a thickness of 50 µm. The ceramic washcoat consists of 4 mg/cm^2 γ-Al_2O_3. The amount of catalytic active material (platinum or palladium) is 1 mg/cm^2.

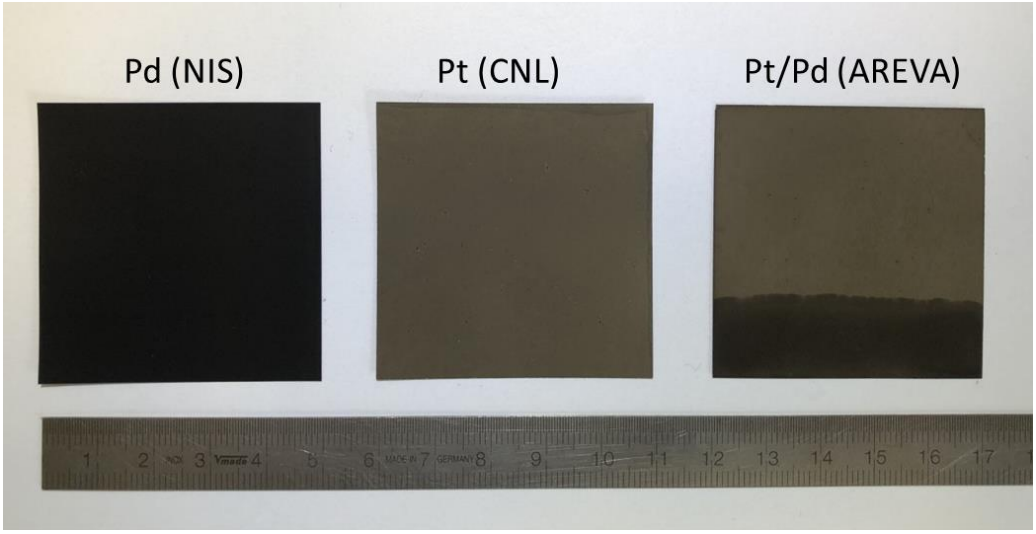

Figure 13: Catalyst samples (5x5 cm^2) – Pt, Pd and Pt/Pd

3.1. REKO-1

The REKO-1 facility has been designed to study the reaction kinetics of the catalytic hydrogen recombination process and to investigate the operational behaviour of catalyst elements under several boundary conditions [26]. It is a modular flow tube reactor which is composed of different tube elements according to the test specifications and requirements. The facility allows investigation of the recombination behavior of one catalyst sample under well-defined and steady-state forced flow boundary conditions.

The small-scale facility consists of a vertical flow channel with an inner diameter of 40 mm. The gas mixture is injected at the bottom inlet and flows to the top outlet. The gas can be composed of different components provided by means of mass flow controllers (MFC). A steam generator provides a continuous steady flow controlled by the electrical power of the heating elements. In this configuration, a catalyst element is exposed to a well-defined gas mixture under controlled flow conditions.

The inlet gas composition is fixed and calculated by the MFCs' real value signals. Part of the outlet gas is conducted through a heated line to the external analysers in order to determine its composition. The outlet gas composition is determined by means of hydrogen (heat conductivity) and oxygen (paramagnetic) analysers. Thermocouples installed in different positions allow the gas temperature measurement. The catalyst temperature is measured by pyrometer through the optical access provided by a glass window. The catalyst sample holder is located in the middle of the flow channel between two heated sections. The optical temperature measurement is limited to temperatures between 70°C and 550°C due to the range of measurement of the pyrometer. The pyrometer accuracy is within 1% of the maximum value. However, many parameters such as the uncertainty of the surface emissivity, the transmissivity of the glass, the adsorption in water vapour should be considered. In this study, it is considered that the pyrometer has a similar accuracy as the thermocouple type K, used for the calibration.

Gas supply

The role of the gas supply is to provide a steady-state volumetric gas flow with constant gas composition and temperature. The gas supply allows the preconditioning of a mixture of different gas species, including air, hydrogen, nitrogen, water vapor and carbon monoxide. The gas components are fed into the system by means of mass flow controllers (MFCs), enabling to

control the volumetric flow rate and the gas mixture. A steam generator provides up to 10 L/h of water vapor. Several gas pre-heaters allow controlling the gas mixture inlet temperature.

Mass flow controllers

The gas mixture is controlled by a set of mass flow controllers (FRC). In the present set-up, the following controllers are used:

- Air
  - FRC 3.02: 10 n-m³/h
  - FRC 3.03: 6 n-m³/h
  - FRC 3.04: 10 n-m³/h
- Nitrogen
  - FRC 3.06: 25 n-m³/h
- Hydrogen
  - FRC 3.05: 0.5 n-m³/h or 2 n-m³/h
- Carbon monoxide
  - FRC 3.07: 0.5 n-m³/h

As specified by the manufacturer, the measurement uncertainty for all mass flow controllers amounts to ≤ +/- 1 % of the measurement range.

Steam generator

Steam is provided by an ATHMOS-RS5 direct steam generator (company ADROP Feuchtemesstechnik GmbH) with a maximum capacity of 10 L/h (liquid water). The water flow is controlled by a Coriolis flow meter with a typical measurement uncertainty of +/- 0.15 % of the measurement range.

The REKO-1 facility, Figure 14, allows to investigate the behavior of a single catalyst sample. Three different types of 5x5 cm² catalyst have been used: platinum, palladium and platinum based with a palladium strip at the bottom. This set of experiments allowed understanding the conditions that lead to poisoning.

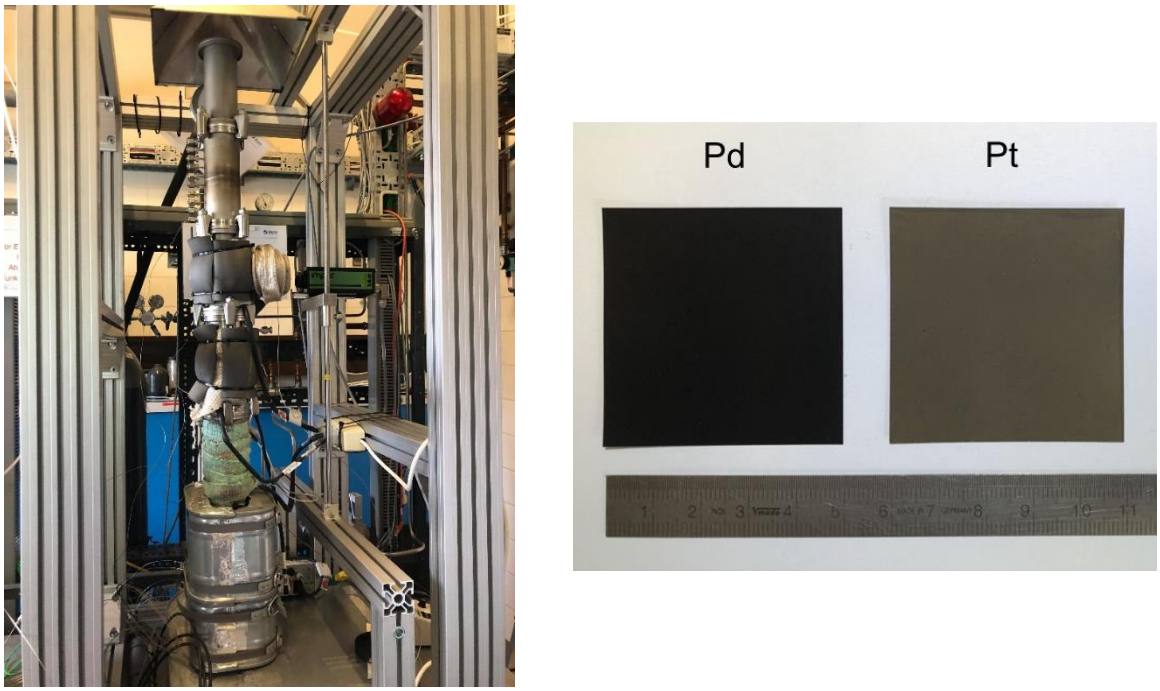

Figure 14: REKO-1 facility (left) and catalyst used in the tests (right).

Experimental procedure

The test matrix for the experiments has been defined based on the conditions of a severe accident scenario, shown in Table 5. The hydrogen fraction varies from 1 to 7 vol.%, carbon monoxide fraction from 0.5 to 6 vol.%, the oxygen fraction is reduced to up to 0.7 vol.%. The experiments have been performed at atmospheric pressure and three initial gas temperatures: 20°C, 80°C and 150°C.

Table 5: Relevant conditions during severe accident late phases scenarios.

	Lower concentration	Higher concentration
Hydrogen	0.26 %	8 %
Oxygen	1.2 %	6 %
Carbon Monoxide	3.5 %	6 %
Temperature	350 K	420 K
pressure	1.2 bar	6.6 bar

A typical test sequence consists of the continuous injection of hydrogen into the reaction channel, followed by the continuous injection of carbon monoxide. After achieving steady-state conditions, the oxygen content is stepwise reduced by increasing the nitrogen fraction of the

air/nitrogen mixture until the catalyst is deactivated. The temperature of the catalyst is measured with a pyrometer indicating when the exothermic reaction occurs.

Pyrometer calibration

The pyrometer has been calibrated before the experiments in order to achieve accurate measurements. For this purpose, a thermocouple has been coupled to a catalyst sample at the same spot where the pyrometer measurement was obtained. Hydrogen was injected in the tube to achieve elevated catalyst temperatures. The emissivity of the pyrometer was adjusted to obtain the same temperature measurement as indicated by the thermocouple. This procedure was performed for both catalyst types and with and without steam. The emissivity used for the platinum catalyst was 60% (dry conditions), while for the palladium was 54%. Figure 15 shows the agreement of temperatures for each emissivity value obtained for the Pt catalyst.

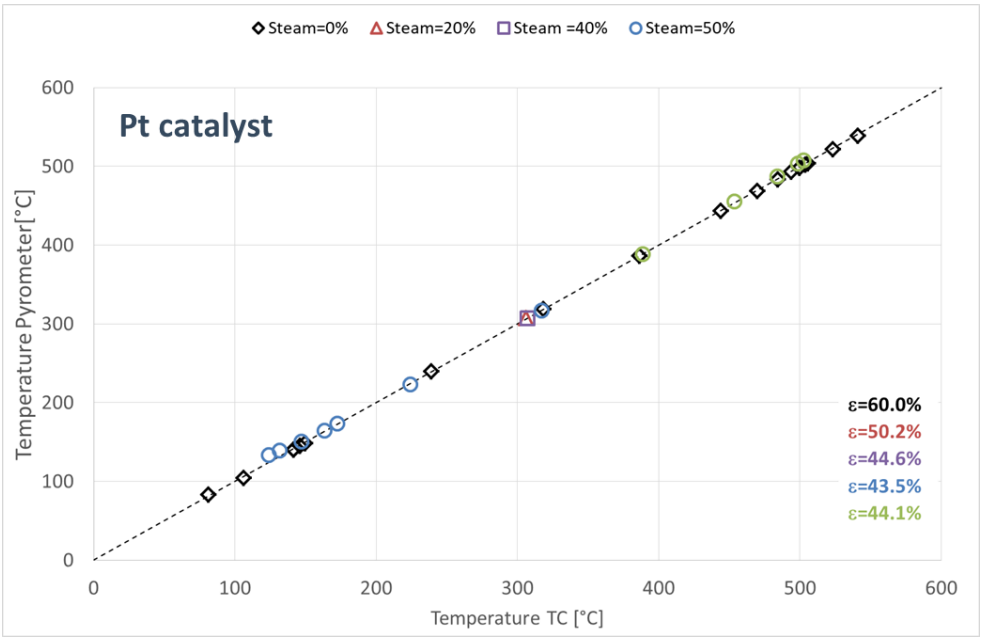

Figure 15: Catalyst temperature measured with the pyrometer versus the catalyst temperature measured with the thermocouple for different emissivities for pyrometer calibration.

Once the emissivity was calibrated, the temperature was measured with the pyrometer in different positions of the catalyst to show the temperature profile, Figure 16. The square indicates the area of the catalyst surface that is available for temperature measurements. For a mixture with hydrogen and carbon monoxide, the temperature is higher than when only

hydrogen is injected. The catalyst temperature corresponds with the recombination rate. The diagram also demonstrates that the temperature at the lower end of the catalyst is higher according to the laws of diffusion-controlled reaction kinetics.

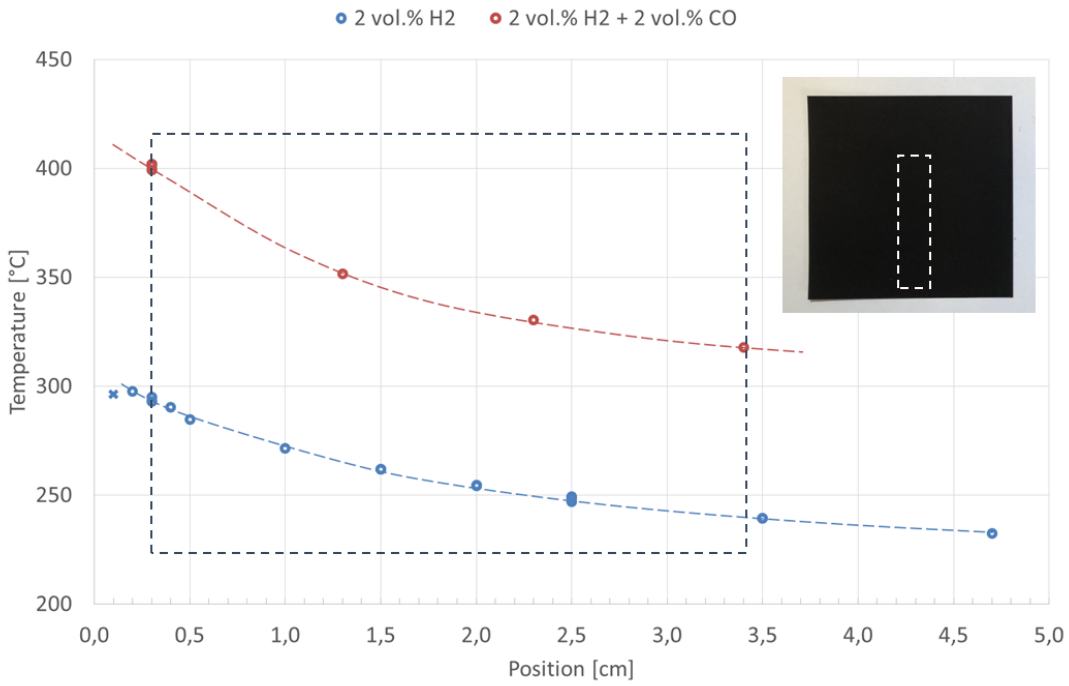

Figure 16: Catalyst surface temperature along catalyst height for mixture of 2 vol.% H_2 (blue) and mixture of 2 vol.% H_2 and 2 vol.% CO (red).

Reference tests without carbon monoxide

In order to prepare for the poisoning tests, the catalyst has been studied under several conditions. Reference experiments have been performed without carbon monoxide to investigate the effect of the hydrogen fraction, the gas temperature, the flow velocity, steam, oxygen fraction and oxygen starvation.

Figure 17 show how the catalyst temperature varies for different hydrogen fractions for a gas mixture at ambient temperature and at 0.5 m/s. It is possible to see that the higher is the hydrogen content, the higher is the catalyst temperature.

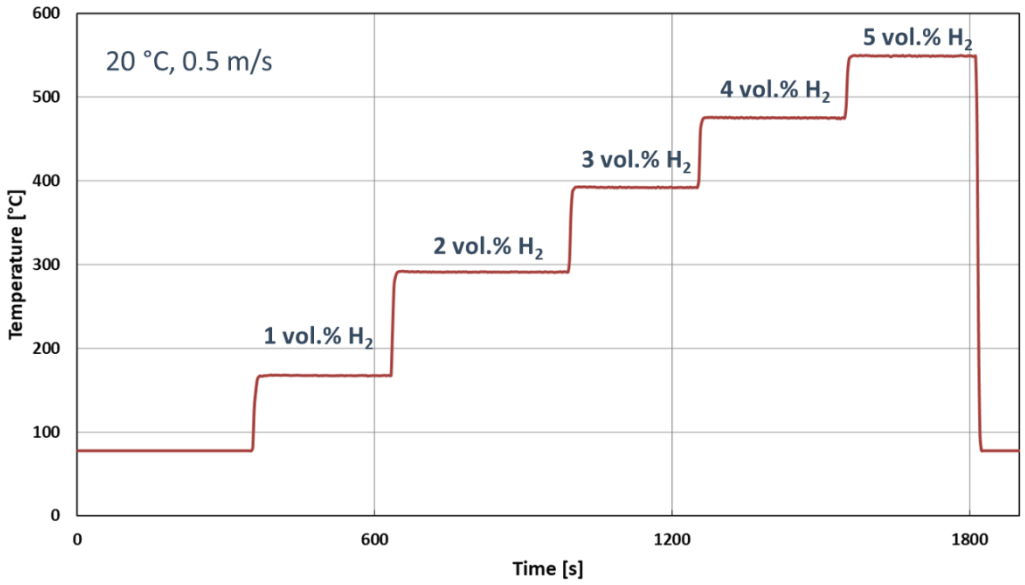

Figure 17: Evolution of the temperature over time when hydrogen fraction is increased from 1 vol.% H_2 to 5 vol.% H_2.

Figure 18 represents the effect of the initial gas temperature on the catalyst behavior. The tests have been performed for gas mixtures initial temperatures fixed at 20°C, 80°C and 150°C, with 0.5 m/s flow velocity.

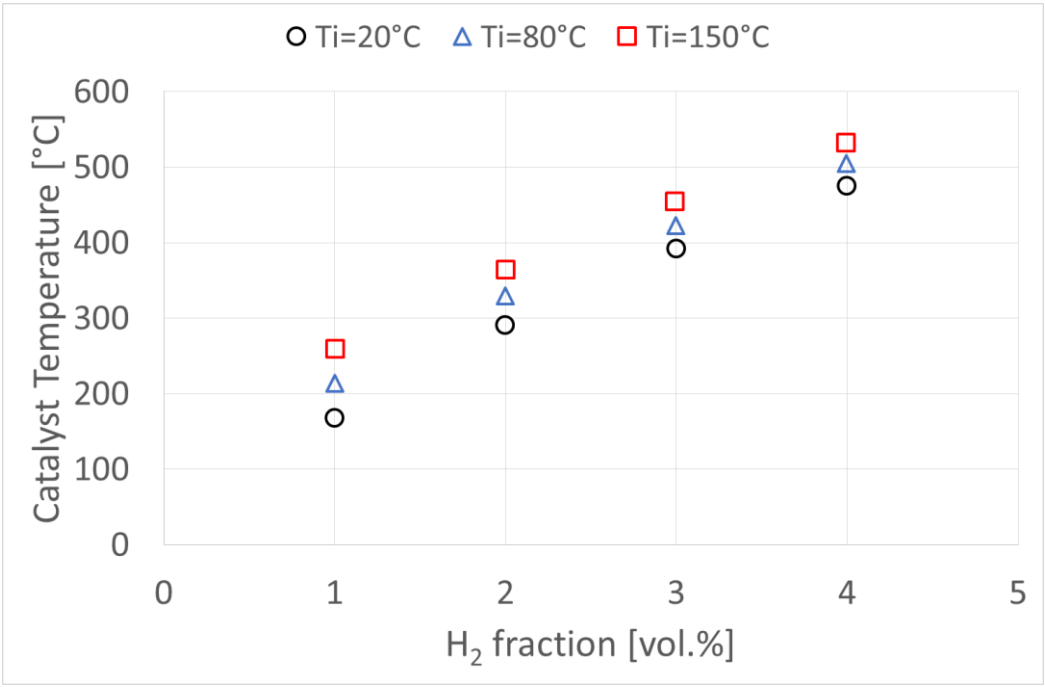

Figure 18: Catalyst temperature at different hydrogen molar percent for three initial gas temperatures: 20°C, 80°C and 150 °C.

The effect of the flow velocity at ambient temperature is shown in Figure 19. The experimental data reveals the small difference in the catalyst temperature for different flow velocities (0.5 and 1.0 m/s).

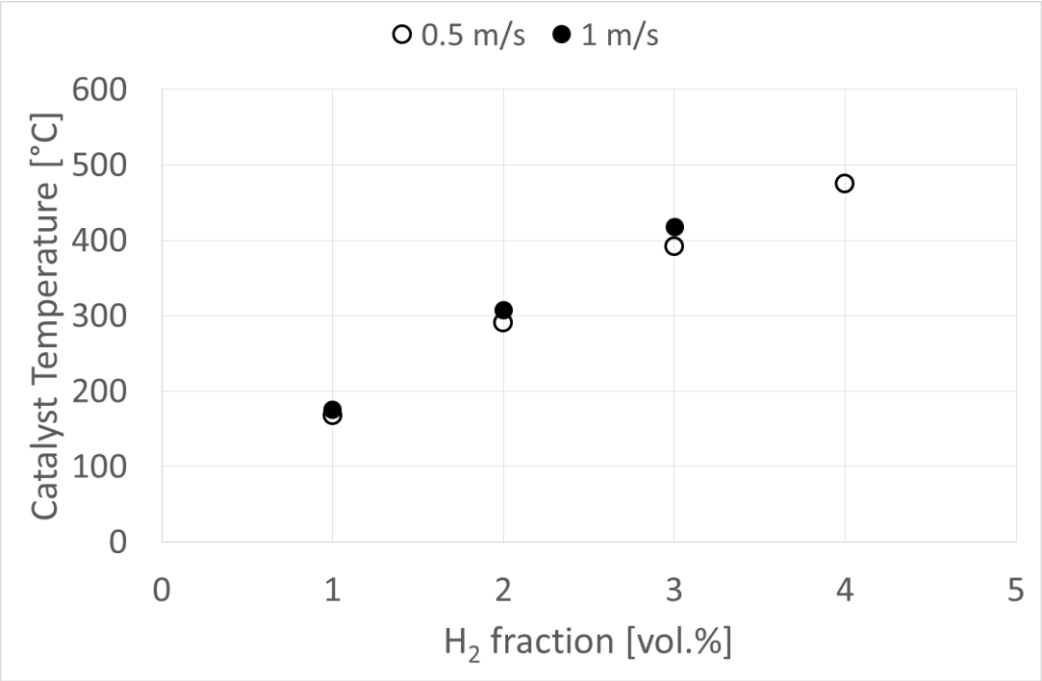

Figure 19: Catalyst temperature at different hydrogen content for two flow velocities.

The catalyst behavior under the presence of steam has also been investigated. Figure 20 shows the catalyst temperature for tests performed with dry conditions and with 100% relative humidity. In this case, there was no significant difference observed.

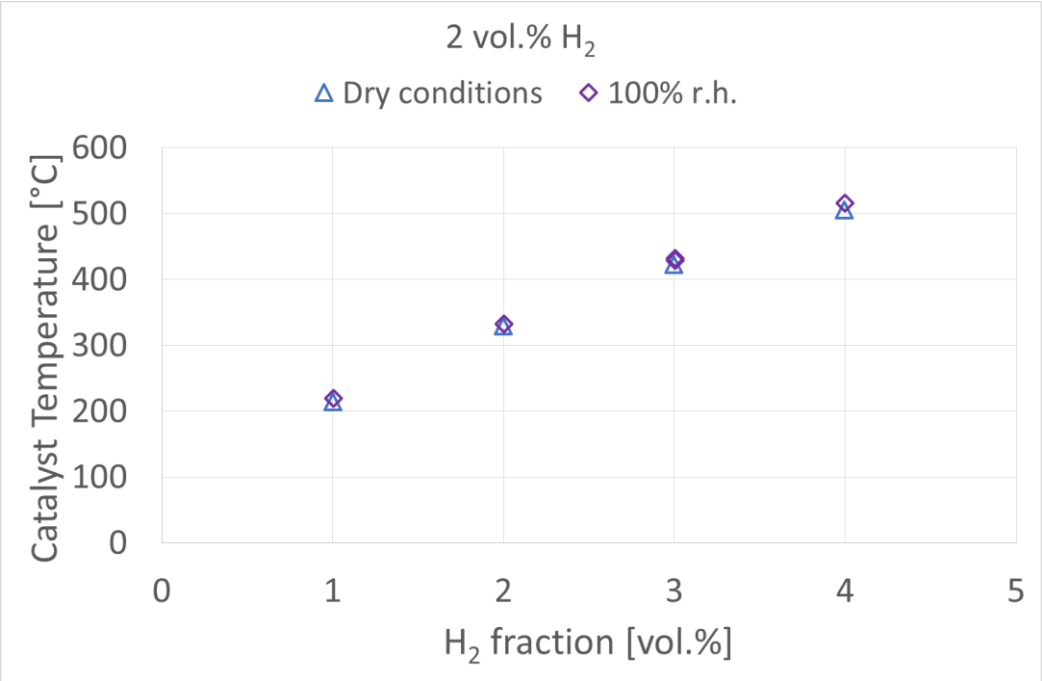

Figure 20: Catalyst temperature at different hydrogen content for dry test and test with steam.

The oxygen starvation was analyzed for several hydrogen fractions. Figure 21 shows that once the oxygen content is below a certain value, the temperature will decrease with the oxygen. In oxygen starvation regime, the recombination rate depends linearly with the oxygen fraction.

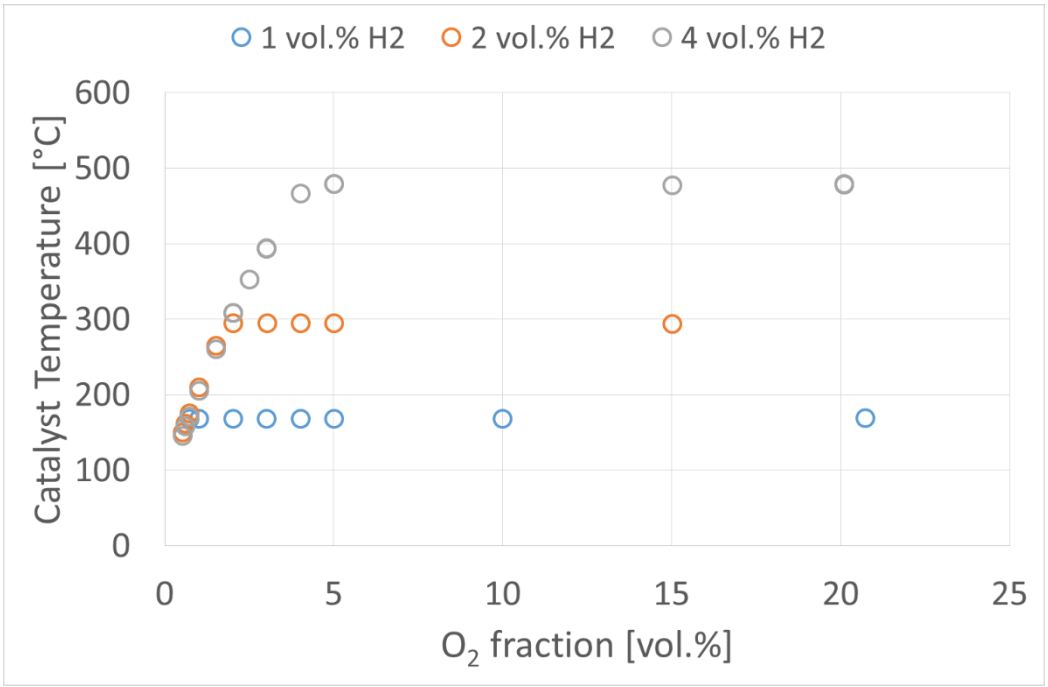

Figure 21: Evolution of the catalyst temperature versus the O_2 content at different H_2 content.

3.2. REKO-3

The REKO-3 facility, in Figure 22, allows small scale tests in order to study the effects of different parameters on the characteristics of catalyst plates inside a vertical flow channel. It is an adaptation of the REKO-1 facility, with different geometry. The catalyst sheets are placed in a parallel arrangement forming vertical rectangular channels. The set-up is a representation of a box-type recombiner section of AREVA design. The rectangular stainless-steel flow channel has a cross-sectional area of 46 mm × 146 mm.

Gas mixtures, consisting of hydrogen, air, nitrogen, carbon monoxide and steam, are supplied by mass flow controllers. A gas analyser with condensate separator allows to determine the gas composition after catalyst reaction so it is possible to calculate the reaction rates of each species. The measuring cells are based on different measuring principles: paramagnetic sensor (O_2), heat conductivity sensor (H_2), infrared sensor (CO/CO_2).

For gas temperature measurements, TCs are placed in the inlet and in the outlet section. A pyrometer allows measuring the temperature of the catalyst surface through a glass window.

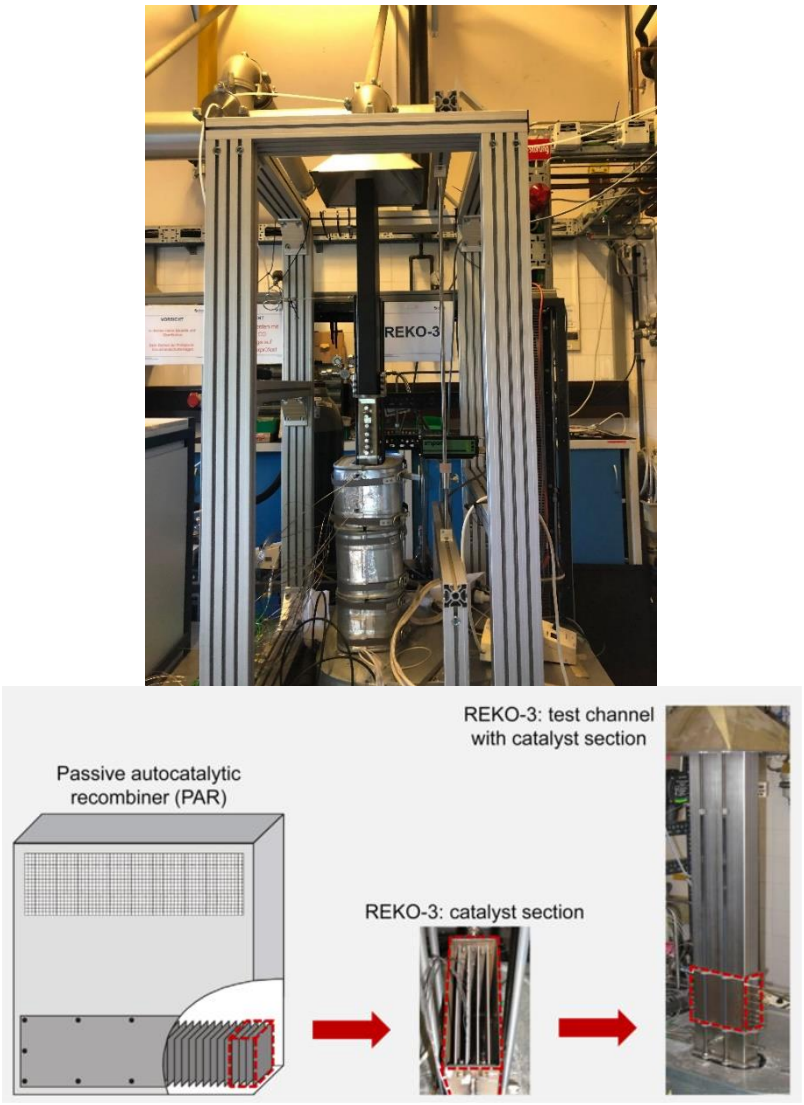

Figure 22: The REKO-3 facility

Experimental procedure

For the experiments in the REKO-3 facility, four catalyst samples, with dimensions of 14.3 x 14.3 cm², have been placed inside the rectangular channel. The preparation of the facility was similar to the preparation of REKO-1. The pyrometer was calibrated with the same procedure already described. However, modifications have been made to obtain more accurate data. The experiments have been performed with a platinum catalyst only.

The catalyst temperature was measured in different positions of the catalyst sheet to obtain the temperature profile for several hydrogen fractions, shown in Figure 23. The temperatures are higher for higher hydrogen contents. Also, the bottom of the catalyst present higher temperatures compared to the top.

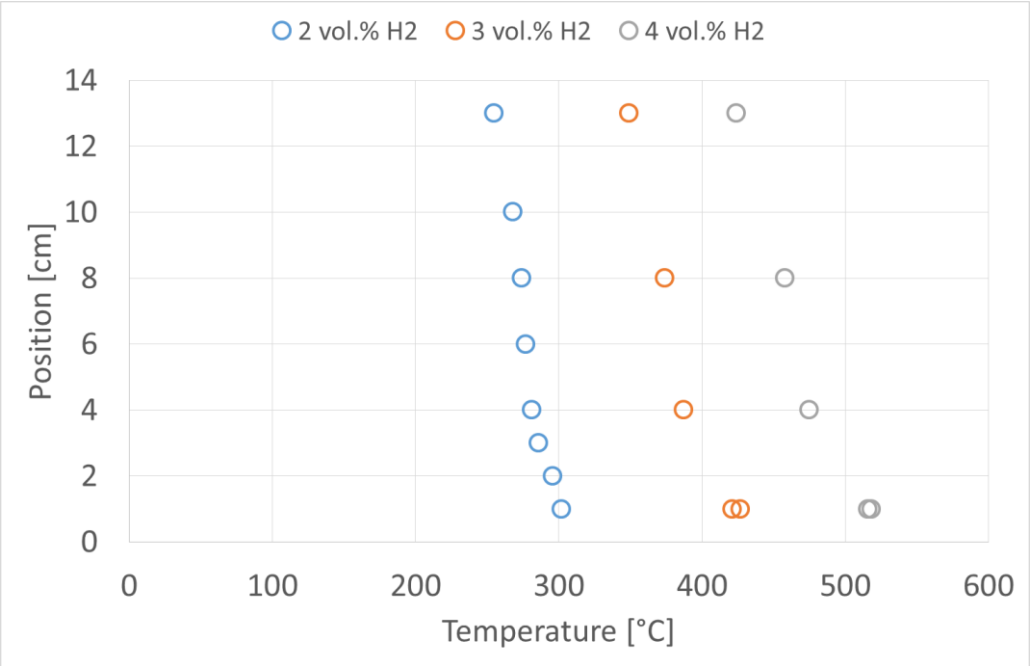

Figure 23: Catalyst height versus catalyst temperature for mixtures of 2 vol.% H_2, 3 vol.% H_2 and 4 vol.% H_2.

The temperature profile was measured for different oxygen content to show how the oxygen starvation occurs, Figure 24. The measurements were performed for a gas mixture with 3 vol.% hydrogen and at 20°C. The temperature profile for 21 vol.% O_2 is represented by the red circles. Then, the oxygen fraction was decreased to 3.5 vol.% O_2, shown by the blue circles, oxygen starvation is first observed at the bottom edge of the catalyst. For this oxygen fraction, the temperature profiles are similar to the ones mentioned before, but the temperature is slightly lower at the bottom. Once the oxygen fraction is decreased to 3 vol.%, the oxygen starvation effect becomes more visible. The temperature decreases along the entire profile. However, the effect is stronger at the bottom, showing that the oxygen starvation also starts at the lower bottom edge of the catalyst. For 2 vol.% O_2, green circles, and 0.8 vol.% O_2, black circles, the temperature profile becomes a flat vertical profile. This behaviour indicates that when oxygen starvation occurs, the discrepancy in the catalyst temperature along the catalyst surface is not significant.

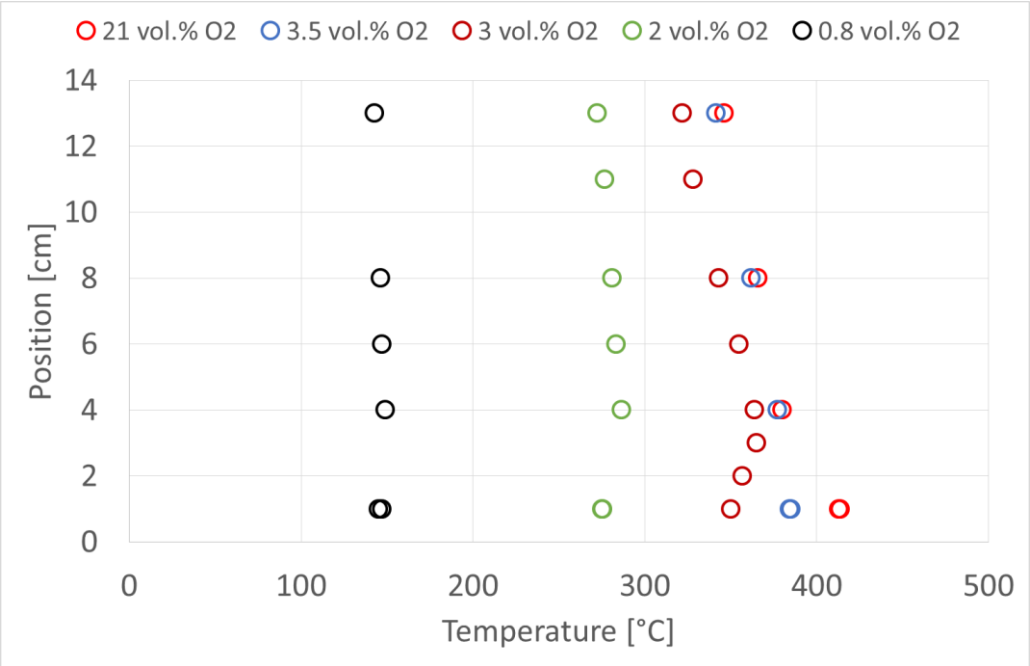

Figure 24: Catalyst height versus catalyst temperature for mixture of 3 vol.% H_2 and oxygen reduction from 21 vol.% O_2 to 0.8 vol.% O_2.

The temperatures profiles obtained helped to define the points of interest for temperature measurement. The catalyst placed close to the glass window was placed in order to reduce heat losses to the wall. Small holes were made in four points along the catalyst sample, so it is possible to measure the temperature of the second catalyst. The modified catalyst is showed in Figure 25 on the left and on the right the channel where the catalysts are placed.

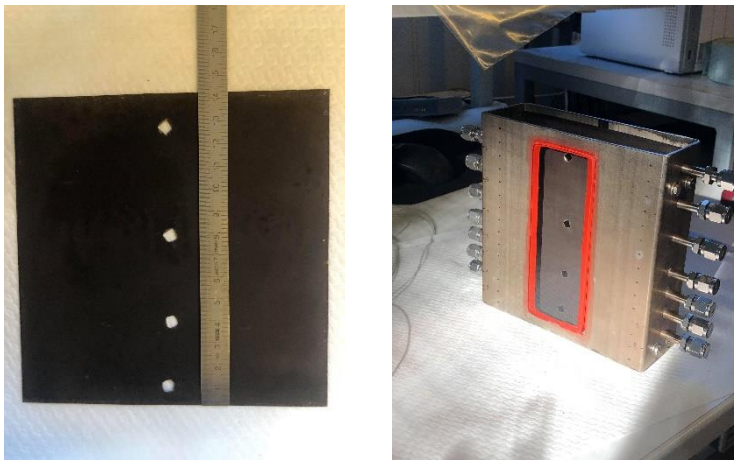

Figure 25: Modified catalyst sample (left) and catalysts placed inside channel with glass window (right).

Once the catalyst has been modified, the temperatures profiles for different hydrogen fractions without carbon monoxide have been measured. Figure 26 shows the temperature profiles for the conditions presented in Table 6. For the case where the hydrogen fraction is 4 vol.%, the temperature at the two lowest points was not measured since the values were higher than 550°C, the upper limit of the pyrometer.

Table 6: Test matrix for REKO-3 reference experiments.

Inlet H_2 fraction [vol.%]	Flow velocity [m/s]
1.0	0.85
2.0	1.00
3.0	1.10
4.0	1.10

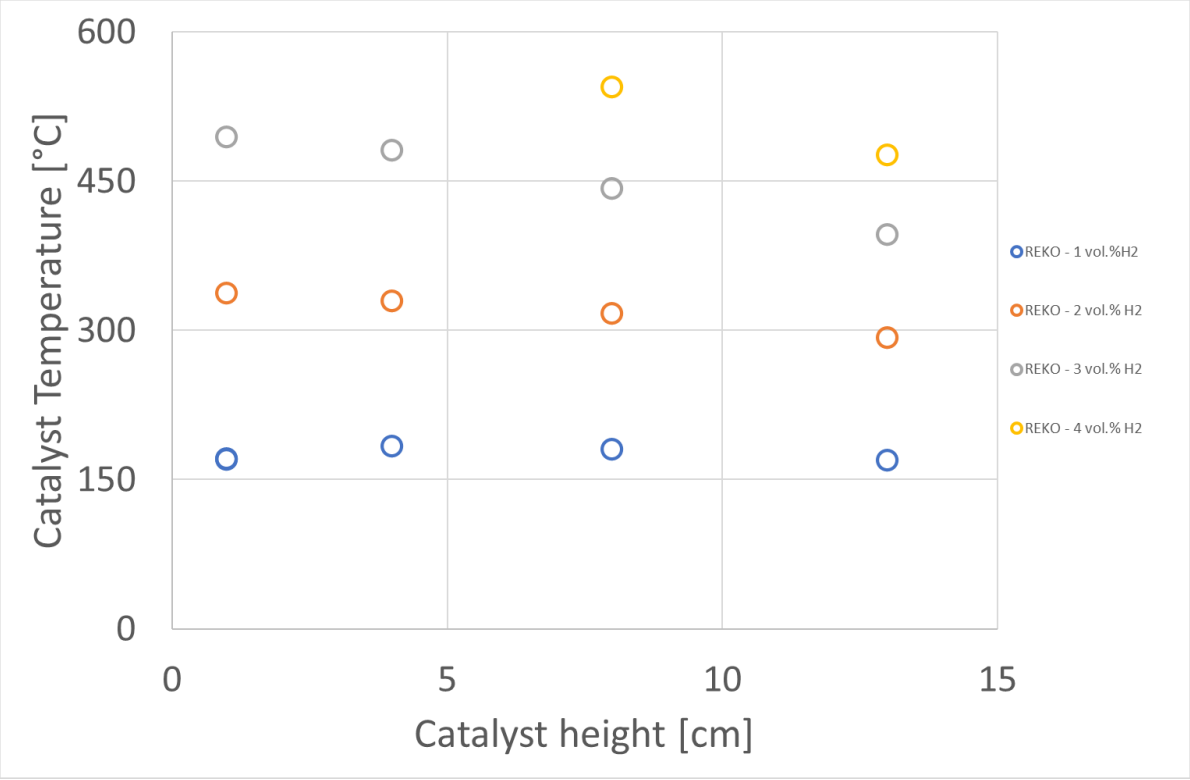

Figure 26: Catalyst surface temperature along catalyst height for different H_2 content.

The temperature profile under oxygen starvation for a mixture with 3 vol.% H_2 and no carbon monoxide was also measured. Figure 27 shows a similar temperature profile for 21, 5 and 4

vol.% O_2, where the temperature is higher at the bottom of the catalyst. When the oxygen fraction reaches 3 vol.%, it is possible to see the impact of the oxygen reduction since the temperature at the lower edge of the catalyst starts to decrease. For 2 vol.% O_2, the temperature is lower, indicating that less hydrogen is being recombined.

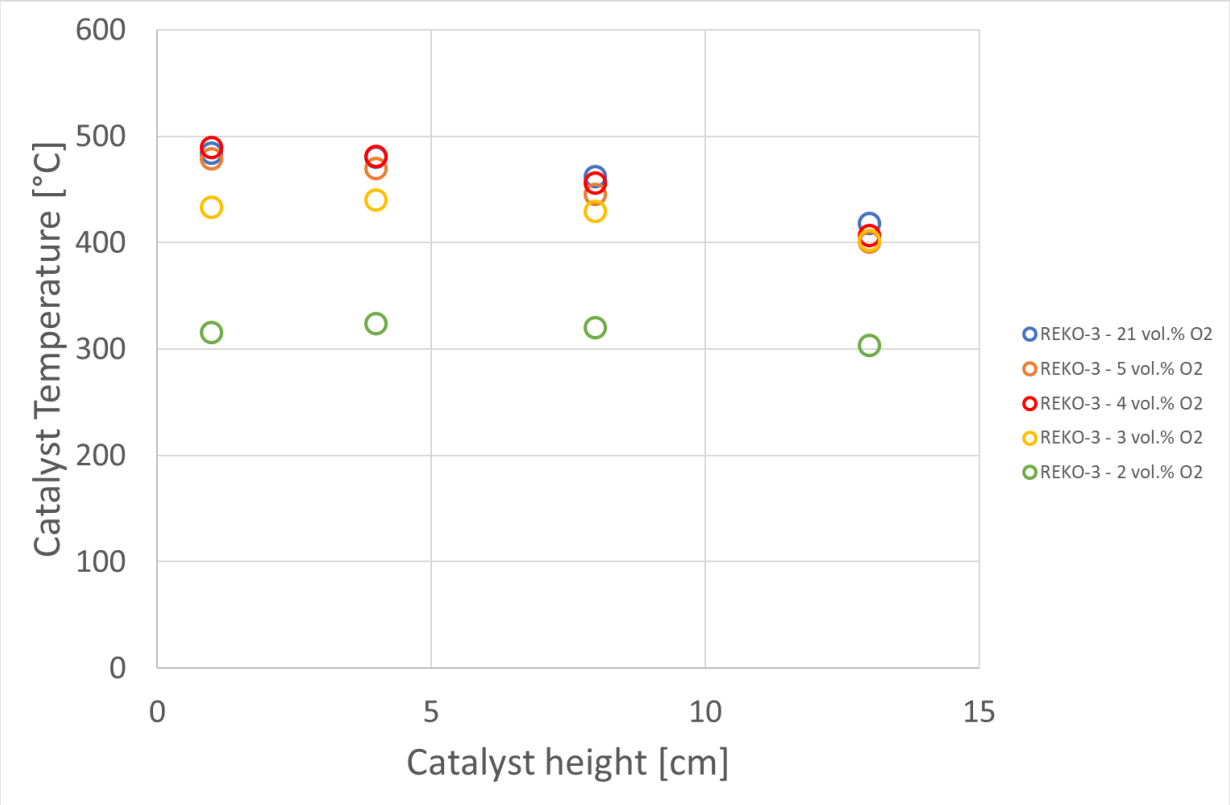

Figure 27: Catalyst surface temperature along catalyst height for mixtures of 3 vol.% H_2 and O_2 reduction.

The experiment test procedure was similar to the one performed in REKO-1.

3.3. REKO-4

The REKO-4 facility has been designed to study recombiners under natural flow conditions. The cylindrical steel pressure vessel has a free volume of 5.45 m³ (1.4 m diameter, 3.7 m height), including wall heating and outer insulation. The vessel is designed to perform experiments with flammable hydrogen/air mixtures up to 2.0 bar operational pressure at 280°C. The vessel is equipped with 32 flanges and a manhole with a diameter of approx. 60 cm (allows the accessibility of the vessel)

The vessel used to perform experiments with hydrogen-air mixtures can resist hydrogen explosions. However, the vessel is designed for controlled hydrogen-oxygen reaction at the catalytic surfaces of the recombiner, not for regular explosions.

The instrumentation of the vessel allows the analysis of the recombiner and its interaction with the vessel atmosphere. Gases (hydrogen, air, nitrogen) are injected in radial direction into the vessel at an elevation of approx. 20 cm above the bottom grid by means of mass flow controllers. Water vapor is provided by a mobile steam generator. The vessel is equipped with thermocouples for gas temperature measurements at different elevations as indicated in Figure 28. To determine the pressure inside the vessel, relative and absolute pressure sensors are applied. The determination of starting conditions and the development of the gas composition during the experiment is possible due to humidity, hydrogen and oxygen sensors.

Gases are injected via mass flow controllers. In the present set-up, a mass flow controller with a maximum flow rate of 2 n-m³/h has been used for hydrogen injection (FRC 4.01). For controlled air injection, a mass flow controller with a maximum flow rate of 6 n-m³/h (FRC 4.02) has been used.

As specified by the manufacturer, the measurement uncertainty for the mass flow controllers amounts to ≤ +/- 1 % of the measurement range.

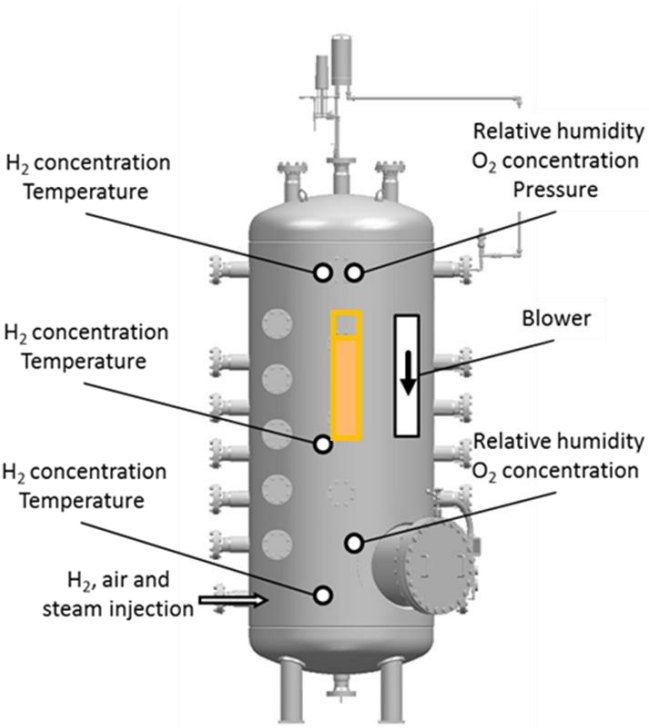

Figure 28: The REKO-4 facility

The experiments have been performed in the REKO-4 facility using a 5 x 5 cm² platinum-based catalyst with a palladium strip at the bottom in order to investigate the impact of oil. Different percentages of oil coverage have been tested. The oil used is the MOBIL DTE 746 grade 46 oil, the same used in the primary pumps in NPP. The oil properties are shown in Table 7. The oil has been placed so that it was possible to investigate the behaviour of the catalyst under different conditions and percentages of oil coverage. The experiment allows to understand how the oil affects the recombiner, whether it will delay the recombination start-up and whether it is possible to have the catalyst at full operation after being covered by oil.

Table 7: MOBIL DTE 746 grade 46 oil properties.

Property	**Oil Mobil DTE 746**
Grade	ISO 46
Density @ 15 C, g/cm3, ASTM D1298	0.86
Flash point, Cleveland Open Cup, °C, ASTM D92	230
Kinematic viscosity @ 40°C, mm^2/s, ASTM D445	44
Kinematic viscosity @ 100°C, mm^2/s, ASTM D445	6.8

The catalyst holder with three catalyst samples has been placed inside a rectangular box to simulate the chimney effect, both shown in Figure 29. The small size recombiner has been positioned on the top middle in REKO-4. Thermocouples have been positioned at the bottom of the facility, at the bottom of the recombiner, inside the recombiner and at the top of the recombiner. Hydrogen sensors have also been placed in strategic positions, including the bottom and the top of the recombiner.

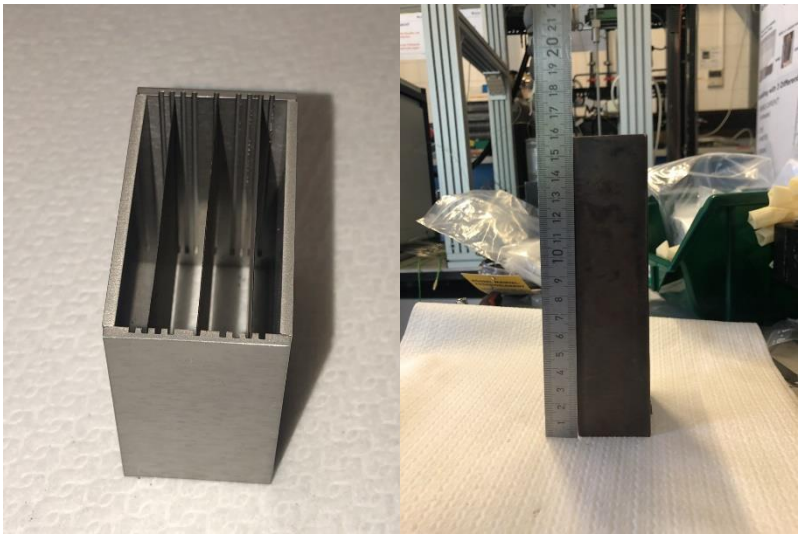

Figure 29: Catalyst holder with the polluted catalyst samples and small recombiner box.

The thermocouples inside and at the top of the recombiner indicates if the hydrogen is being converted by an increase in the temperature. The hydrogen sensors allow to observe the recombination rate once the injection has stopped. The hydrogen sensors at the recombiner outlet allow determining when the conversion of the hydrogen starts.

The oil has been deposited directly on the catalyst sample with a pipette. First, a test with three catalyst samples without oil deposition has been performed for reference data. Then different oil coverages have been tested. One test with the entire three catalyst 100% covered with a thin film of oil has been performed to represent the worst scenario. Later, experiments in which only one of the three catalysts was covered with oil have been carried out. The same amount of oil has been applied to the catalysts in the experiments.

3.4. REKO-Fire

The newly built REKO-Fire facility, shown in Figure 30, combines a flow tube reactor for catalyst investigation with a steady-state tube furnace for the constant generation of cable fire products at varying combustion conditions. The facility was designed in order to allow simultaneous exposure of the catalyst to cable fire products and to hydrogen/air mixtures. That was, it is possible to better quantify the influence of gaseous and particulate components on the catalysts' behavior. The installation has been used to study the effect of combustion products generated from flame-retardant power cables under three different fire conditions on the start-up behavior of three types of catalyst for hydrogen recombination.

Figure 30: REKO-Fire facility

The flow chart of REKO-Fire is shown in Figure 31. The facility consists of vertical cylindrical reaction tube (1), where the catalyst is placed, connected with 3 feed lines: cable fire product generator (2), hydrogen/air mixture and steam generator (3), and dilution air (4). The outlet of the reaction tube is connected to the off-gas treatment system. The gas temperature is measured by means of thermocouples (TCs) installed at the inlet and the outlet of the reaction channel. Several heating elements allow heating the tube in order to reduce both heat losses and the deposition of fire products on the inner tube wall.

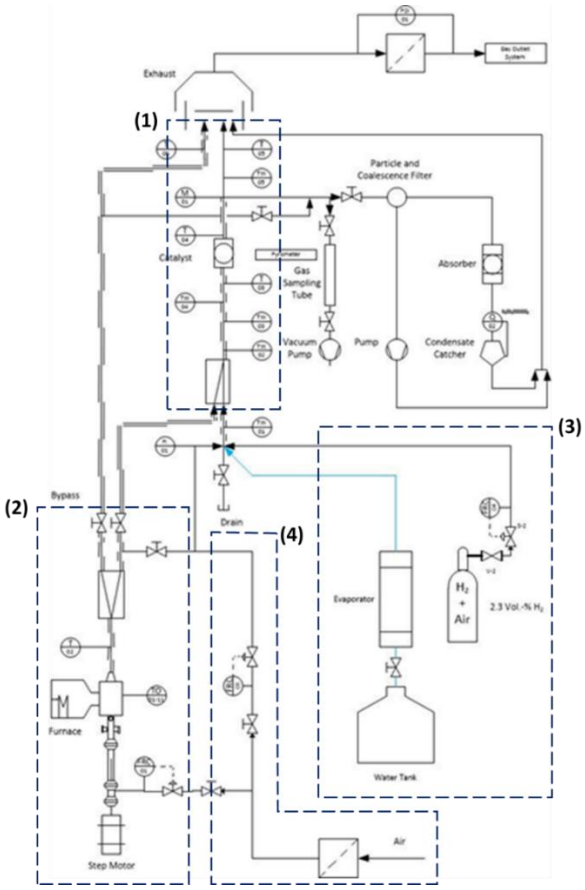

Figure 31: REKO-Fire facility flow chart

The reaction tube has an inner diameter of 6.7 cm. The gas temperature is measured by means of thermocouples installed at the inlet and the outlet of the tube. Heating elements are used to reduce heat losses and deposition of fire products on the inner tube wall. The 5x5 cm² catalyst sample is placed with a specific holder in the central position of the tube.

The concept of cable fire product generation system is based on the "steady state tube furnace" described in ISO/TC 19700. The system consists of a feed unit which continuously moves a quartz glass slide inside the tube furnace, and it is capable of burning cable samples under well-controlled and reproducible boundary conditions. The furnace by GERO Carbolite Company is operated at a constant internal temperature of between 30 and 3000°C. The sample cable is placed on a quartz glass sample tray, which is transported by a stepper motor coupled to a linear drive at a feed rate of approx. 10 mm/s through a quartz glass channel into the furnace. The glass channel is coupled to the reaction tube by means of a specifically manufactured coupling in order to minimize mechanical loads on the quartz glass. An Emerson gas analyzer system

continuously extracts a gas sample via a probe in the tube, which is then analyzed in four serially coupled measuring cells. The cells are available to determine oxygen, hydrogen, carbon monoxide and carbon dioxide concentrations. While the oxygen analyzer uses a paramagnetic sensor, the hydrogen content of the gas mixture is determined via an integrated thermal conductivity sensor. The combustion gases CO and CO2 are measured within the gas analyzer using infrared sensors. The accuracy of the gas analyzer used is specified by the manufacturer as 1% of the full-scale value of each gas.

Experimental procedure

Generally, cables consist of conductors, insulation, filling material and cable sheathing. The cables used in the experiments are of the type FRNC-BX 4 x 2.5 mm², a representative power cable for German Convoi-type NPPs, manufactured by company Prysmian Kabel und Systeme GmbH. To improve the continuity of the combustion process, the cable is pressed before being placed inside the carriage (Figure 32). Pressing is necessary to override the physical fire protection properties of the cable sheath by uniformly violating its integrity and to facilitate the insertion of the flexible cable into the straight sledge.

Figure 32: Flame retardant non-corrosive (FRNC) power cable sample (left), pressed cable sample (right).

This work focuses on cable fire products (CFPs) generated in well-ventilated combustion, under-ventilated combustion and oxidative pyrolysis. The catalyst samples used in this test series are thin sheets with a size of 5 x 5 cm². For each catalyst, two tests have been performed. In case of oxidative pyrolysis, each test has been repeated twice. Table 8 shows the test matrix with the basic boundary conditions.

Table 8: Test matrix for cable fire experiments.

Combustion condition	Catalyst	Primary air flow	Furnace temperature	Test
Well ventilated	Pt	20 l/min	680 °C	RF-A-02/07
	Pd	20 l/min	680 °C	RF-B-01/04
Under ventilated	Pt	4 l/min	680 °C	RF-A-05/08
	Pd	4 l/min	680 °C	RF-B-02/05
Oxidative pyrolysis	Pt	4 l/min	380 °C	RF-A-06/09/10
	Pd	4 l/min	380 °C	RF-B-03/06/07

A typical test sequence starts with the cable fire which is led into the bypass. After steady-state conditions are achieved, the CFPs are led through the reaction channel. Measurements indicate what happens

The different gas concentration measurements during bypass operation are given in Figure 33. For well-ventilated conditions, we observe the large portion of oxygen and a high CO_2/CO ratio. In the under-ventilated case, the off-gas contains almost no oxygen and a high CO_2/CO ratio. In the pyrolysis case, almost no CO_2/CO is produced and high oxygen concentration.

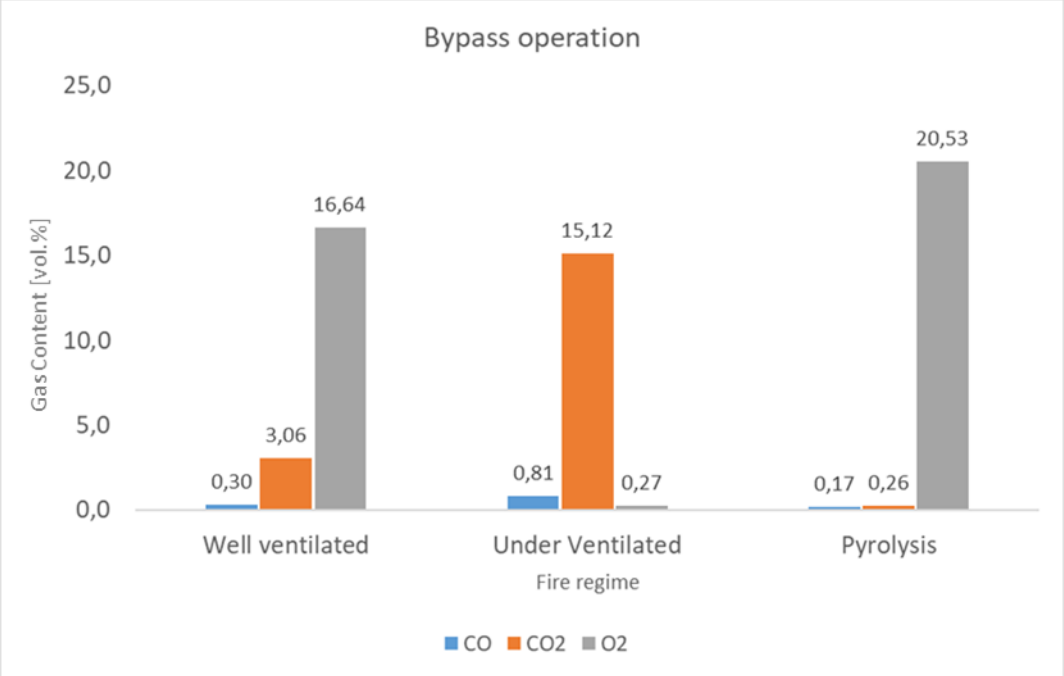

Figure 33: Outlet gas concentrations during bypass operation

3.5. Conclusion

This chapter presents the experimental platforms and the qualification tests results performed before addressing the poisoning effect investigation. First, the pyrometer was calibrated to assure a good measurement of the catalyst temperature. Then, experiments with H_2/air gas mixtures were performed to investigate the effect of different parameters on the behavior of the catalyst during normal operation. Tests were performed for gas mixtures at 20°C, 80°C and 150°C in order to analyze the impact of the initial gas temperature. The impact of the flow velocity was investigated. For flow velocities of 0.5 and 1.0 m/s, the experimental results reveal small difference in the catalyst temperature. Experiments performed with steam were compared to those under dry conditions and there was no significant difference observed in the catalyst temperature. The catalyst behavior was also analyzed under oxygen starvation conditions. The experimental data shows that the catalyst temperature decreases with the oxygen content below a certain value, indicating that the recombiner is less efficient for this case but hydrogen is still converted into steam. These results serve as a reference for the normal operation of the catalyst.

4. NUMERICAL TOOL

The SPARK (Simulation for Passive Autocatalytic Recombiners' risK) code is a CFD code dedicated to the numerical simulations of catalytic recombiners. The calculation tool, developed at IRSN, solves the two-dimensional steady-state Navier–Stokes equations in the vorticity-velocity formulation by including complex gas phase and surface chemistry, multicomponent transport and heat radiation.

The code allows the description of the thermochemistry and transport mechanisms governing the catalytic conversion of hydrogen and of carbon monoxide and to numerically predict the transition of the catalytic combustion regime (without flames) to the combustion in gas phase (with flames).

The detailed modelling makes possible to investigate and to predict the behaviour of recombiners during severe accidents and to evaluate the associated risks. The SPARK code had been used to study the ignition of hydrogen by recombiners for different gas mixtures, to investigate the interaction of recombiners with the carbon monoxide, to predict the performance of recombiners for various thermo-hydraulic conditions, and others applications that allow the evaluation of the recombiners behaviour [27]. In the following, the SPARK code is briefly described and the new model implemented to the investigate the poising experiments is presented.

4.1.1. Hypotheses

In order to justify the planar channel geometry with catalytic plates adopted in SPARK with regard to the real geometry of recombiners installed in French nuclear plants, some hypotheses have been made.

Flow symmetry

The effects on the boundary caused by the heat losses at the outside walls of the recombiner and by the channels next to them are neglected. This hypothesis allows considering a symmetric flow inside each vertical channel formed by the catalytic plates in the lower case of the recombiner.

Infinitely thin two-dimensional plates

The catalytic sheets are considered two-dimensional plates due to the relation between the depth of the plates (≈ 130 mm) and the width (≈ 10 mm) of the channel. The plates are also considered infinitely thin and it is justified by the relation between the thickness of the plates (≈ 0.1 mm) and the width of the channel. The last hypothesis permits to ignore the thermal conduction in the plates.

Laminar flow

Under normal operation conditions, the average gas flow speed between the catalytic plates is in the order of 1 to 2 m/s with Reynolds number Re_{4h} lower than 2500, so the flow can be considered as laminar.

Pseudo-stationary flow

The recombiners represent only a small volume of the containment as the dimensions of the recombiners are in the order of 1 m of width, 1 m of height and 20 cm of depth and the characteristic dimensions of a real containment are in the order of several tenths of meters in all directions. The stratification in the containment atmosphere is less perceptible for the scale of the recombiner since the inlet composition of the mixture changes slowly compared to kinetics of the recombiner. Moreover, the activation of the recombiners by natural convection indicates low inlet speed on the bottom and contributes to slow variations of the inlet conditions. These remarks lead to the assumption of a pseudo-stationary flow.

4.1.2. Numerical Domain

The numerical domain is a consequence of the box-type PAR geometry with a row of vertical catalytic sheets as show in Figure 34. Infinitely thin catalytic sheets are assumed in order to neglect possible horizontal solid heat conduction. Since external heat losses are not considered, the flow can be assumed to be symmetrical so the numerical domain is reduced to half channel between two catalytic sheets in the median plane of the recombiner.

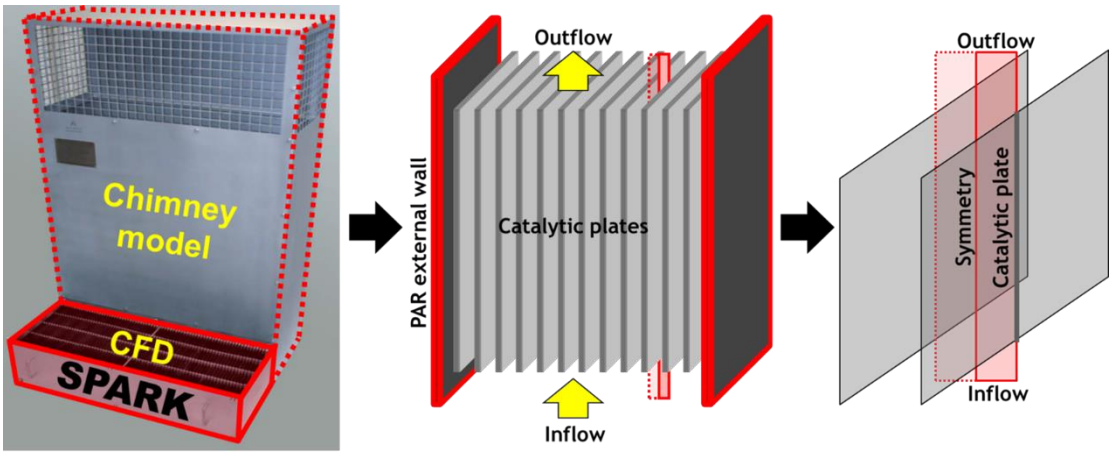

Figure 34: Recombiner configuration and numerical domain

4.1.3. Governing equations

The conservation equations in the gaseous phase are defined with the vorticity-velocity formulation. They result from multi-species reactive compressible flow equations in the limit of low Mach numbers:

$p = \bar{p} + \tilde{p}$ with $\tilde{p} = \bar{p}O(M^2)$ and $M \ll 1$,

where the pressure p can be split into a uniform pressure $\bar{p}$ and an aerodynamic disturbance pressure $\tilde{p}$. The vorticity-velocity formulation has the advantage of eliminating the aerodynamic disturbance $\tilde{p}$ which has a heavy impact on the calculation time.

Equation of the vorticity

$$\partial^2_{xx}(\mu\omega) + \partial^2_{yy}(\mu\omega) = \rho u \partial_x \omega + \rho v \partial_y \omega + 2\partial_x \mu \, \partial_y(\partial_x u + \partial_y v) - 2\partial_y \mu \, \partial_x(\partial_x u + \partial_y v) + \partial_y \rho \, \partial_x(u^2/2) - \partial_x \rho \, \partial_y(v^2/2) + 2\partial_y u \partial^2_{xx}\mu - 2\partial_x v \, \partial^2_{yy}\mu - 2\partial_x u \partial^2_{yx}\mu + 2\partial_y v \, \partial^2_{xy}\mu + \partial_x \rho g,$$

where ρ is the density of the mixture, u the horizontal velocity, v the vertical velocity, t the time, the symbol ∂ the operator for the partial derivation, μ the shear viscosity, and ω the vorticity defined as: $\omega = \partial_x v - \partial_y u$.

Equation of the gaseous species

$$\rho u \partial_x Y_k + \rho v \partial_y Y_k + \partial_x(\rho U_k Y_k) + \partial_y(\rho V_k Y_k) - M_k \omega_k = 0 \quad \text{for} \quad k = 1 \ldots n,$$

where M_k is the molar mass of the k^{th} gaseous species, U_k the horizontal diffusion velocity of the k^{th} gaseous species, V_k the vertical diffusion velocity of the k^{th} gaseous species, w_k the molar

production rate in the gaseous phase of the k^{th} species, n the amount of gaseous species, and Y_k the mass fraction of the k^{th} gaseous species.

Equation of the surface species

$$\sigma_k = 0 \quad \text{for} \quad k = n+1 \ldots n+\hat{n},$$

where σ_k is the fraction of occupied catalytic sites by the k^{th} absorbed species and $\hat{n}$ the amount of surface species. This simply serves for the formulation of the absence of surface species in the gaseous phase.

Equation of the horizontal velocity

$$\partial_{xx}^2 u + \partial_{yy}^2 u - \partial_y \omega + \partial_x \left[\frac{u}{\rho} (\partial_x \rho) + \frac{v}{\rho} (\partial_y \rho) \right] = 0.$$

Equation of the vertical velocity

$$\partial_{yy}^2 v + \partial_{xy}^2 u + \partial_y \left(\frac{u}{\rho} \partial_x \rho + \frac{v}{\rho} \partial_y \rho \right) = 0.$$

Equation of the temperature

$$\rho c_p u \partial_x T + \rho c_p v \partial_y T + \partial_x \left(q_x - \sum_{k=1}^{n} h_k F_{kx} \right) + \partial_y \left(q_y - \sum_{k=1}^{n} h_k F_{ky} \right)$$
$$+ \left(\sum_{k=1}^{n} c_{pk} F_{kx} \right) \partial_x T + \left(\sum_{k=1}^{n} c_{pk} F_{ky} \right) \partial_y T + \sum_{k=1}^{n} h_k M_k \omega_k = 0,$$

where c_p is the specific heat at constant pressure in the mixture, c_{pk} the specific heat at constant pressure of the k^{th} gaseous species, F_{kx} and F_{ky} the horizontal and vertical diffusion flows of the k^{th} gaseous species, q_x and q_y the horizontal and vertical heat flux, h_k the specific enthalpy of the k^{th} gaseous phase and T the temperature.

State equation for the gaseous mixture

$$\rho = \frac{\bar{p}\bar{M}}{RT} \quad \text{with} \quad \bar{M} = \left(\sum_{k=1}^{n} \frac{Y_k}{M_k} \right)^{-1}$$

where $\bar{M}$ is the average molar mass of the gaseous mixture.

4.1.4. Multicomponent transport

The transport fluxes are evaluated as given in the detailed modeling of the multi-component transport which is derived from the kinetic gas theory [27].

Horizontal diffusion flux of the gaseous species

$$F_{kx} = \rho U_k Y_k \quad \text{with} \quad U_k = -\sum_{l=1}^{n} D_{kl}\partial_x X_l - \theta_k \partial_x \log T \quad \text{for} \quad k = 1\ldots n,$$

where D_{kl} is the diffusion coefficient of the k^{th} gaseous species into the l^{th} gaseous species, q_k the thermal diffusion coefficient of the k^{th} gaseous species and X_l the molar fraction of the l^{th} gaseous species. The first term of the diffusion velocity corresponds to the multi-species diffusion and the second term to the thermal diffusion (i.e. diffusion induced by the temperature gradient).

Vertical diffusion flux of the gaseous species

$$F_{ky} = \rho V_k Y_k \quad \text{with} \quad V_k = -\sum_{l=1}^{n} D_{kl}\partial_y X_l - \theta_k \partial_y \log T \quad \text{for} \quad k = 1\ldots n.$$

Horizontal heat flux

$$q_x = \sum_{k=1}^{n} h_k F_{kx} - \lambda\, \partial_x T + p\sum_{k=1}^{n} \chi_k U_k,$$

where λ is the thermal conductivity of the gaseous mixture and χ_k the ratio of the thermal diffusion of the k^{th} gaseous species. The first term of the heat flux corresponds to the enthalpy flux due to the species' diffusion, the second term to the heat conduction (Fourier's Law) and the last term to the heat flux induced by the species' diffusion.

Vertical heat flux

$$q_y = \sum_{k=1}^{n} h_k F_{ky} - \lambda\, \partial_y T + p\sum_{k=1}^{n} \chi_k V_k.$$

4.1.5. Boundary conditions

The surface conditions include all the conservation relations at the interface solid-gas on the catalytic plate. More detailed boundary conditions, like the symmetry or the inert wall are presented in the SPARK guide report [27].

Gaseous species balance

$$F_{kx} = -M_k \hat{\omega}_k, \quad k = 1 \ldots n,$$

where $\hat{\omega}_k$ is the molar surface production rate of the k^{th} gaseous species.

Surface species balance

$$\hat{\omega}_k = 0 \quad \text{for} \quad k = n+1 \ldots n+\hat{n}.$$

This condition constitutes the absence of mass accumulation on the catalytic surface.

Heat flux balance

$$\lambda \partial_x T + \sum_{k=1}^{n} h_k M_k \hat{\omega}_k - \sum_{k=1}^{n} p \chi_k U_k + q_{rad} = 0.$$

4.1.6. Complex chemistry

The combustion in the gaseous phase and the catalytic recombination of hydrogen are modeled by using the approach with complex chemistry. This modeling allows treating the kinetic-chemical mechanisms with any amount of chemical species and reactions. More details concerning the modeling with complex chemistry and the terms of chemical production can be found in SPARK report [27].

Elementary reactions

The complex chemistry approach allows the description of the reactive mechanism with n chemical species, which react in n_r reversible reactions. It can be formalized as:

$$\sum_{k=1}^{n} \nu_{ki}^{d} \mathcal{X}_k \Leftrightarrow \sum_{k=1}^{n} \nu_{ki}^{r} \mathcal{X}_k \quad \text{for} \quad i = 1 \ldots n_r,$$

where $\mathcal{X}_k$ is the symbol of the k^{th} species, ν_{ki}^{d} and ν_{ki}^{r} the respectively forward and backward stoichiometric coefficients of the k^{th} gaseous species in the i^{th} reaction.

Gaseous molar production rate

$$\omega_k = \sum_{k=1}^{n_r} \nu_{ki}\tau_i \quad \text{with} \quad \nu_{ki} = \nu_{ki}^r - \nu_{ki}^d,$$

where τ_i is the reaction rate of the i^{th} reaction.

Reaction rate

The reaction rate τ_i of the i^{th} reaction is expressed as:

$$\tau_i = K_i^d \prod_{k=1}^{n} [X_k]^{\nu_{ki}^d} - -K_i^r \prod_{k=1}^{n} [X_k]^{\nu_{ki}^r},$$

where K_i^d and K_i^r are the forward and backward reaction constants of the i^{th} reaction, and $[X_k]$ the molar fraction of the k^{th} gaseous species defined as:

$$[X_k] = \frac{\overline{P}}{RT} X_k.$$

The reaction coefficients are evaluated by Arrhenius laws whose parameters are listed in chemical mechanisms. The same formalism is used for the surface chemistry in order to define the surface molar production rate $\hat{\omega}_k$ and the surface reaction rate $\hat{\tau}_i$.

4.1.7. Numerical methods

The solution algorithm has been developed on the basis of a laminar Bunsen flame code [9][27]. The governing equations and boundary conditions are discretized on a two-dimensional tensor-product grid using a finite difference technique. The resulting system of highly nonlinear coupled equations is solved with a damped Newton's method [10]. A preconditioned Bi-CGSTAB algorithm is used to solve the large sparse linear systems arising during Newton iterations [27].

Additionally, the numerical evaluation of the chemical production rates, thermodynamic properties, and transport coefficients imposes particular attention in order to limit the computational cost of the solution. Thus, all properties are calculated using vectorized and highly optimized libraries for gas phase chemistry, surface chemistry and transport, respectively named: CHEMKIN II, SURF CHEM, and EGLIB.

Continuation technique

The technique of pseudo-continuation used in SPARK V2 consists in the estimation of the continuation step according to the error estimation given by an Euler predictor scheme. The continuation variable is chosen out of the main parameters of a recombiner, namely: $X_{H_2}^{in}$, x_{Air}^{in}, $X_{H_2O}^{in}$, v_{in}, T_{in} and $\bar{p}$. After each stationary solution of the branch $Q_g^{tot} = f(X)$, the step is determined as:

$$\left\| Z^{k+1} - \left(Z^k + \Delta X_k \left(\partial_X Z \right)_k \right) \right\| \approx \left\| \frac{1}{2} \left(\Delta X_k \right)^2 \left(\partial_X^2 Z \right)_k \right\| \leq \varepsilon_c,$$

where Z^k is the k^{th} discrete solution of the solution branch, X the variable de continuation, ΔX_k the k^{th} continuation step and ε_c the pseudo-continuation tolerance. This tolerance directly determines the refinement of the curvature of the branch $Q_g^{tot} = f(X)$. Figure 35 illustrates the technique of pseudo-continuation.

The characteristic "pseudo" is due to the fact that this technique does not permit to overpass a turning point. In fact, an infinite slope associated to this kind of singular points avoids an application of the presented technique. Nevertheless, this method permits an automatic pursuit of the solution branch and assures an adequate refinement in the zones with strong curvature, especially during the ignition.

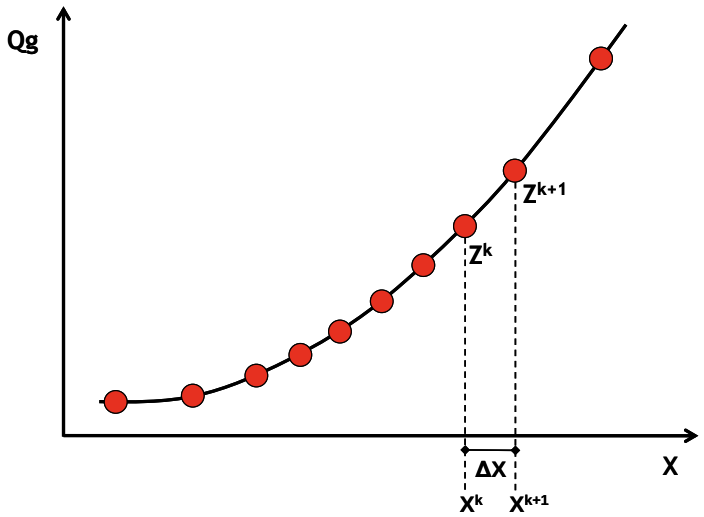

Figure 35: Pseudo-continuation algorithm [27].

4.1.8. Surface chemistry

The surface mechanism used for the catalytic oxidation of hydrogen and carbon monoxide over platinum was proposed by Deutschmann [28]. It contains 8 surface species and 8 gaseous species and consists of 20 reactions. Table 9 shows the surface reactions of the kinetic-chemical mechanism. For each reaction, the pre-exponential coefficient *A* and the activation energy *E* of the Arrhenius Law are given. The reaction mechanisms were updated, as presented in Table 10, in order to allow simulation during deactivation conditions.

Table 9: Reaction mechanisms for the catalytic oxidation of H_2 and CO over Pt [28].

Adsorption reactions[a]		s	
1[c].	$H_2 + 2Pt^{(s)} \rightarrow 2H^{(s)}$	0.046	
2.	$H + Pt^{(s)} \rightarrow H^{(s)}$	1.000	
3.	$O_2 + 2Pt^{(s)} \rightarrow 2O^{(s)}$	0.023	
4[d].	$O_2 + 2Pt^{(s)} \rightarrow 2O^{(s)}$	0.070	
5.	$O + Pt^{(s)} \rightarrow O(s)$	1.000	
6.	$H_2O + Pt^{(s)} \rightarrow H_2O^{(s)}$	0.750	
7.	$OH + Pt^{(s)} \rightarrow OH^{(s)}$	1.000	
8[e].	$CO + Pt^{(s)} \rightarrow CO^{(s)}$	0.840	
Surface reactions[b]		A	E
9.	$H^{(s)} + O^{(s)} \Leftrightarrow OH^{(s)} + Pt^{(s)}$	$3.7\ 10^{21}$	2749
10.	$H^{(s)} + OH^{(s)} \Leftrightarrow H_2O^{(s)} + Pt^{(s)}$	$3.7\ 10^{21}$	4159
11.	$OH^{(s)} + OH^{(s)} \Leftrightarrow H_2O^{(s)} + O^{(s)}$	$3.7\ 10^{21}$	11520
12.	$CO^{(s)}+O^{(s)} \rightarrow CO_2{}^{(s)}+Pt^{(s)}$	$3.7\ 10^{21}$	25096
13.	$C^{(s)}+O^{(s)} \rightarrow CO^{(s)}+Pt^{(s)}$	$3.7\ 10^{21}$	15010
14.	$CO^{(s)}+Pt^{(s)} \rightarrow C^{(s)}+O^{(s)}$	$1.0\ 10^{18}$	43977
Desorption reactions[b]		A	E
15.	$H^{(s)} + H^{(s)} \rightarrow H_2 + 2Pt^{(s)}$	$3.7\ 10^{21}$	$16109 - 1434\ \sigma_H$
16.	$O^{(s)} + O^{(s)} \rightarrow O_2 + 2Pt^{(s)}$	$3.7\ 10^{21}$	$50908 - 14340\ \sigma_O$
17.	$H_2O^{(s)} \rightarrow H_2O + Pt^{(s)}$	$1.0\ 10^{13}$	9632
18.	$OH^{(s)} \rightarrow OH + Pt^{(s)}$	$1.0\ 10^{13}$	46128
19.	$CO^{(s)} \rightarrow CO + Pt^{(s)}$	$1.0\ 10^{13}$	30115
20.	$CO_2{}^{(s)} \rightarrow CO_2 + Pt^{(s)}$	$1.0\ 10^{13}$	4900

[a] Sticking coefficients: s.
[b] Reaction rate coefficients: k = A exp(-E/RT) with A [mole-cm- Kelvin-sec] and E [cal/mole].
[c] The hydrogen adsorption is first order with respect to platinum.
[d] The oxygen sticking coefficient is temperature dependent: $s_{O2} = 0.07(T_0/T)$ with T_0=300 K.
[e] The carbon monoxide adsorption is second order with respect to platinum.

Table 10: Reactions are updated with kinetic data from [28]. R6–R11 are added HCOO reactions. R1 is given in terms of a sticking coefficient (S0) and is second order with respect to Pt(s). Units: S0 [–], A [cm, s, K], Ea [J/mol], coverage h [–]. Table adapted from [43]

Reactions		S_0 (A)	n	E_a
Adsorption and desorption reactions				
R1[a]	CO + Pt(s) → CO(s)	8.4E-2	0	0
R2[a]	CO(s) → CO + Pt(s)	2.13E+13	0	136,190–33,000θCO(s)
Surface reactions				
R3[a]	CO(s) + O(s) → CO2(s) + Pt(s)	3.70E+20	0	108,000–33,000θCO(s)
R4[a]	H(s) + O(s) → OH(s) + Pt(s)	3.70E+20	0	70500
R5[a]	OH(s) + Pt(s) → H(s) + O(s)	1.00E+20	0	130690
R6	OH(s) + CO(s) → HCOO(s) + Pt(s)	3.70E+21	0	94200
R7	HCOO(s) + Pt(s) → OH(s) + CO(s)	1.33E+21	0	870
R8	HCOO(s) + O(s) → OH(s) + CO2(s)	3.70E+21	0	0
R9	OH(s) + CO2(s) → HCOO(s) + O(s)	2.79E+21	0	151050
R10	HCOO(s) + Pt(s) → CO2(s) + H(s)	3.70E+21	0	0
R11	CO2(s) + H(s) → HCOO(s) + Pt(s)	2.79E+21	0	90050

4.1.9. Chemistry in the gaseous phase

The kinetic-chemical mechanism used for the combustion of hydrogen and carbon monoxide in air consists of 12 gaseous species and 31 reactions [27].

Table 11 lists the reaction of the kinetic-chemical mechanism describing the combustion in the gaseous phase. For each reaction, the pre-exponential coefficient *A*, the temperature coefficient *n*, and the activation energy *E* of the Arrhenius Law are given in Table 11

.

Table 11: Reaction mechanism for the gaseous combustion of H_2 and CO

H_2/O_2 reactions[a]		A	n	E_a
1.	$H + O_2 \Leftrightarrow O + OH$	$3.55\ 10^{15}$	-0.40	16600
2.	$O + H_2 \Leftrightarrow H + OH$	$5.08\ 10^{04}$	2.70	6290
3.	$H_2 + OH \Leftrightarrow H_2O + H$	$2.16\ 10^{08}$	1.50	3430
4.	$O + H_2O \Leftrightarrow OH + OH$	$2.97\ 10^{06}$	2.00	134000
5[b].	$H_2 + M \Leftrightarrow H + H + M$	$4.58\ 10^{19}$	-1.40	104000
6[b].	$O + O + M \Leftrightarrow O_2 + M$	$6.16\ 10^{15}$	-0.50	0
7[b].	$O + H + M \Leftrightarrow OH + M$	$4.71\ 10^{18}$	-1.00	0
8[b].	$H + OH + M \Leftrightarrow H_2O + M$	$3.80\ 10^{22}$	-2.00	0
9[c,e].	$H + O_2 (+M) \Leftrightarrow HO_2 (+M)$	$1.48\ 10^{12}$	0.60	0
		$6.37\ 10^{20}$	-1.72	525
10.	$HO_2 + H \Leftrightarrow H_2 + O_2$	$1.66\ 10^{13}$	0.00	823
11.	$HO_2 + H \Leftrightarrow OH + OH$	$7.08\ 10^{13}$	0.00	295
12.	$HO_2 + O \Leftrightarrow O_2 + OH$	$3.25\ 10^{13}$	0.00	0
13.	$HO_2 + OH \Leftrightarrow H_2O + O_2$	$2.89\ 10^{13}$	0.00	-497
14.	$HO_2 + HO_2 \Leftrightarrow H_2O_2 + O_2$	$4.20\ 10^{14}$	0.00	12000
	$HO_2 + HO_2 \Leftrightarrow H_2O_2 + O_2$	$1.30\ 10^{11}$	0.00	-1630
15[b,f].	$H_2O_2 (+M) \Leftrightarrow OH + OH (+M)$	$2.95\ 10^{14}$	0.00	48400
		$1.20\ 10^{17}$	0.00	45500
16.	$H_2O_2 + H \Leftrightarrow H_2O + OH$	$2.41\ 10^{13}$	0.00	3970
17.	$H_2O_2 + H \Leftrightarrow HO_2 + H_2$	$4.82\ 10^{13}$	0.00	7950
18.	$H_2O_2 + O \Leftrightarrow OH + HO_2$	$9.55\ 10^{06}$	2.00	3970
19[b].	$H_2O_2 + OH \Leftrightarrow HO_2 + H_2O$	$1.00\ 10^{12}$	0.00	0
	$H_2O_2 + OH \Leftrightarrow HO_2 + H_2O$	$5.80\ 10^{14}$	0.00	9560

CO reactions[a]		A	n	E_a
20[b].	$CO + O (+M) \Leftrightarrow CO_2 (+M)$	$1.80\ 10^{10}$	0.00	2380
		$1.55\ 10^{24}$	-2.79	4190
21.	$CO + O_2 \Leftrightarrow CO_2 + O$	$2.53\ 10^{12}$	0.00	47700
22.	$CO + HO_2 \Leftrightarrow CO_2 + OH$	$3.01\ 10^{13}$	0.00	23000
23.	$CO + OH \Leftrightarrow CO_2 + H$	$2.23\ 10^{05}$	1.90	-1160
HCO reactions[a]		**A**	**n**	**E_a**
24[d].	$HCO + M \Leftrightarrow H + CO + M$	$4.75\ 10^{11}$	0.70	14900
25.	$HCO + O_2 \Leftrightarrow CO + HO_2$	$7.58\ 10^{12}$	0.00	410
26.	$HCO + H \Leftrightarrow CO + H_2$	$7.23\ 10^{13}$	0.00	0
27.	$HCO + O \Leftrightarrow CO + OH$	$3.02\ 10^{13}$	0.00	0
28.	$HCO + OH \Leftrightarrow CO + H_2O$	$3.02\ 10^{13}$	0.00	0
29.	$HCO + O \Leftrightarrow CO_2 + H$	$3.00\ 10^{13}$	0.00	0
30.	$HCO + HO_2 \Leftrightarrow CO_2 + OH + H$	$3.00\ 10^{13}$	0.00	0
31.	$HCO + HCO \Leftrightarrow H_2 + CO + CO$	$3.00\ 10^{12}$	0.00	0

[a] Reaction rate coefficients: $k = A\ T^n \exp(-E/RT)$ with A [mole-cm-Kelvin-sec] and E [cal/mole].
[b] Third body efficiencies: $\alpha_{H2} = 2.5$, $\alpha_{H2O} = 12.0$, $\alpha_{CO} = 1.9$, $\alpha_{CO2} = 3.8$.
[c] Third body efficiencies: $\alpha_{H2} = 2.0$, $\alpha_{H2O} = 11.0$, $\alpha_{CO} = 1.9$, $\alpha_{CO2} = 3.8$, $\alpha_{O2} = 0.78$.
[d] Third body efficiencies: $\alpha_{H2} = 2.5$, $\alpha_{H2O} = 6.0$, $\alpha_{CO} = 1.9$, $\alpha_{CO2} = 3.8$.
[e] Reaction 9 is a Troe reaction with $F_c = 0.8$ (first entries are for high pressures).
[f] Reaction 15 is a Troe reaction with $F_c = 0.5$ (first entries are for high pressures).

4.2. Implementation of new conditions

The previous versions of SPARK have been designed for hydrogen and carbon monoxide combustion and recombination in recombiners. As of today, the code contains the reaction mechanisms for the catalytic oxidation of H_2 and CO over platinum. However, Pd and Pt may react differently. Even though most recombiners use platinum as the catalyst, some recombiners use palladium or bimetallic Pt-Pd catalyst. It is necessary to enhance the SPARK code with the reaction mechanisms for the H_2 and the CO over palladium. This will allow a further comparison between the different catalysts and a better understanding of how the poisoning products act when in contact with palladium or platinum.

The literature presents the surface reaction scheme for hydrogen and oxygen over palladium based on thermochemical and kinetic data for the interaction of these elements [28], showed in 12. The surface reaction mechanism for hydrogen over palladium is shown in Table 12. It is possible to observe that palladium leads to the same reaction mechanisms as platinum but with different rate coefficients.

Table 12: Surface reaction mechanism on palladium (units: A [mol, cm, s], Ea [kJ/mol], S0). Pd(s) denotes bare surface sites [28]. Reaction rate: k = A T^n exp(-E_a/RT)

#	Reaction	A	E_a	S^0
1	H_2+2Pd(s) => 2H(s)			0.7
2	H+Pd(s) => H(s)			1.00
3	2H(s) => H_2+2Pd(s)	4.80 x 10^{21}	$84 - 15 \cdot HH(s)$	
4	O_2+2Pd(s) => 2O(s)			0.40
5	O+Pd(s) => O(s)			1.00
6	2O(s) => O_2+2Pd(s)	7.10 x 10^{21}	230	
7	H_2O+Pd(s) => H_2O(s)			0.75
9	H_2O(s) => H_2O+Pd(s)	1.30 x 10^{13}	44.0	
10	OH+Pd(s) => OH(s)			1.00
11	OH(s) => OH+Pd(s)	1.30 x 10^{13}	213	
12	H(s)+O(s) <=> OH(s)+Pd(s)	6.50 x 10^{21}	11.5	
13	H(s)+OH(s) <=> H_2O(s)+Pd(s)	6.50 x 10^{21}	17.4	
14	OH(s)+OH(s) <=> H_2O(s)+O(s)	6.5 x 10^{21}	48.2	

The reaction mechanisms have been established based on data from the literature. The initial sticking coefficient for the dissociative hydrogen adsorption was chosen to be 0.7, which presents an average value of the existing data. For the associative hydrogen desorption, $A = 4.8 \times 10^{21}$ cm^2 (mol s^{-1}) and $E_a^{max} = 84$ kJ mol^{-1} are used. An additional decrease of the activation energy with increasing hydrogen coverage due the adsorbate-adsorbate interactions is considered: $E_a = E_a^{max} - \Theta_{H(s)} \times 15$ kJ mol^{-1}. For the interaction of oxygen with palladium, the following values are adopted: $S^0 = 0.4$ and $E_a^{des} = 230$ kJ mol^{-1}. The pre-exponential factor was derived from the vibrational frequency of a Pd-O bond of 1.1×10^{13} s^{-1}. For the remaining reactions, the kinetic data derived for a platinum surface were used. All those values have been established by Deutschmann et al [28] based on previous works.

4.3. Reference simulations

The catalyst temperature is the parameter used in the REKO experiments to identify catalyst deactivation by CO. For this reason, first calculations have been performed for hydrogen-air mixtures in order to verify that the SPARK code is able to reproduce it, notably with low-oxygen content. The calculations using conditions from normal operation allow to compare with the results from the reference tests performed in REKO facilities.

SPARK simulations with REKO-1

Simulations with the REKO-1 geometry have also been performed. Since the geometry of REKO-1 is a cylinder with a single catalyst sample, the 2D simulations performed at SPARK may not be the most adapted.

Figure 36 show the catalyst temperature measured at the lower edge of the catalyst for mixtures with different hydrogen fractions at 0.5 m/s and no carbon monoxide. During normal operation of the catalyst, SPARK predictions of the catalyst temperature is in a very good agreement with the experimental values.

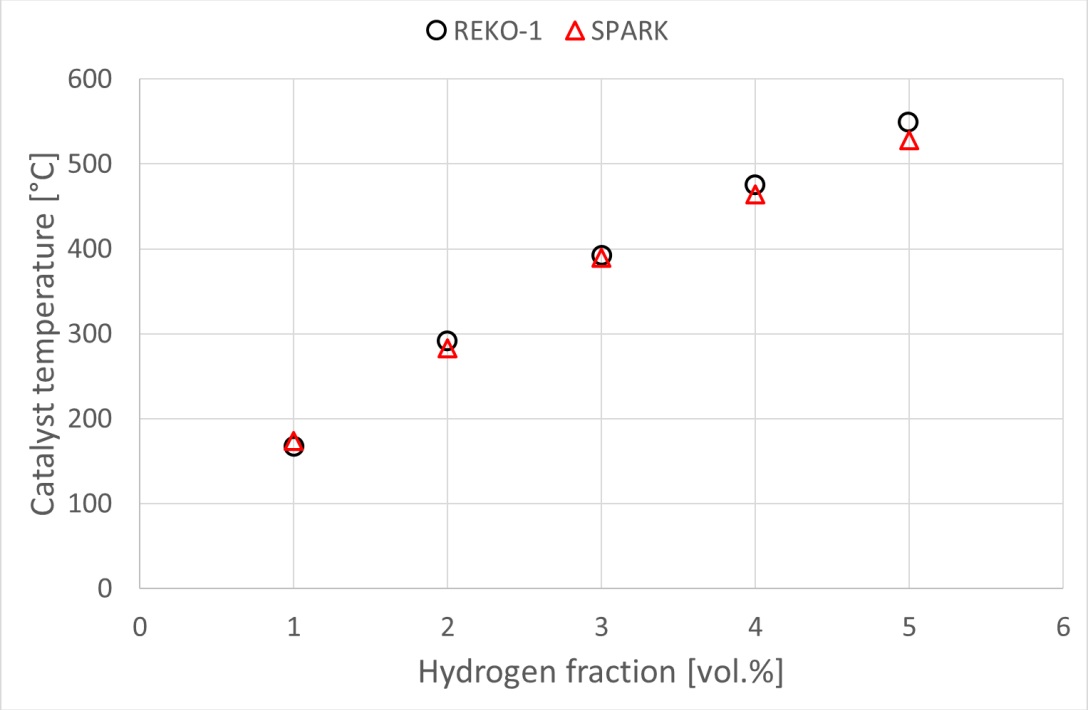

Figure 36: Evolution of catalyst temperatures measured at the bottom of the catalyst versus the H_2 molar percent for mixtures without CO and at 0.5 m/s.

Figure 37 represents the temperature profile for a mixture of 4 vol.% H_2, without carbon monoxide and during oxygen starvation. The circles represent the values measured experimentally at REKO-1 and the lines the values calculated with SPARK. Until 4.5 vol.% of oxygen, SPARKS predicts the temperature of the catalyst in a good agreement with the experimental results. However, the results show that SPARK predicts the on-set of oxygen starvation already for an oxygen fraction of 3.5 vol.%, which is slightly earlier than observed experimentally.

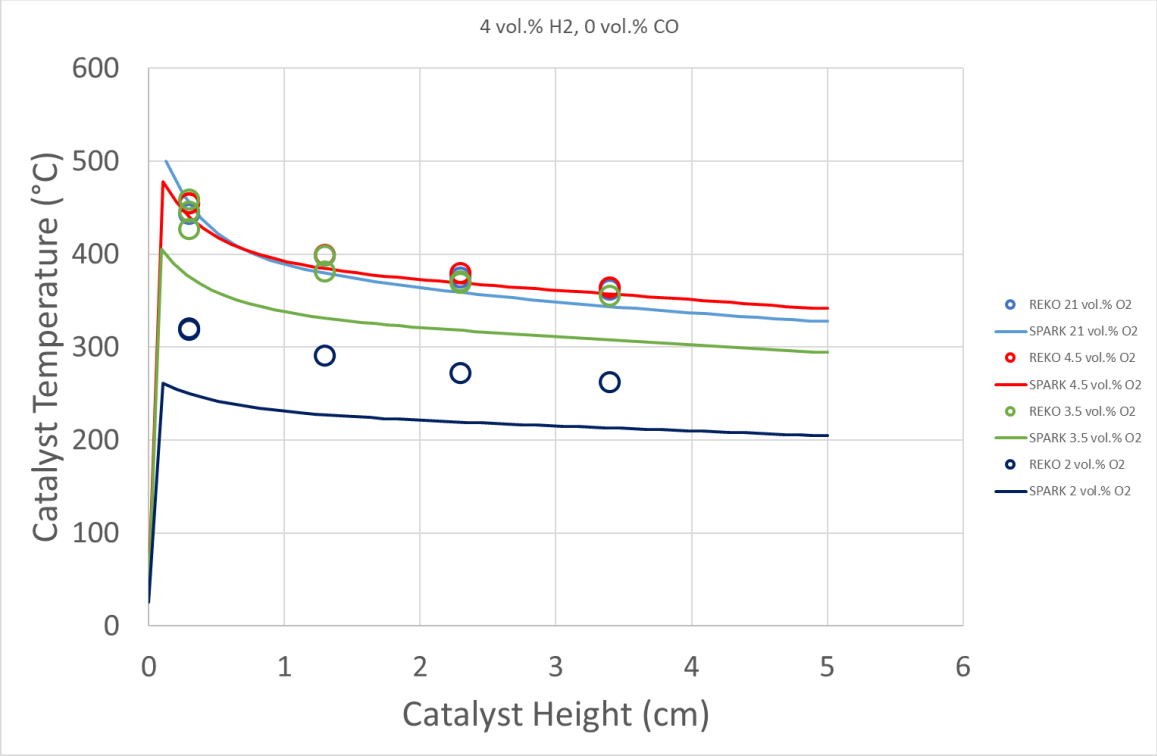

Figure 37: Catalyst surface temperature along catalyst height for 4 vol.% H2 and O2 content varying from 21 to 2 vol.%: Comparison between REKO-1 results and SPARK simulations.

SPARK simulations with REKO-3

The REKO-3 geometry was also used for SPARK simulations. Figure 38 show the temperature profile along the catalyst height for different hydrogen fractions with 21 vol.% of oxygen and at ambient temperature. The circles represent the experimental results while the line represents the values calculated by the SPARK code. For 4 vol.% of hydrogen, there is no available data for the lower positions of the catalyst since the temperature was higher than the upper limit of

the pyrometer. The experimental and numerical results are in very good agreement, confirming that the SPARK code can predict the catalyst temperature for rich-oxygen conditions.

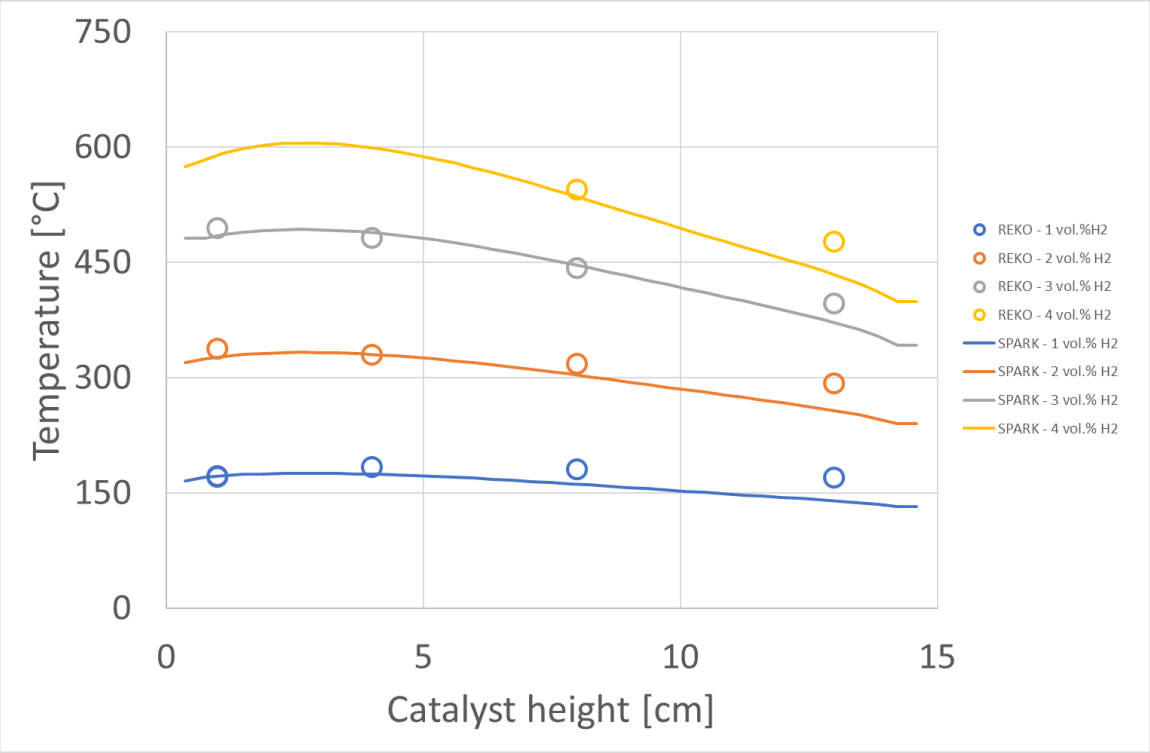

Figure 38: Catalyst surface temperature along catalyst height for different H_2 content: Comparison between REKO-3 results and SPARK simulations.

As mentioned earlier, once the oxygen content is below a certain value, the catalyst temperature decreases with the oxygen fraction, and gets eventually uniform along the catalyst height. A test series with 3 vol.% of hydrogen and the oxygen content varying from 21 to 2% at 1.15 m/s have been calculated with SPARK (Figure 39). The numerical results are consistent with the experimental results: from 21 vol.% O_2 to 4 vol.%, there are no changes in the catalyst temperature, showing that the efficiency of the recombiner is maintained and once the oxygen content is 3 vol.%, the effect of oxygen starvation is observed.

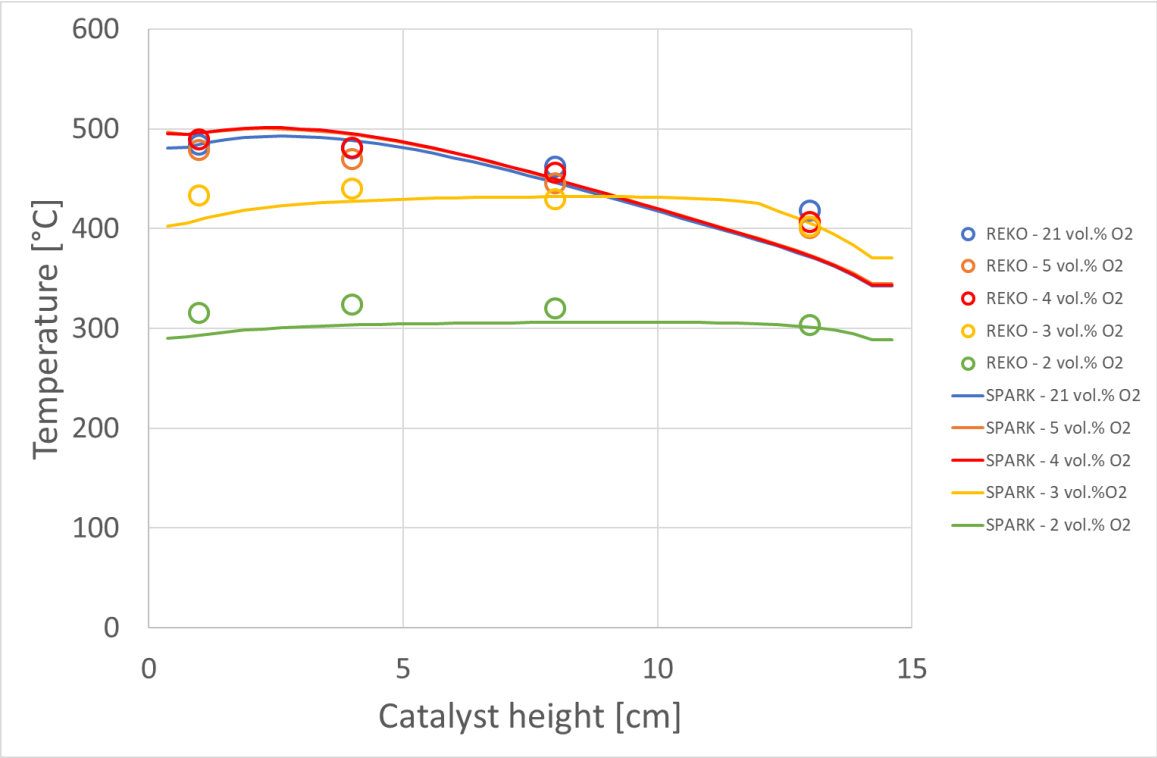

Figure 39: Catalyst surface temperature along catalyst height for 3 vol.% H_2 and O_2 content varying from 21 to 2 vol.%: Comparison between REKO-3 results and SPARK simulations.

The effect of steam on the catalyst temperature has also been analyzed with the presence of carbon monoxide and no restriction of oxygen. For a mixture of 2 vol.% H2, 100% relative humidity and carbon monoxide varying from 0 to 4 vol.% at 0.5 m/s and 80°C, the results are shown in Figure 40. The catalyst temperature obtained with SPARK are coherent with the temperatures measured at the bottom of the catalyst.

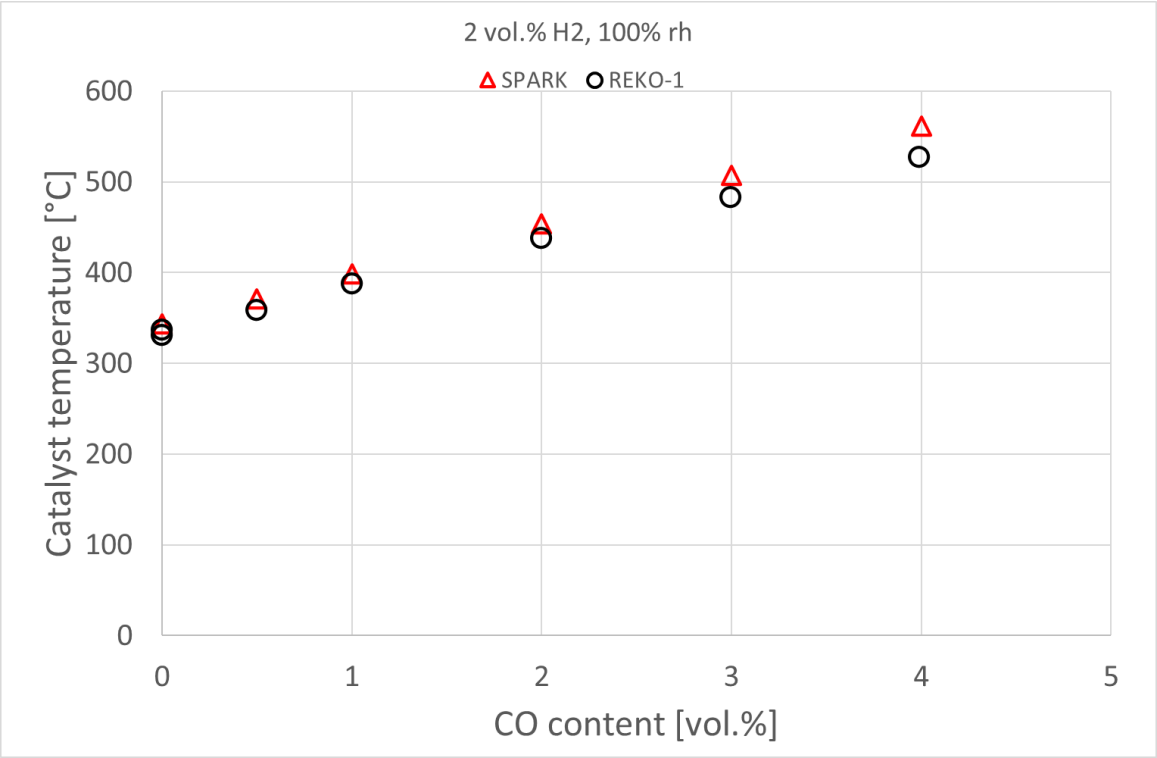

Figure 40: Catalyst temperatures for a mixture of 2 vol.% H2 versus CO content under dry and steam conditions.

4.4. Conclusion

Calculations have been performed for hydrogen-air mixtures in order to verify that the SPARK code is able to reproduce the experimental results. Simulations using REKO-1 geometry have been performed. The results using normal operation conditions are consistent with the experimental data. However, during oxygen starvation the results indicate that SPARK predicts the phenomena slightly earlier than observed in the experiments. Since the geometry of REKO-1 is a cylinder with a single catalyst sample, the 2D simulations performed with SPARK is not the most adapted.

The simulations using REKO-3 geometry have been conducted as well using different H_2/air mixtures. The catalyst behavior for conditions where there is oxygen reduction has also been simulated. The effect of steam on the catalyst temperature has also been analyzed with the presence of carbon monoxide and no restriction of oxygen. The numerical results are consistent with the experimental results for all the cases, confirming that the SPARK code can predict the catalyst temperature for rich-oxygen conditions, oxygen starvation conditions and when in presence of steam.

5. IMPACT OF CARBON MONOXIDE ON CATALYST DEACTIVATION

This chapter presents the experimental and numerical work carried out on the catalyst deactivation by carbon monoxide. First, the scoping experiment performed at the REKO-1 facility is presented, followed by the experiments performed at REKO-3. Finally, the numerical work performed with SPARK code is presented and compared to the experimental results.

In order to investigate the catalyst deactivation by carbon monoxide, experiments have been performed in two different experimental facilities. First, scoping tests have been performed with the REKO-1 facility to understand the deactivation process and how the different parameters impact platinum and palladium catalyst behaviour. Experiments have been performed at the REKO-3 facility to characterize the poisoning by carbon monoxide on a recombiner section with four full size catalyst samples. These experiments have been performed in the frame of the AMHYCO project, a European project that aims to improve the experimental knowledge and simulation capabilities in combustion risk management of hydrogen and carbon monoxide mixtures in severe accidents in nuclear power plants.

5.1. Scoping experiments: REKO-1

Previous experimental data indicates that recombiners operation in the presence of hydrogen and carbon monoxide can be divided into three different regimes [41]:

- Regime I: Undisturbed parallel reaction of hydrogen and carbon monoxide with oxygen;
- Regime II: Constrained parallel reaction of hydrogen and carbon monoxide with oxygen;
- Regime III: Reaction stop due to catalyst deactivation.

The results obtained with the REKO-1 facility confirmed these three regimes. The exothermic catalytic conversion of H_2 and CO has been observed by means of the catalyst temperature measurement. The behavior of the catalyst sample is shown in Figure 41. In this case, the composition of the gas mixture initially introduced in REKO-1 was 2 vol.% H_2, 4 vol.% CO and 7 vol.% O_2 at 0.5 m/s and ambient temperature. It is possible to observe that the catalyst temperature increases to 300°C when hydrogen is injected which means that the catalytic

reaction is happening thus hydrogen is being recombined into steam. Once carbon monoxide is injected in the flow channel, the catalyst temperature increases to 500°C, showing its conversion into carbon dioxide. Every step takes five minutes in order to achieve steady-state conditions. Finally, oxygen starts being stepwise reduced. Until 4 vol.% O_2, there is no change in the temperature, showing that the catalyst operation is still in the regime I, where there is a parallel reaction of hydrogen and carbon monoxide with oxygen. As soon as the oxygen fraction is decreased to 3.5 vol.%, the temperature also decreases to 452 °C, showing that the reaction is now under oxygen starvation, confirming regime II. When the oxygen content is reduced to 2.9 vol.%, there is a significant drop in the catalyst temperature and then it continuously decreases, showing that the reaction is slowly being reduced until total stop, around 4 200s. This last case corresponds to deactivation of the catalyst by carbon monoxide. Later, the injection of carbon monoxide was stopped and the catalyst temperature increased once again to the same temperature as the same step, indicating that hydrogen was being converted.

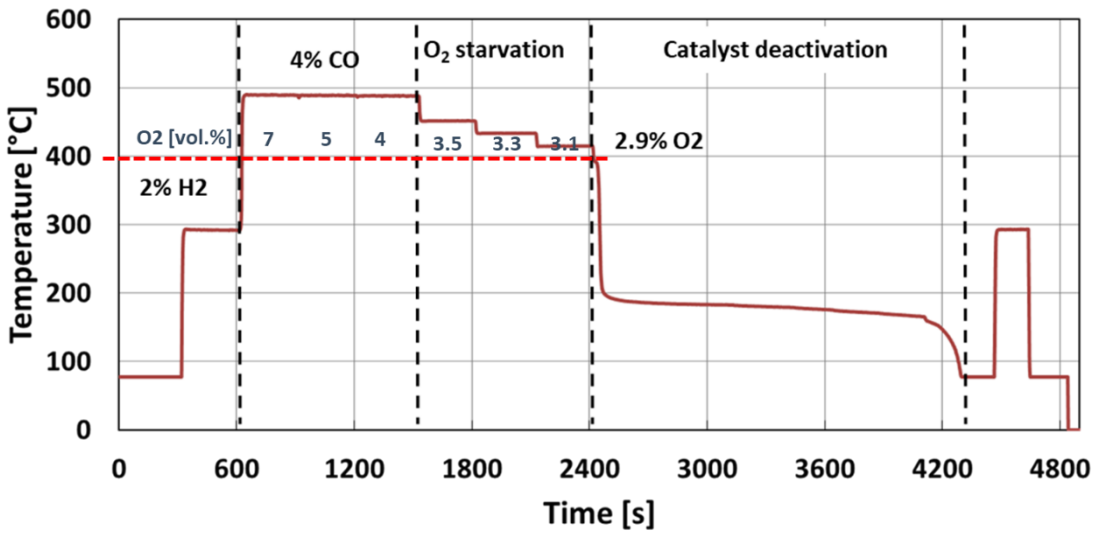

Figure 41: Catalyst temperature over time during a poisoning experiment.

Figure 42 shows at which catalyst temperature the poisoning occurs for different carbon monoxide fractions. Each symbol represents a different hydrogen fraction. Each point on the diagram is a different test where the poisoning was observed. The tests have been performed at 20°C with 0.5 m/s flow rate. The poisoning temperature seems to be a function of the carbon monoxide fraction, but independent from the hydrogen fraction. It is possible to observe that for different hydrogen contents, the catalyst poisoning temperature is the same for each carbon

monoxide, except for 1 vol.% of hydrogen. For this case, the catalyst temperature was not high enough to sustain the reaction and the catalyst was deactivated before oxygen starvation was observed.

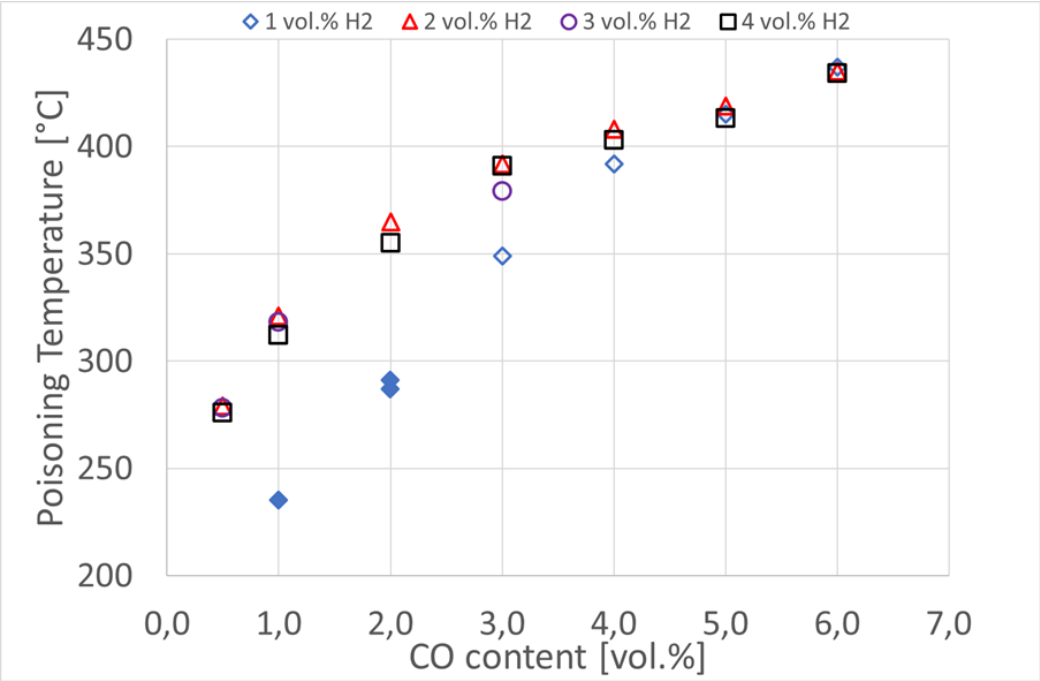

Figure 42: Evolution of the poisoning Temperature versus the CO molar percent for different H_2 molar percent. P_{ini} = 1 bar.

A typical test sequence starts with a fixed hydrogen and carbon monoxide mixture and then oxygen is decreased. In order to verify the effect of the test procedure, another type of experiments has been performed where the hydrogen and oxygen composition is fixed and then the carbon monoxide fraction is increased. Both types of test sequence lead to the same catalyst poisoning temperature, which can be seen in Figure 43.

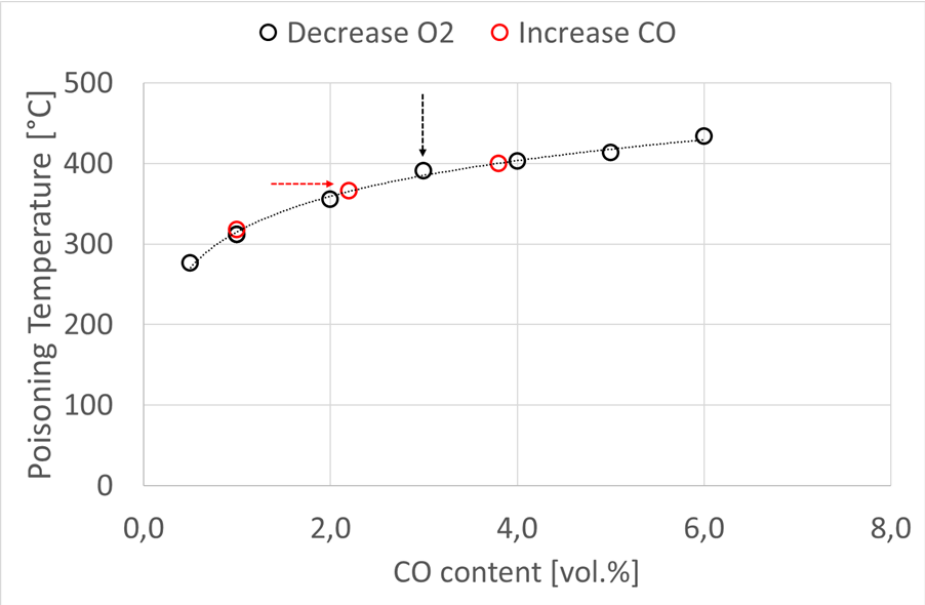

Figure 43: Evolution of the poisoning temperature versus the CO molar percent. Comparison between two test procedures.

The effect of the initial gas temperature can be observed for platinum-based catalyst in Figure 44. Three initial gas temperatures have been tested. The poisoning temperature seems to be independent from the gas temperature for the platinum catalyst. The poisoning seems to occur once the catalyst temperature is below the poisoning temperature indicated for each carbon monoxide concentration. The deactivation of the catalyst seems to be a function of catalyst temperature and carbon monoxide fraction.

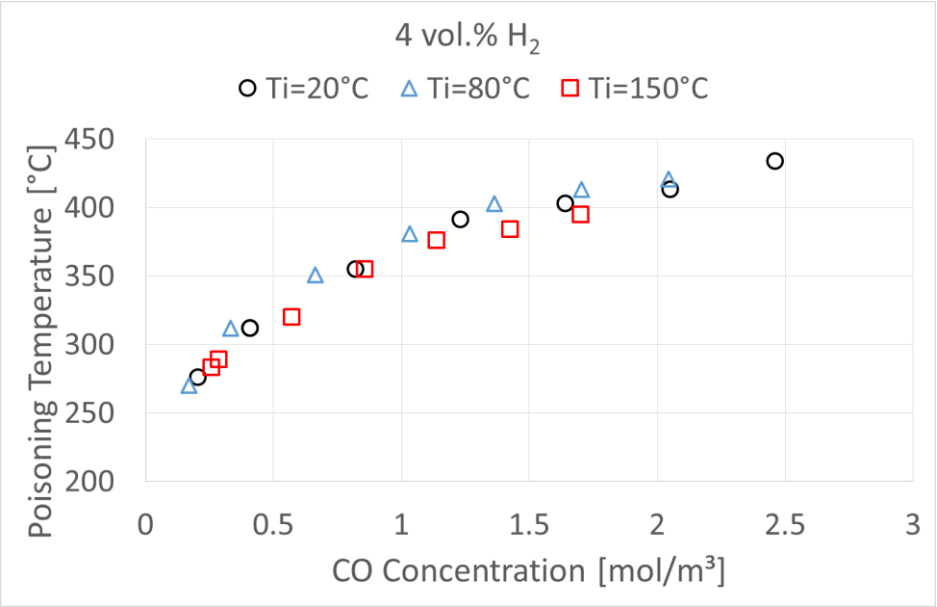

Figure 44: Catalyst poisoning temperature at different carbon monoxide concentrations for three initial gas temperatures: 20°C, 80°C and 150 °C.

The effect of flow velocity in the catalyst deactivation by carbon monoxide for platinum-based catalyst is showed in Figure 45. The poisoning temperature seems to be independent from the flow velocity. For two different flow velocities, the poisoning occurs at the same catalyst temperature for each carbon monoxide fraction.

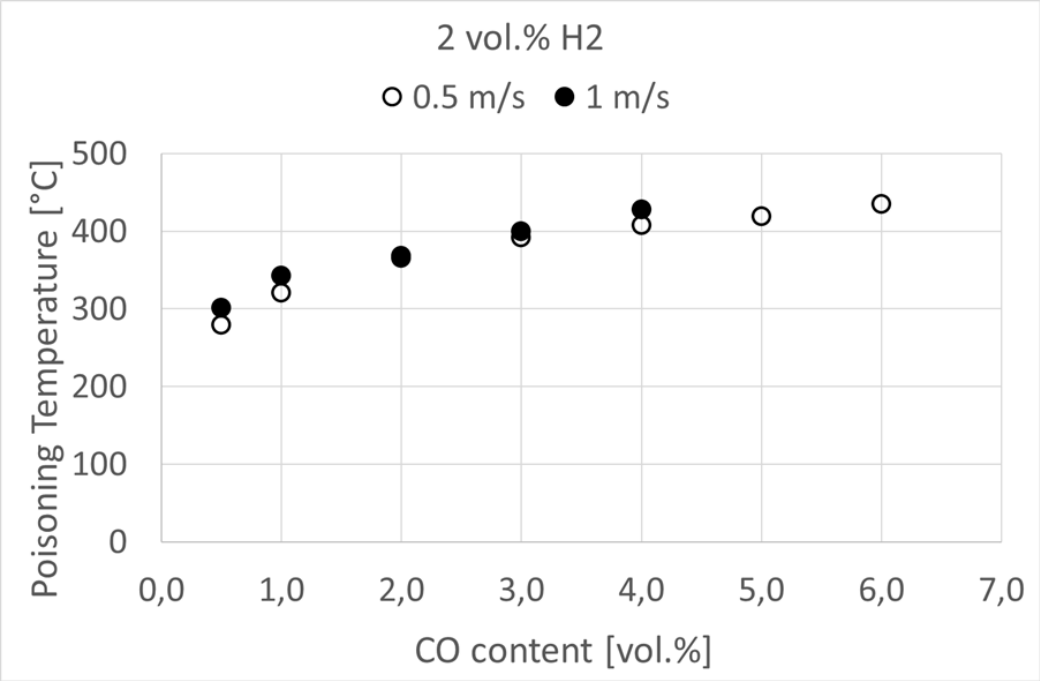

Figure 45: Catalyst poisoning temperature at different carbon monoxide fractions for different flow velocities.

The comparison of the catalyst deactivation for dry and humid conditions is represented in Figure 46. The tests have been performed at 80°C and 100% relative humidity with the platinum catalyst. The poisoning temperature is significant higher in high humidity, probably due to limited H_2O desorption from the catalyst surface.

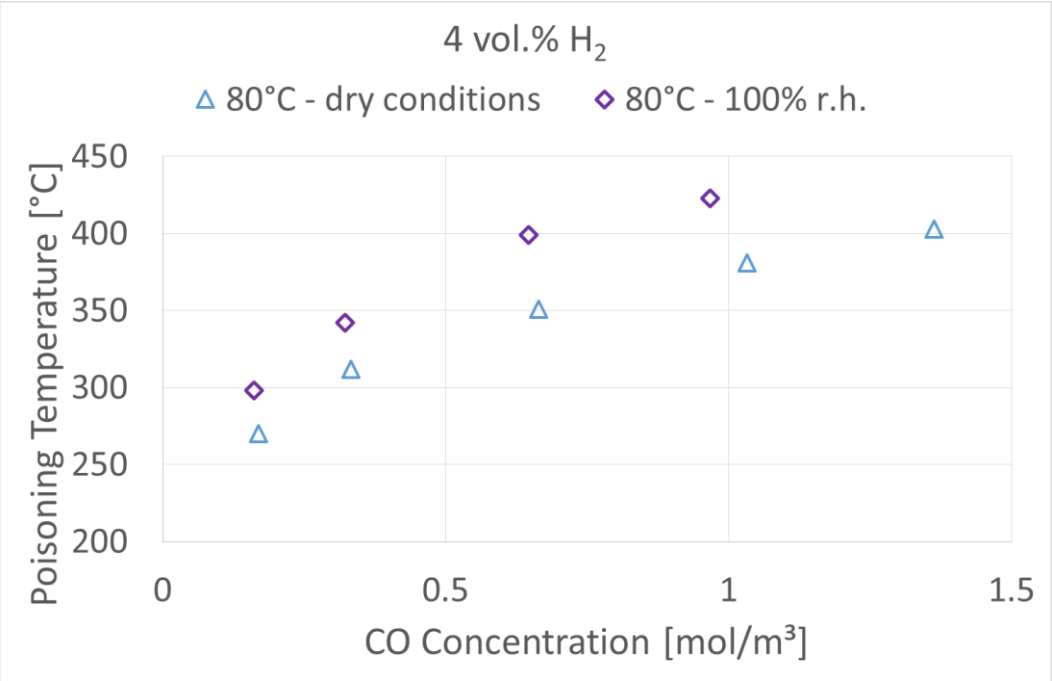

Figure 46: Catalyst poisoning temperature at different carbon monoxide concentrations for dry test and test with steam.

The difference from platinum and palladium-based catalyst has been investigated. Figure 47 shows the catalyst temperature where poisoning takes place for each concentration of carbon monoxide. Platinum-based catalyst are represented in black and palladium-based catalyst in red. In order to study the influence of the gas temperature, the experiments have been performed at 20°C, 80°C and 150°C. It is possible to observe that the poisoning temperature is higher for higher concentrations of carbon monoxide. The results showed that the palladium catalyst is deactivated at lower catalyst temperatures than the platinum-based one. Furthermore, the catalyst temperature in which the platinum is deactivated is not impacted by the gas temperature, while for the palladium catalyst the gas temperature has a significant influence. The results showed that the deactivation can be predicted by the carbon monoxide fraction, the oxygen fraction and the catalyst temperature.

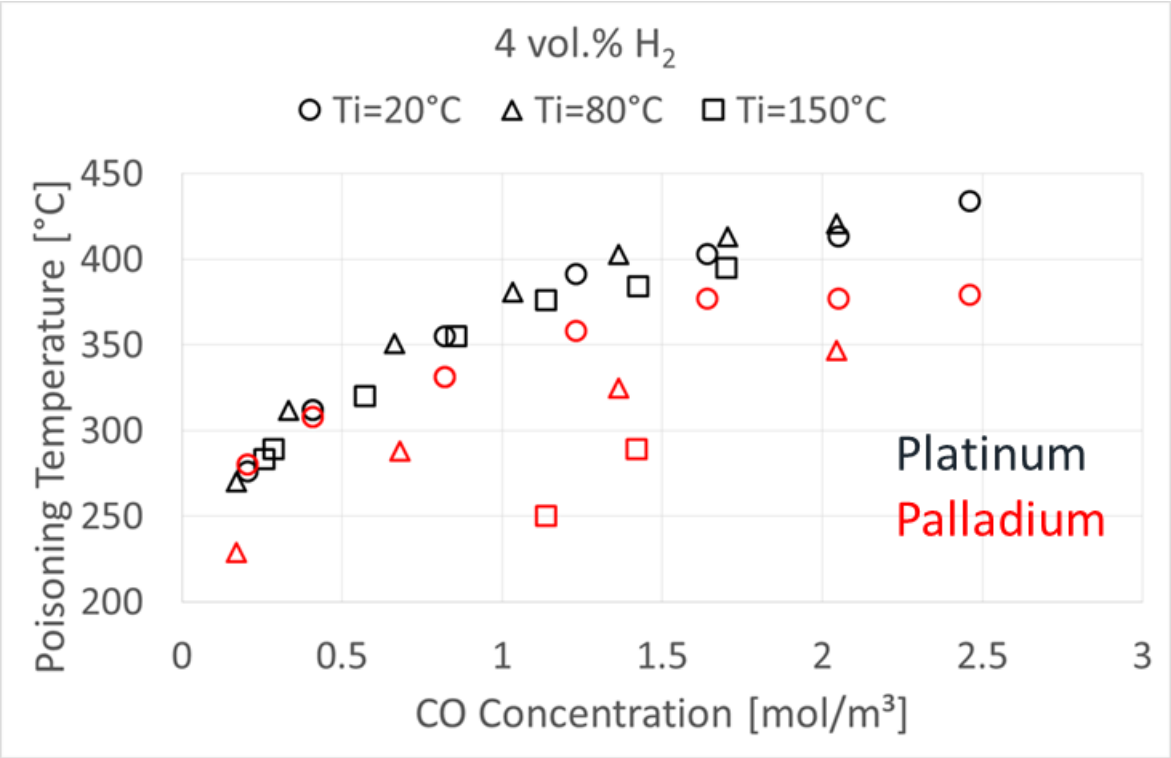

Figure 47: Comparison of catalyst poisoning temperature versus CO concentration for platinum and palladium catalysts.

5.2. Recombiner section experiments: REKO-3

REKO-3 facility, described in chapter 3, has been used to investigate poisoning by carbon of monoxide on a section of a PAR under forced flow conditions. The facility uses real scale catalyst sheets and it provides data for validation on numerical codes.

First experiments have been performed with a platinum catalyst at 20°C and 80°C. The experiments are not completed yet. However, the first data obtained in the recombiner section with four full scale catalysts appears to be coherent with the results achieved in REKO-1. The comparison of the results obtained with a platinum catalyst in REKO-1 and REKO-3 are shown in Figure 48. The catalyst temperature seems to not be influenced by the gas temperature. The deactivation temperature of the platinum-based catalyst in REKO-3 seems to follow the same pattern as the one presented for the small catalyst in REKO-1. The poisoning temperatures are higher in this case probably due to minimized heat losses. Experiments still need to be done in order to confirm the results from the single catalyst sample.

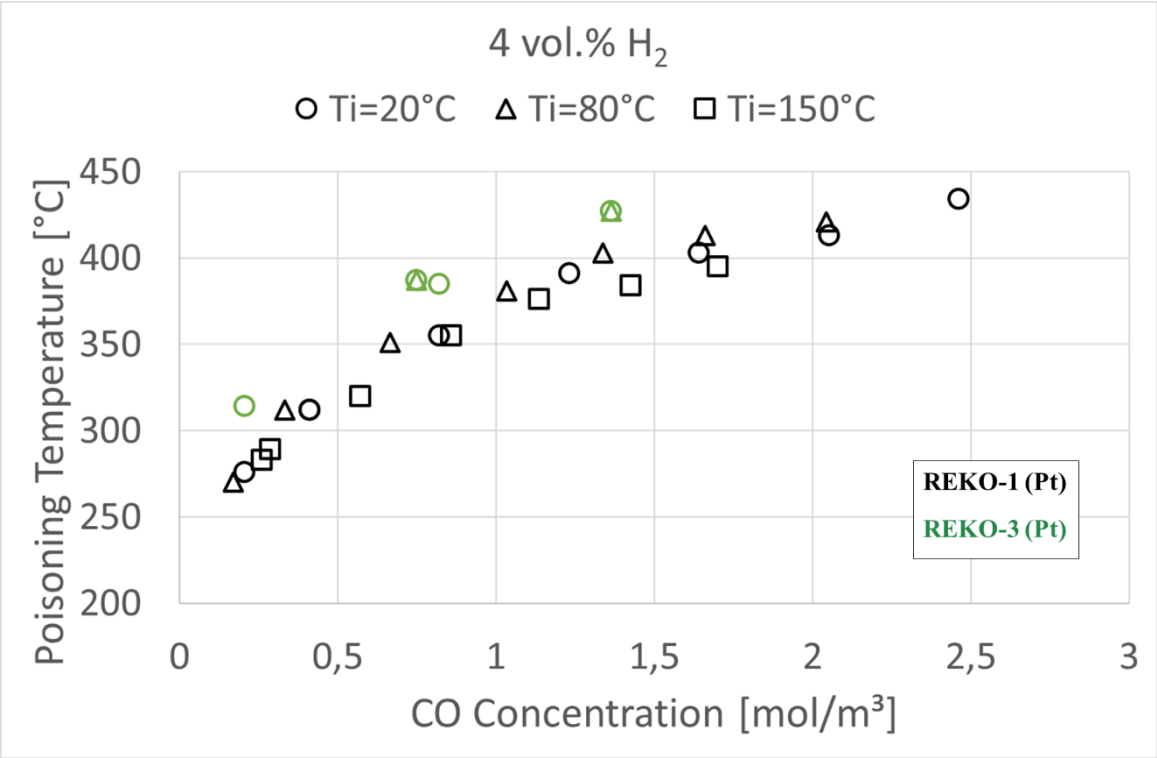

Figure 48: Comparison of catalyst poisoning temperature versus CO concentration for REKO-1 and REKO-3.

5.3. Numerical simulation using SPARK code

In this section, simulations of REKO-3 tests with the SPARK code are presented and discussed, with the objective to assess its capability to predict catalyst deactivation by CO. First, simulations for H_2/CO/air mixtures are presented in order to show that SPARK is able to predict deactivation. Then, calculations performed to analyze the impact of different parameters on the catalyst deactivation are shown. Finally, the numerical simulations are compared to the experimental results.

The calculations were performed using REKO-3 geometry since it is more appropriate for the 2D SPARK simulations. However, they are compared with REKO-1 and REKO-3 experimental data since the difference in the catalyst deactivation observed in REKO-1 and REKO-3 (Figure 48) is not so significant. The difference between the two facilities can be explained by the fact that with REKO-1 facility there is a lot of heat losses due to its geometry so the same difference is expected for SPARK simulations.

5.3.1. Simulations for H_2-CO-air mixtures

Catalyst deactivation was identified in the REKO experiments by a significant drop of the catalyst temperature, indicating that the hydrogen is no longer being recombined as it is during normal operation. The same parameter has been used with the SPARK code. Figure 49 shows the temperature at the lower edge of the catalyst for different values of the oxygen fraction for a mixture of 4 vol.% H_2, 0.5 vol.% CO at 0.5 m/s with inlet gas temperature of 20°C. The black circles represent the measured temperature and the red triangles represents SPARK results. Oxygen is reduced until the catalyst is deactivated. The measured temperatures at REKO-3 are slightly higher than the ones calculated with SPARK. As can be seen, the catalyst deactivation is predicted by the SPARK code, when the oxygen fraction reaches 2.8 vol.% and the catalyst temperature is 383°C. In the experiments, the catalyst deactivation was observed for lower values, when the oxygen fraction was around 2 vol.% O_2 and the catalyst temperature was 340°C.

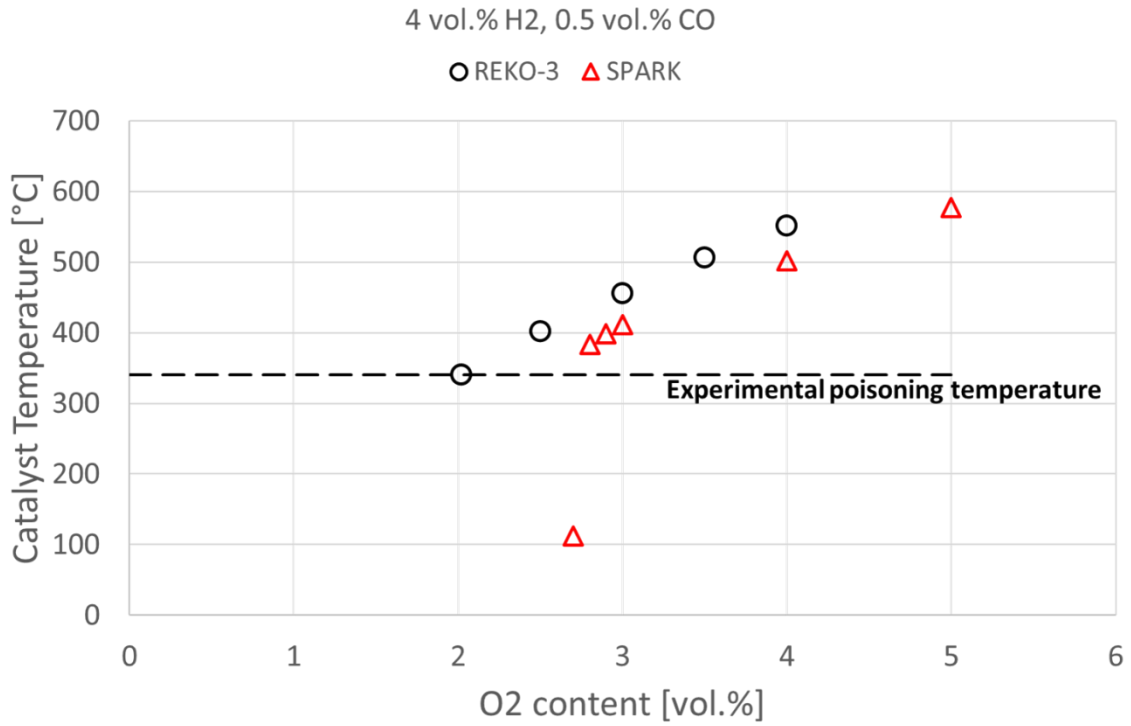

Figure 49: Catalyst temperature for a mixture with 4 vol.% H2, 0.5 vol.% CO and reduction of oxygen.

Figure 50 shows the temperature at the bottom of the catalyst for a mixture of 4 vol.% H_2, 2 vol.% CO at 0.5 m/s with inlet gas temperature of 80°C. Once again, the SPARK code predicts

deactivation at higher oxygen fraction and catalyst temperature. It was observed at 2.4 vol.% O_2 and a catalyst temperature of 390°C while it is predicted at 2.6 vol.% O_2 and a catalyst temperature of 400°C.

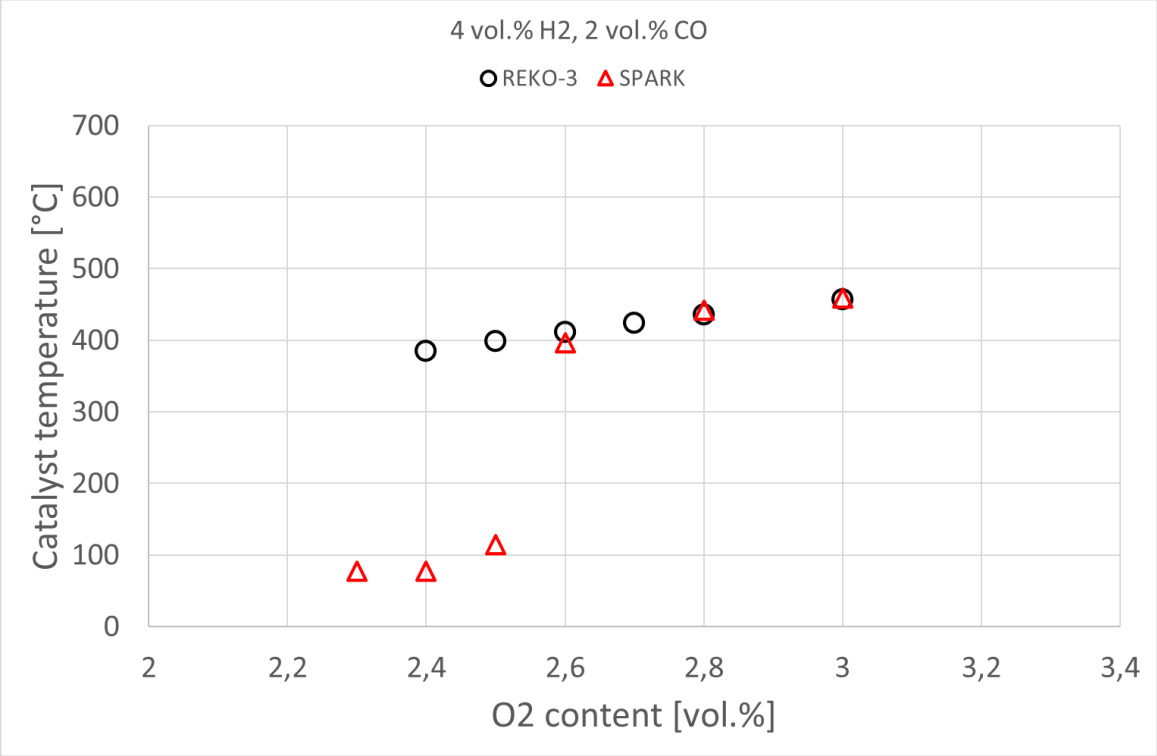

Figure 50: Catalyst temperature for a mixture with 4 vol.% H2, 2 vol.% CO, gas at 80°C and reduction of oxygen.

The SPARK code allows a detailed analysis of the REKO-3 tests. Figure 51 shows the hydrogen fraction present in the gas phase in the channel between two catalyst sheets for the previous mixture: 21 vol.% O_2 on the left and 3 vol.% on the right. Hydrogen starts being converted once it is in contact with the catalytic plate, confirming what was observed with the temperature field. It can be noted that the conversion is less efficient for a mixture with 3 vol.% of oxygen. Most of hydrogen is recombined at the entry of the recombiner, at the bottom of the catalyst.

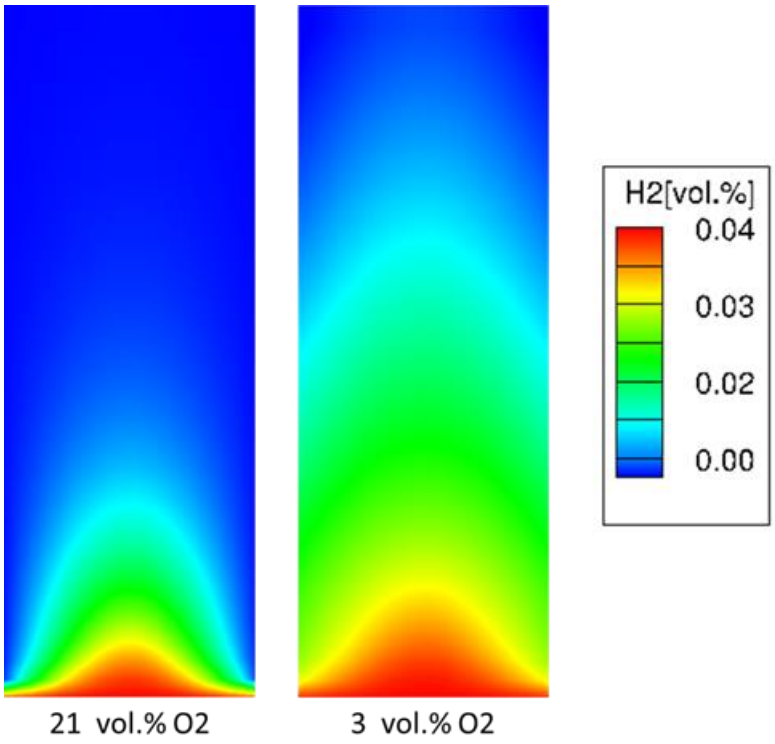

Figure 51: Hydrogen distribution on the channel between catalysts, for 21 vol.% O2 (left) and 3 vol.% O2 (right).

The carbon monoxide present in the channel for the same gas mixture during normal operation are shown in Figure 52. The figure shows that not all carbon monoxide is converted, indicating that the conversion of hydrogen is privileged in these conditions. However, carbon monoxide is still recombined and it does not block the catalytic surface.

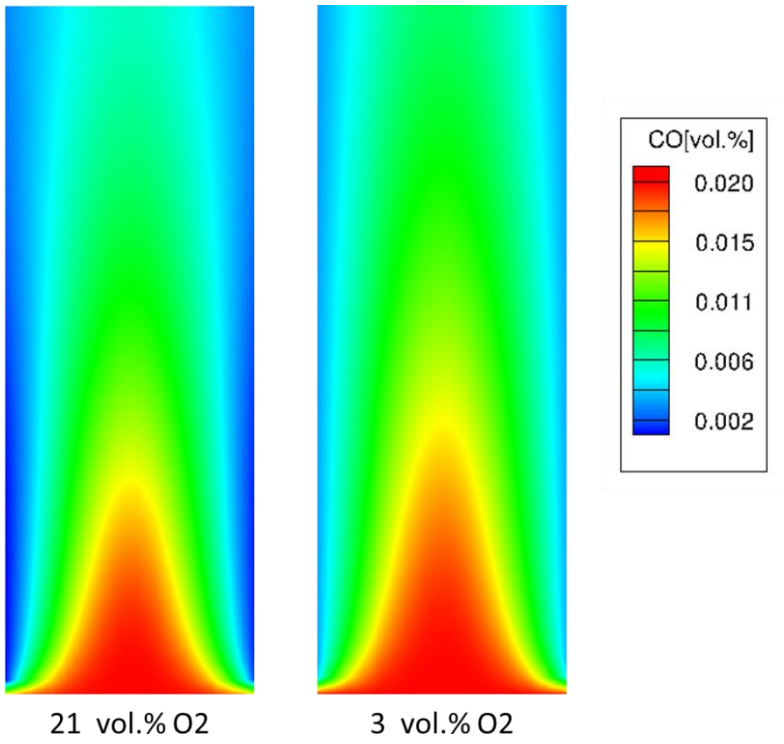

Figure 52: Carbon monoxide distribution in the REKO-3 channel between two catalyst plates, for 21 vol.% O2 (left) and 3 vol.% O2 (right).

Figure 53 represents the catalyst temperature during normal operation for the same mixture previous presented in Figure 39: 21 vol.% O_2 on the left and 3 vol.% O_2 on the right. For both cases, it is possible to observe that hydrogen starts being recombined at the lower edge of the catalyst. However, when the oxygen content is 21 vol.%, the temperature at the bottom of the catalyst is higher while for 3 vol.%, the temperature starts decreasing at this point. This behavior inidcates that the effects of oxygen starvation is first observed at the lower edge of the catalyst, confirming what was observed in the experiments.

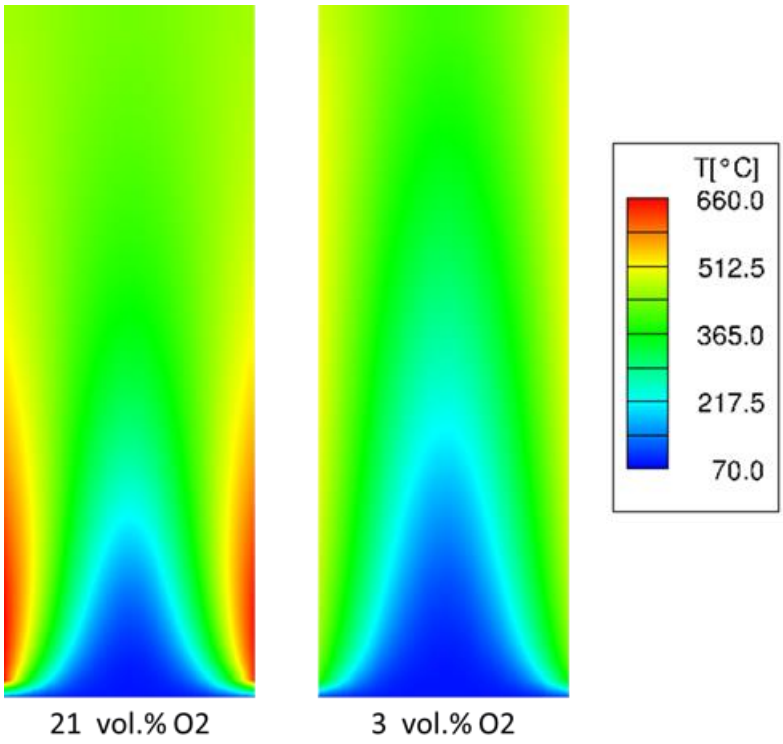

Figure 53: Temperature fields for a mixture with 4 vol.% H_2, 2 vol.% CO, gas at 80°C and 21 vol.% O_2 on the left and 3 vol.% O_2 on the right.

For the considered mixture (4 vol.% H_2, 2 vol.% CO), the catalyst deacativation is predicted around 2.6 vol.% O_2. Figure 54 shows the hydrogen distribution for three different fractions of oxygen during deactivation: on the left, 2.6 vol.% O_2 represents the beginning of poisoning, in the middle during the deactivation process and on the left 2.3 vol.% O_2, showing the catalyst already completely deactivated. On the left, for 2.6 vol.% O_2, the hydrogen fraction at the inlet of the channel is unchanged, indicating that the lower edge of the catalyst is no longer converting hydrogen. In the middle, for 2.5 vol.% of oxygen, the part of the catalyst that is not recombining the hydrogen increases, going up on the catalyst. However, once the gas mixture reaches the part of the catalyst that is not deactivated, the hydrogen is recombined. On the right, for 2.3 vol.% O_2, the entire catalyst seems to be deactivated and almost no hydrogen is being converted. The same can be observed for the carbon monoxide fraction between plates in Figure 55.

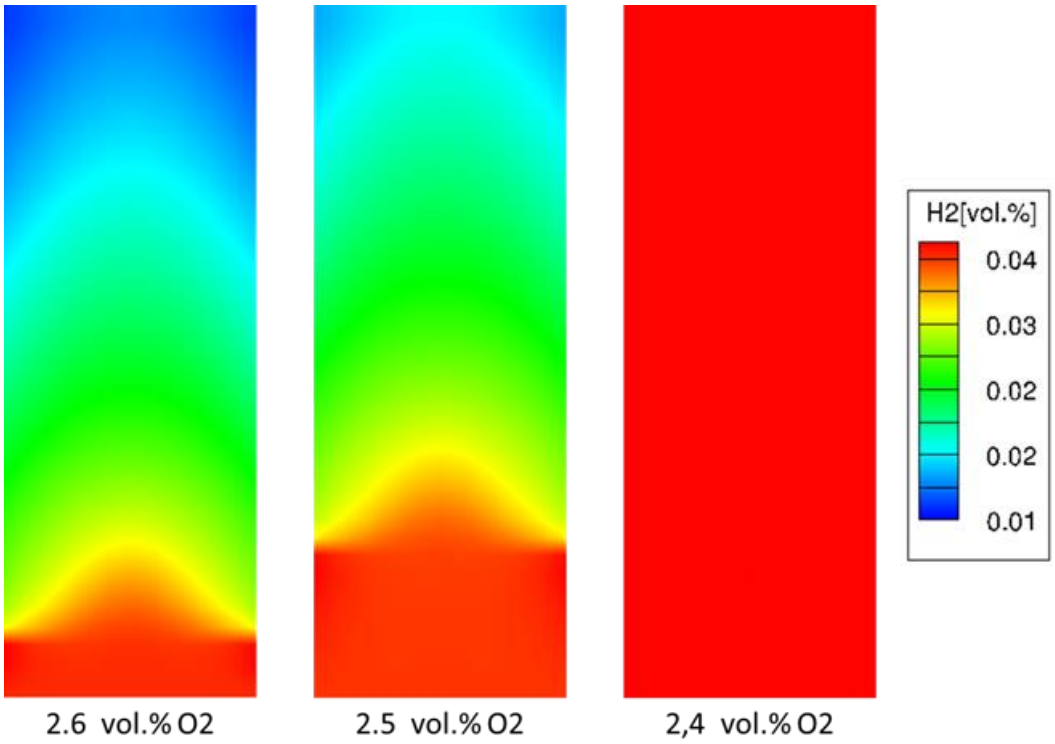

Figure 54: Hydrogen distribution in the REKO-3 channel between two catalyst plates for a mixture with 4 vol.% H2, 2 vol.% CO and the following O2 content: 2.6 vol.% O_2 (left), 2.5 vol.% O_2 (middle) and 2.3 vol.% O_2 (right).

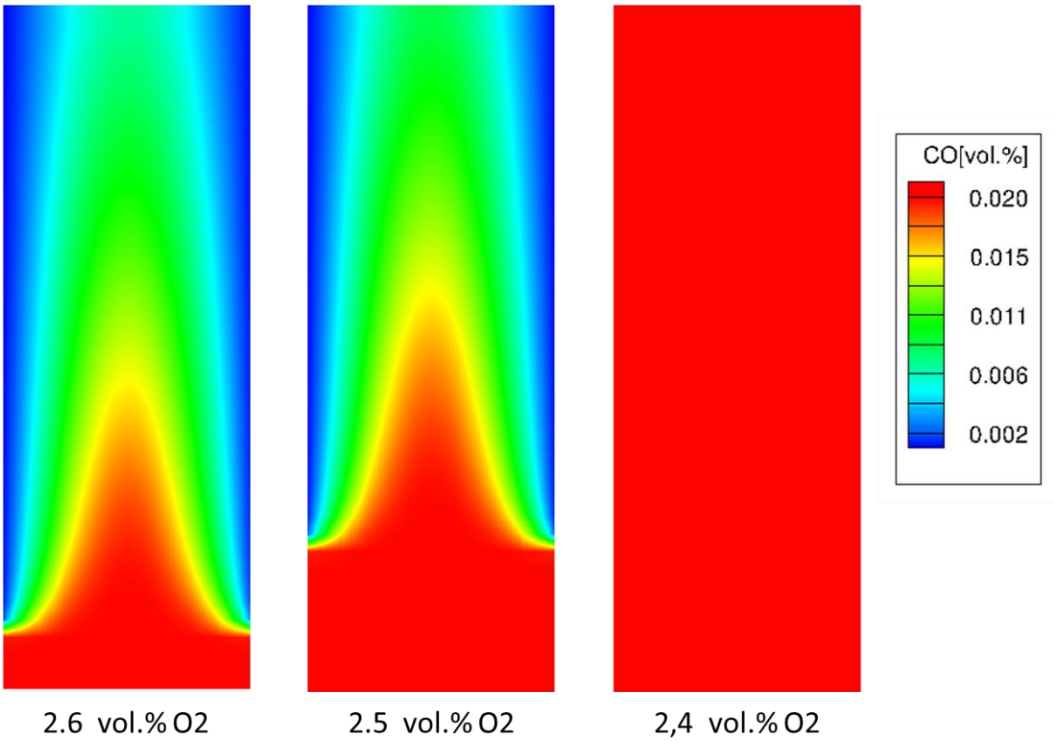

Figure 55: Carbon monoxide distribution in the REKO-3 channel between two catalyst plates for 2.6 vol.% O_2 (left), 2.5 vol.% O_2 (middle) and 2.3 vol.% O_2 (right).

Figure 56 show the temperature field between two plate for the three different contents of oxygen during deactivation.The temperature at the bottom of the catalyst when the fraction of oxygen is 2.6 vol.% starts to decrease showing that there is no reaction occuring at that spot. When futher decreasing the oxygen fraction to 2.5 vol.%, the temperature starts decreasing in the upper parts of the catalyst as well. At 2.3 vol.%, the entire catalyst temperature is around 78°C, indicating complete deactivation.

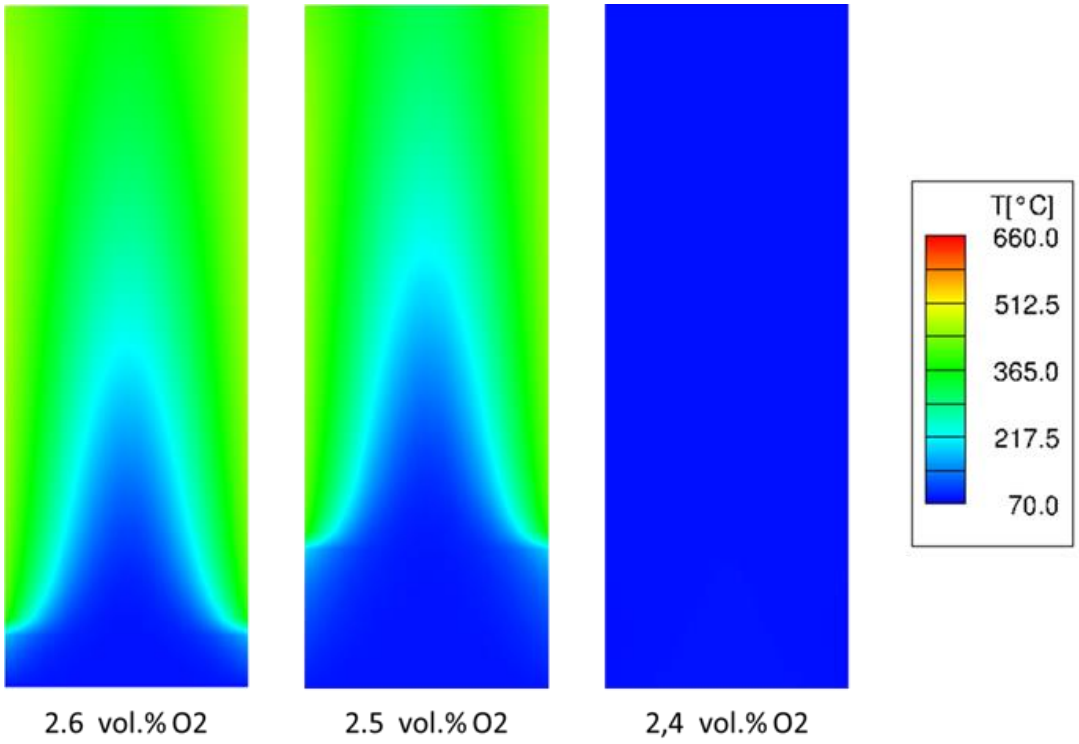

Figure 56: Temperature fields for a mixture with 4 vol.% H_2, 2 vol.% CO, gas at 80°C during deactivation: 2.6 vol.% O_2 (left), 2.5 vol.% O_2 (middle) and 2.3 vol.% O_2 (right).

Figure 57 shows the fraction of carbon monoxide on the catalytic surface. At the beginning of catalyst deactivation (2.6 vol.% O_2), on the left, the carbon monoxide blocks the lower edge of the catalytic surface. At 2.5 vol.% of oxygen, the surface blocked by carbon monoxide is extended by a few centimeters. At 2.3 vol.%, the entire surface of the catalyst is blocked by carbon monoxide, confirming the catalyst deactivation by this product.

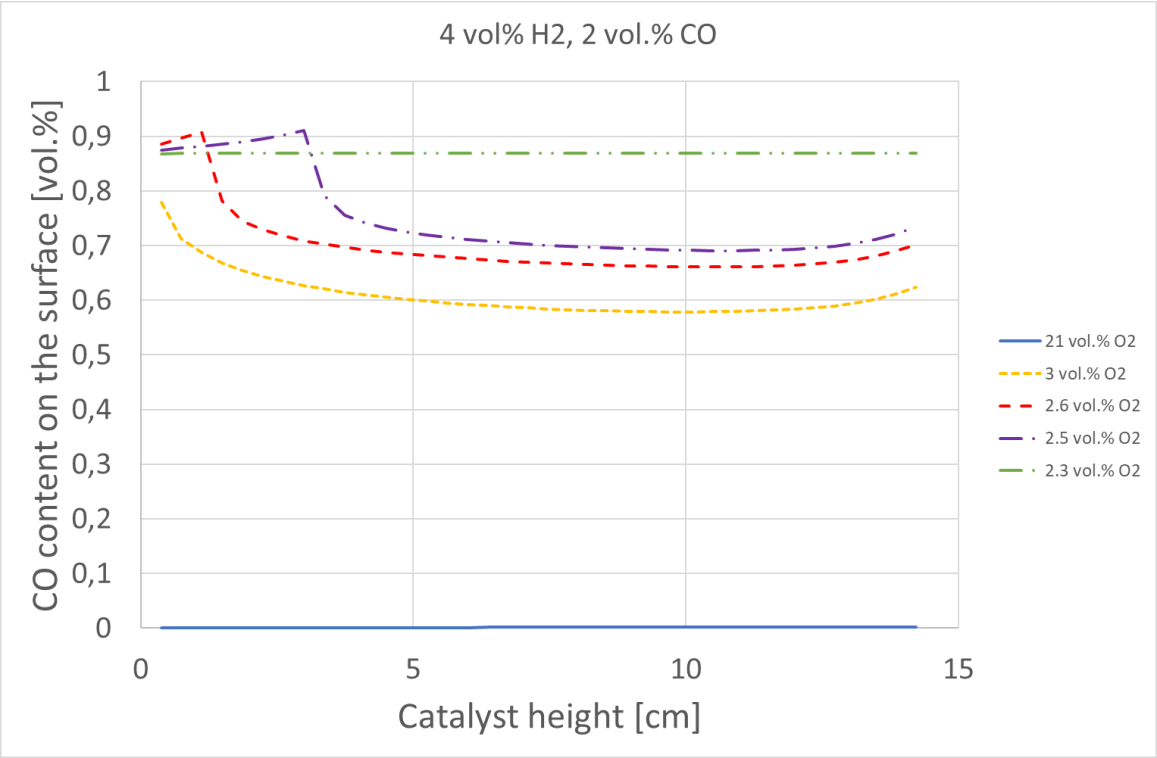

Figure 57: Carbon monoxide distribution along the catalyst plate for a mixture with 4 vol.% H_2, 2 vol.% CO and oxygen varying from 21 to 2.3 vol.%.Characterization of catalyst deactivation for different parameters

A set of calculations have been performed to evaluate the poisoning temperature for different combinations of hydrogen, carbon monoxide, initial gas temperatures and flow velocities.

Impact of H_2 content on the poisoning temperature

Figure 58 illustrates the poisoning temperature predicted by SPARK for different hydrogen and CO fractions at 0.5 m/s, using a platinum catalyst. The blue symbols represent the poisoning for mixtures with 1 vol.% of hydrogen. The red triangles represent 2 vol.% hydrogen; purple circles indicate 3 vol.% H_2 and the black squares for hydrogen fraction of 4 vol.%.

The deactivation is predicted at similar temperature for the different hydrogen fractions. However, for 1 vol.% of hydrogen the poisoning temperature is lower. Also, the higher is the carbon monoxide fraction, the higher the poisoning temperature is.

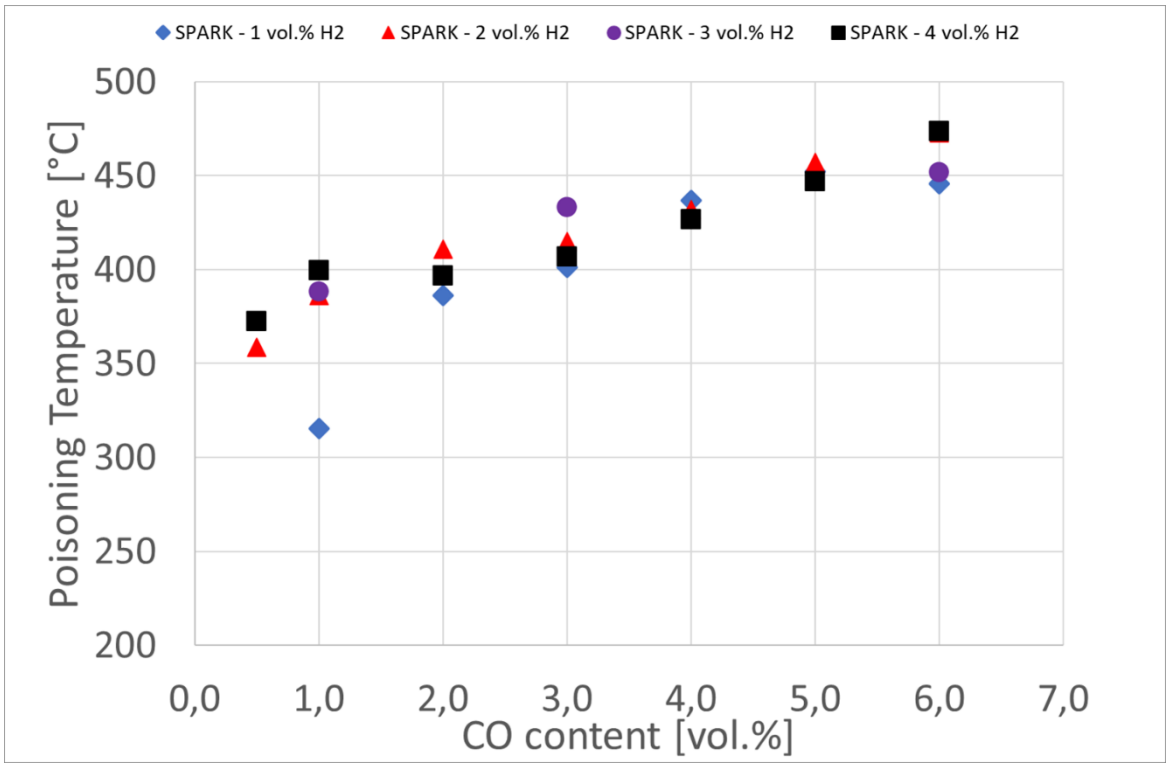

Figure 58: Poisoning temperature predicted by SPARK versus the CO content at different H_2 content. Pini = 1 bar.

Impact of inlet velocity on the poisoning temperature

Figure 59 represents the poisoning for a mixture with 2 vol.% H_2 for two different flow velocities and for each carbon monoxide fraction. The open triangle represents the poisoning for mixtures at 0.5 m/s while the filled triangles represent 1 m/s. The values of the temperature when deactivation occurs are similar for both cases. The flow velocity seems to not have a significant impact on the poisoning.

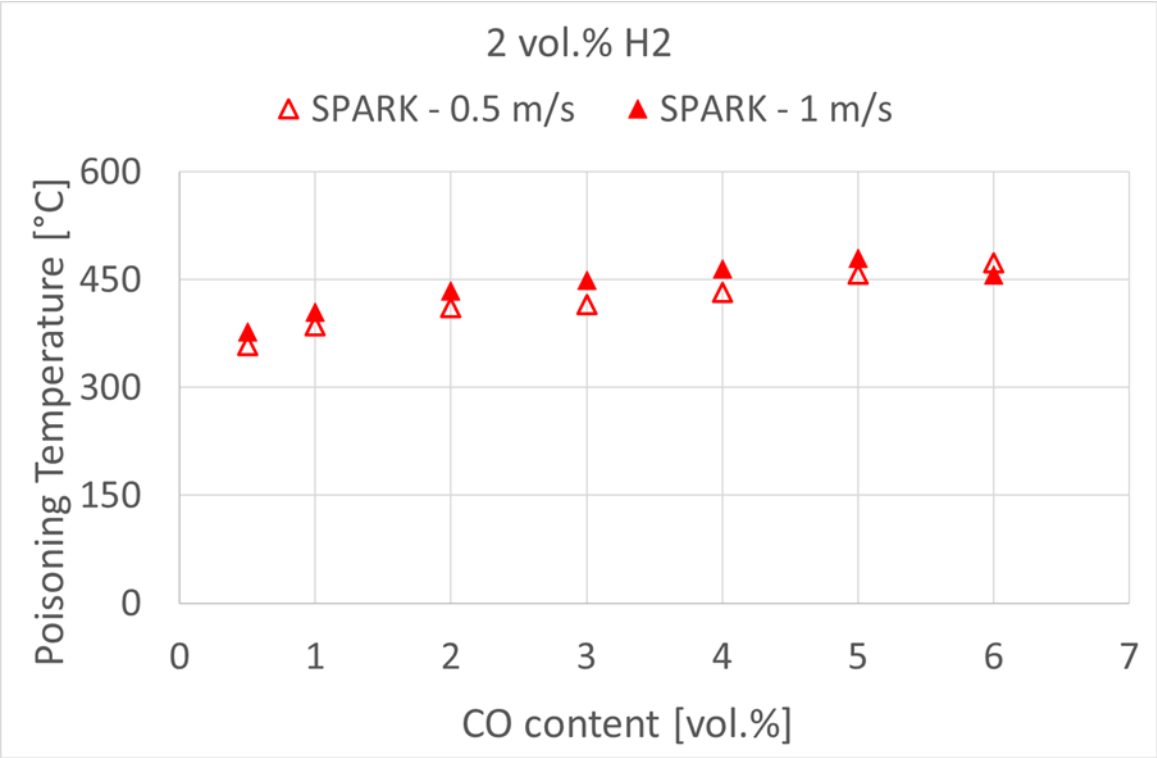

Figure 59: Poisoning temperature predicted by SPARK versus the CO molar percent at different for two flow velocities: 0.5 m/s and 1 m/s. P_{ini} = 1 bar.

Impact of inlet gas temperature on the poisoning temperature

Figure 60 show the impact of the initial inlet gas temperature on the poisoning of a mixture of 4 vol.% H_2 for different carbon monoxide concentrations using a platinum catalyst. Figure 60 shows the carbon monoxide concentration and not fraction as the previous one in order to compare the different gas temperatures. The circle represents the case where the initial gas temperature was 20°C, triangle for 80°C and squares for 150 °C. For this type of catalyst, the inlet gas temperature seems to have no impact on the poisoning temperature.

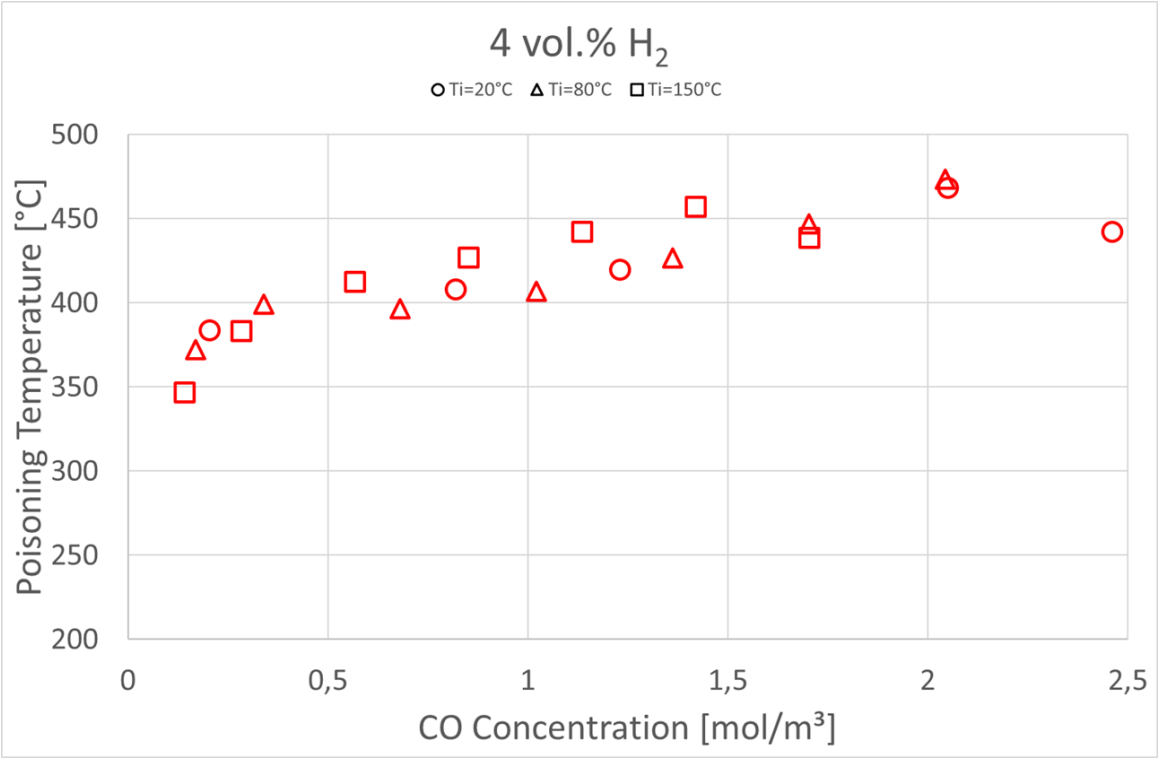

Figure 60: Catalyst poisoning temperature predicted by SPARK at different carbon monoxide concentrations for three initial gas temperatures: 20°C, 80°C and 150 °C.

Impact of steam content on the poisoning temperature

Figure 61 represents the effect of steam on the deactivation for a mixture of 4 vol.% H_2. The red triangles represent the case where there is no steam and the initial gas temperature is 80°C while the purple triangles represent the case with steam at 100 % relative humidity at 80°C. The deactivation occurs at a higher temperature when the catalyst is under steam conditions.

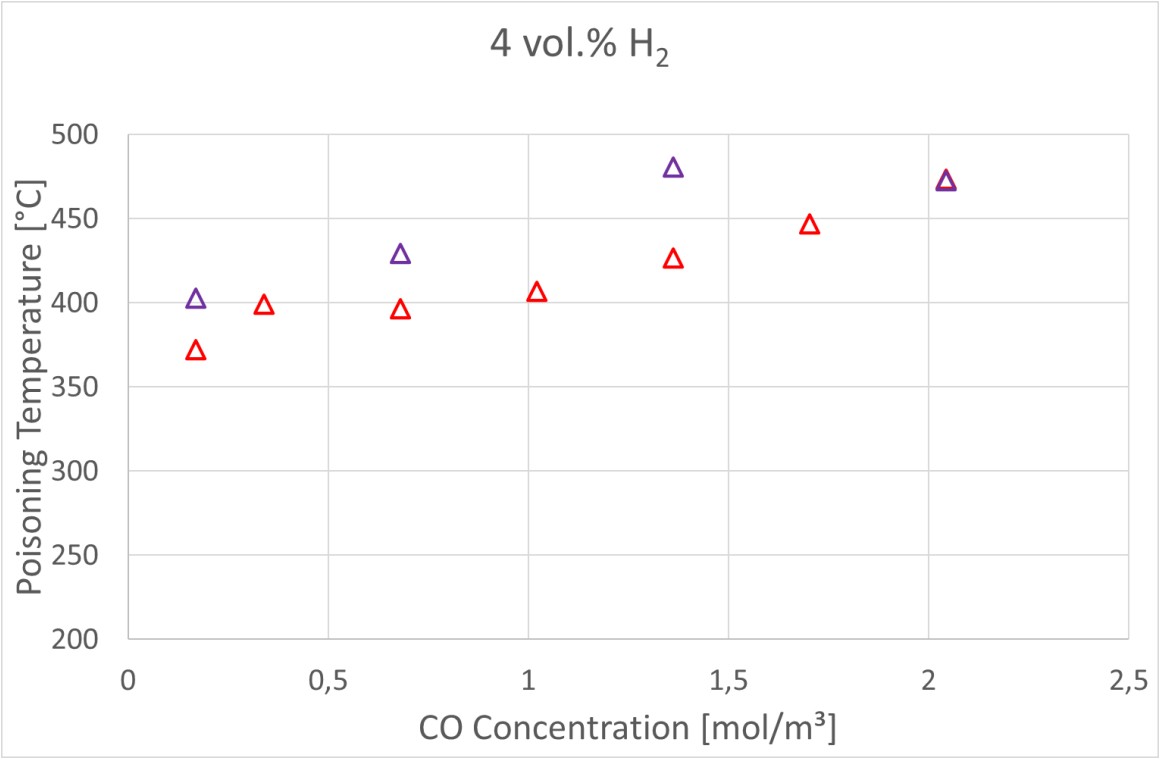

Figure 61: Catalyst poisoning temperature predicted by SPARK at different carbon monoxide concentrations for dry test and test with steam.

O_2 content when catalyst deactivation occurs

Figure 62 represents the oxygen fraction at beginning of catalyst deactivation for each hydrogen and carbon monoxide mixture. The oxygen fraction when catalyst deactivation occurs increases with H_2+CO content and decreases with inlet gas temperature.

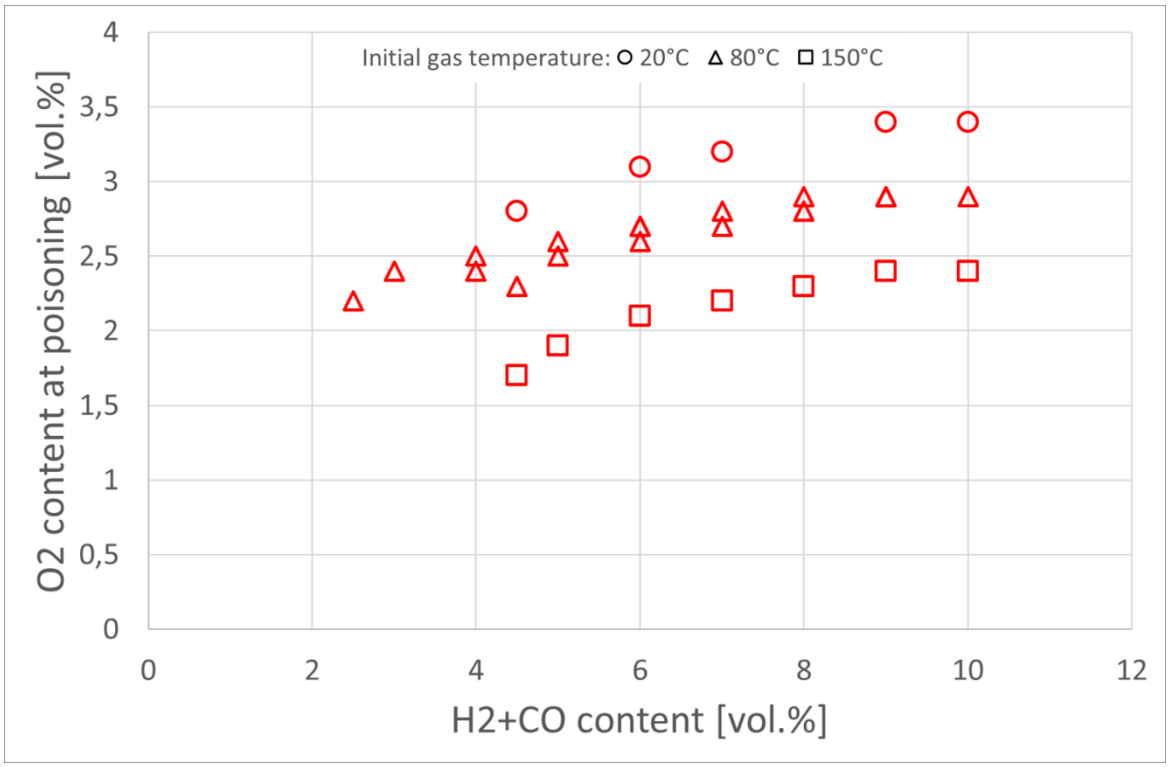

Figure 62: Oxygen content at poisoning versus the H_2+CO molar percent at different initial gas temperatures predicted by SPARK. P_{ini} = 1 bar.

5.3.2. Comparison with experimental data

Figure 63 represents the comparison between the data obtained from the experiments performed at REKO-1 and SPARK results using REKO-3 geometry since this geometry is more suitable for the calculations and more representative of a real recombiner. The open symbols represent the experimental results and the filled symbols the numerical results. Even though SPARK predicts the poisoning at a higher temperature, it is possible to observe that the deactivation trend is similar to the one observed on a single catalyst sample. This difference in the temperature can be explained by the fact that, with REKO-1 facility, the heat losses are more important due to its geometry.

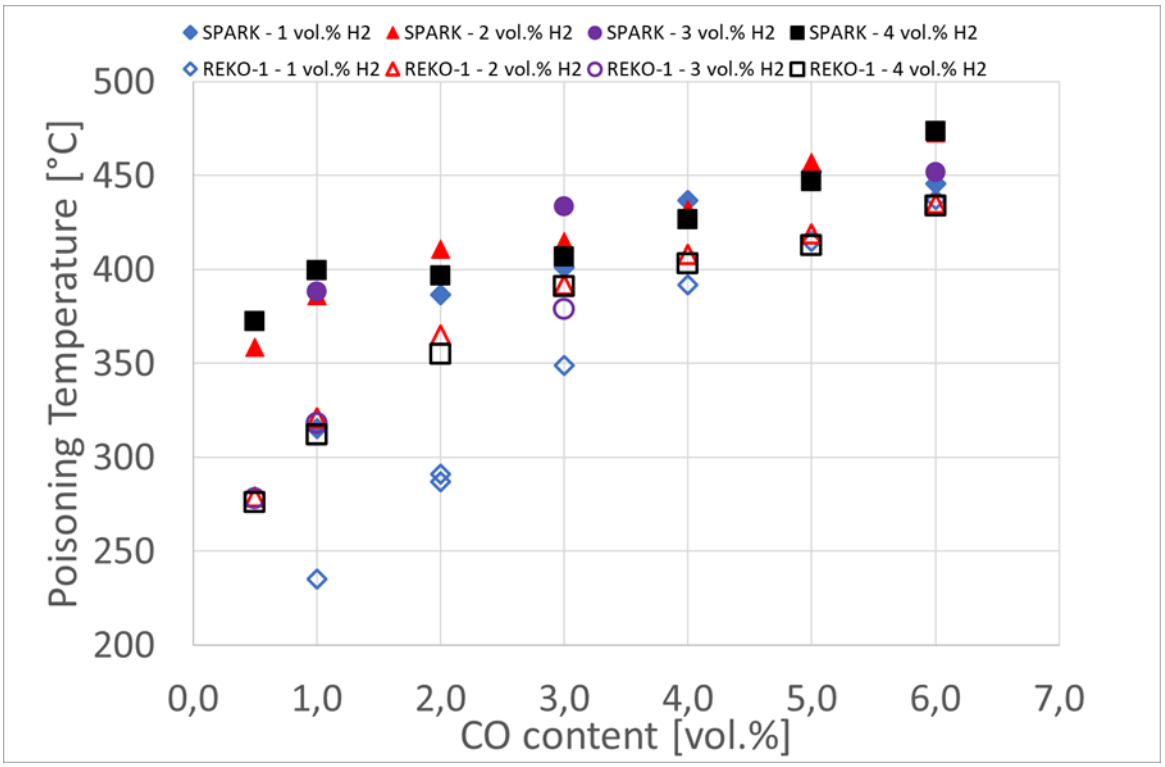

Figure 63: Evolution of the poisoning Temperature versus the CO molar percent at different H2 content. Comparison between experiments (open symbols) and simulation (solid symbols). P_{ini} = 1 bar.

The comparison of the experimental and numerical results for the effect of the flow velocity on the poisoning temperature is showed in Figure 64. Once again, the experimental data is obtained from REKO-1 and the simulations using REKO-3 geometry, explaining the discrepancy in the temperature values. However, the catalyst presents the same behavior.

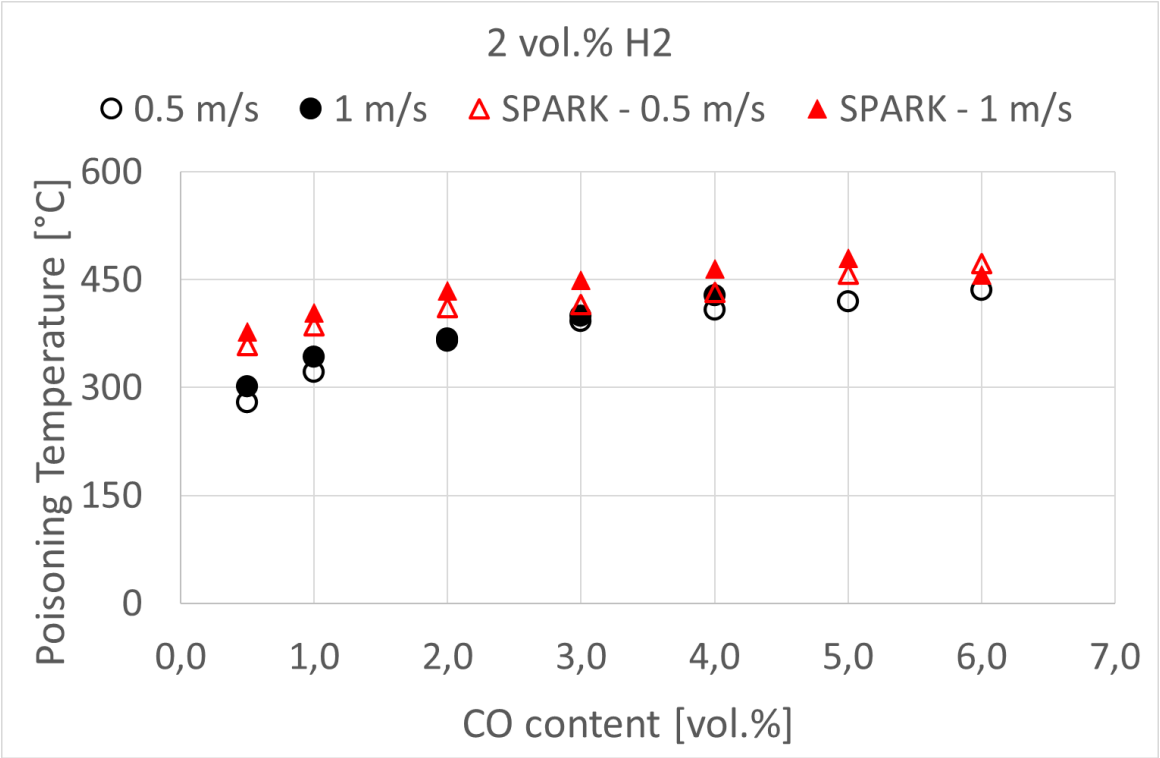

Figure 64: Evolution of the poisoning temperature versus the CO molar percent at different flow velocities: 0.5 m/s and 1 m/s. Comparison between experimental results and SPARK simulation. P_{ini} = 1 bar.

Figure 65 indicates the poisoning temperature for a mixture of 4 vol.% H_2 for each carbon monoxide concentration and different initial gas temperatures for platinum catalyst. The black symbols represent the results obtained from REKO-1, the orange symbols the results from REKO-3 and the red ones from the results calculated with SPARK. The poisoning temperature predicted by SPARK seems to be coherent with the ones measured at REKO-3. Even though the simulated temperature is higher than the ones measured at REKO-1, it can be noted that the both curves have the same trend, and the temperature difference can be explained by the heat losses due to REKO-1 geometry.

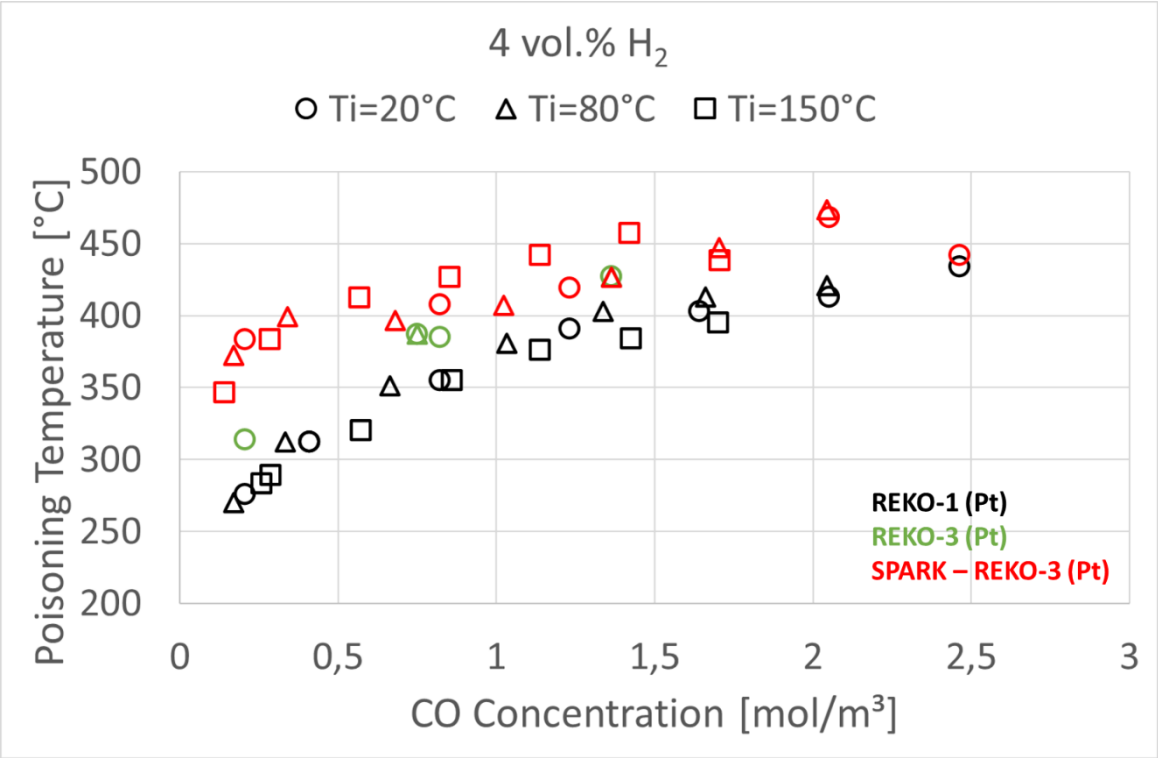

Figure 65: Catalyst poisoning temperature at different carbon monoxide concentrations for three initial gas temperatures: 20°C, 80°C and 150 °C. Comparison of data obtained at REKO-1, REKO-3 and simulated with SPARK.

5.4. Conclusion

In order to enhance the knowledge on the impact of carbon monoxide on the catalyst behavior, experiments have been performed at the REKO facilities. In a first scoping test series, the deactivation conditions of a single catalyst sample have been investigated in the REKO-1 facility. For this purpose, platinum- and palladium-based catalyst samples have been exposed to mixtures of hydrogen, carbon monoxide, air, nitrogen and steam at different temperatures and flow velocities. The experiments revealed that the poisoning can be predicted by the carbon monoxide fraction, the oxygen fraction and the catalyst temperature. Furthermore, the palladium catalyst is deactivated at lower catalyst temperatures than the platinum catalyst. The results show that the catalyst temperature in which the platinum is poisoned is independent from the gas temperature, while for the palladium catalyst the gas temperature seems to influence the poisoning temperature. In a second step, the REKO-3 facility is used to study the effect of carbon monoxide on a section of a recombiner with four full scale catalyst sheets arranged

vertically inside a rectangular channel. These experiments provide data for the further enhancement of numerical codes in the framework of the AMHYCO project and the SPARK code.

SPARK simulations for H_2/CO/air mixtures were performed and the impact of different parameters was analyzed. The comparison of the simulations with the numerical results reveals that SPARK code is able to reproduce catalyst deactivation by CO, and notably to capture the transition from partial to complete deactivation. The code predicts higher poisoning temperature than the ones observed in the experiments.

Even though a new reaction mechanism for H_2/CO on palladium was presented, the calculations could not be finished, and more experimental data is necessary to validation. This will be addressed in future work.

6. EFFECT OF CABLE FIRES ON THE CATALYST START- UP

Products of cable fires can also induce catalyst deactivation, leading to start-up delay. The deactivation is due to the significant amount of aerosols alongside specific combustion gases (e.g. CO, CO_2) released into the containment. In order to further understand how products of cable fires influence the start of the recombination reaction, experiments have been performed at the REKO-Fire platform (see section 3.4).

This chapter provides a comprehensive overview of the findings regarding the catalyst start-up behavior for three different fire regimes and for both catalyst materials used. The presentation of the results is structured according to the respective fire regimes and compares the results of the different catalyst materials within each of them. At the end of each subsection, the main start-up characteristics of all the tests carried out in this particular regime are summarized in the form of a table.

6.1. Well-ventilated regime

Experimental results of the tests with well-ventilated combustion with excess air for the two catalysts are given in Figure 66 and Figure 67. The history plots illustrate the gas temperature above the catalyst foil as an indicator of catalyst behavior (red curve, values of the primary ordinate axis), the hydrogen inlet concentration (blue line, secondary ordinate axis) and the CO_2 and CO outlet concentrations (purple and green lines, secondary ordinate axis) over time.

Figure 66 shows the experiment RF-A-07 performed with a Pt catalyst. After switching from bypass to reaction tube operation at about 14,400 s, the gas temperature inside the reaction tube increases from ~75 °C to ~90 °C due to the introduction of the hot combustion gases. Steady-state combustion conditions are established at approx. 15,000 s at ~2.0 vol.% CO_2 and very low CO concentration close to the detection limit.

At about 16,000 s, hydrogen injection starts at a level of ~1.0 vol.%. The sharp drop in CO_2 concentration during the H_2 injection phase is due to the change in the addition of the hydrogen/air mixture. The instantaneous increase in gas temperature above the catalyst of ~15 K indicates that the exothermic catalytic conversion of H_2 to H_2O starts without any delay.

At about 17,600 s, H_2 is injected for a second time period, this time at a lower concentration (~0.65 vol.%). Again, an instantaneous start of the reaction can be observed from the instantaneous increase in the gas temperature. At this point, however, the sharply decreasing CO_2 concentration indicates that the combustion process of the cable is almost complete and no more combustion gases are being produced. Shortly thereafter, the experiment is terminated and the gas temperature drops as a result of the now gradually decreasing furnace temperature.

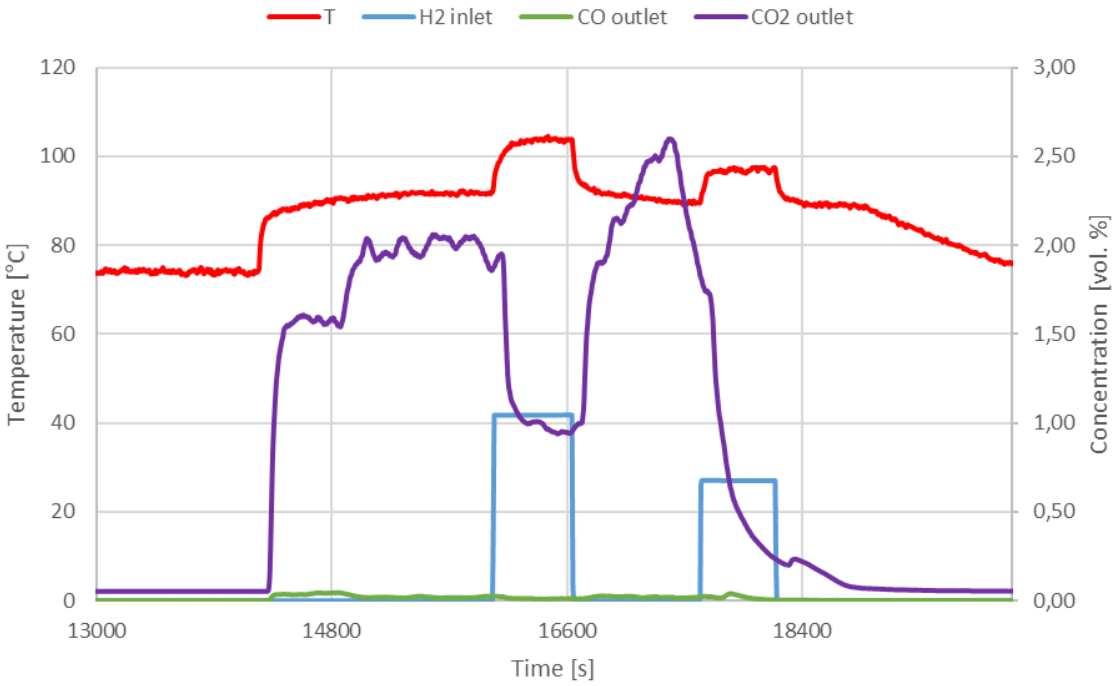

Figure 66: Pt catalyst behavior during well-ventilated combustion (RF-A-07)

Figure 67 shows experiment RF-B-04 performed with a palladium catalyst under the same combustion conditions and similar experimental procedure. Note, however, that during H_2 injection in the experiments with the Pd-based catalyst, the secondary air flow was reduced by the same amount in order not to further dilute the combustion gas (CO and CO_2 volumetric fractions in this diagram). After the catalyst foil is exposed to the combustion products, three hydrogen injection phases are performed from ~17,400 s, ~18,900 s and ~20,350 s. The hydrogen content is subsequently diminished with each new injection phase from 1.0 vol.% to 0.5 vol.% and 0.25 vol.%. In each of these cases, catalyst start-up occurs immediately after start of the injection as indicated by the temperature measurement. Again, the end of the cable combustion process is indicated by the final drop of the CO_2 concentration starting at ~20,500 s during the third hydrogen injection.

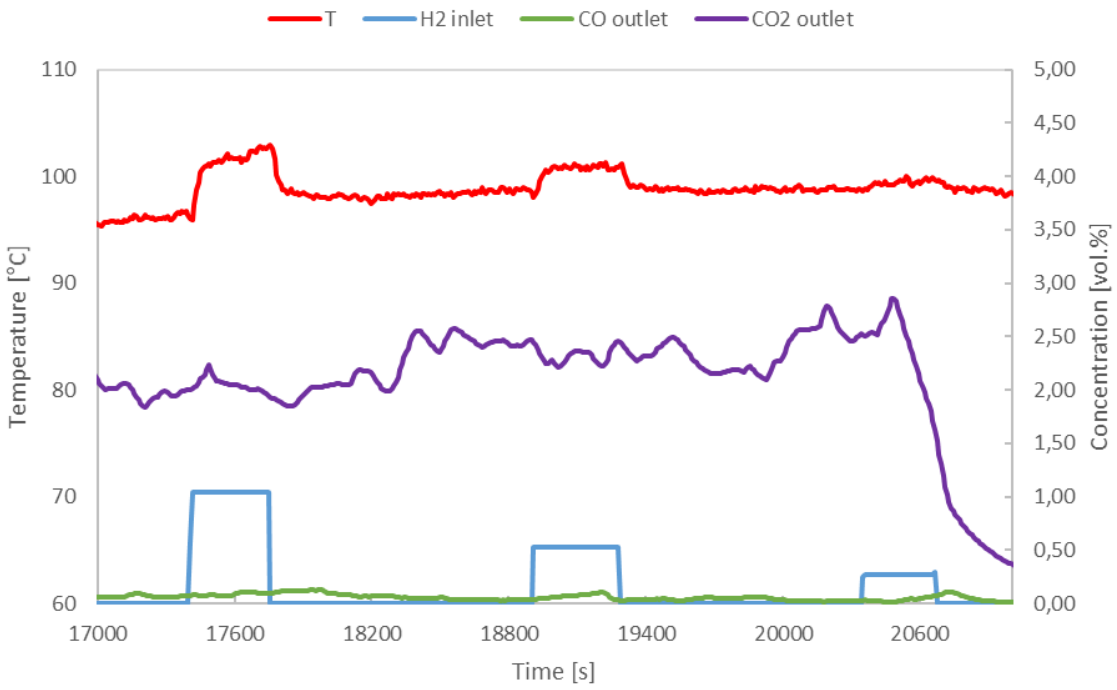

Figure 67: Pd catalyst behavior during well-ventilated combustion (RF-B-04)

Table 13 summarizes the findings of all tests performed under well-ventilated cable fire. The given concentration values for CO, CO_2 and O_2 are average values measured during the corresponding hydrogen injection phase. No impairment of the catalyst behavior has been observed in either case. Neither gaseous (CO_2 in relatively large amounts and very little CO) nor particulate (mainly soot) cable fire products obtained from well-ventilated cable combustion seem to affect the onset of the catalytic H_2 conversion of both Pt and Pd-based catalysts.

Table 13: Summary of catalyst start-up behavior in well-ventilated combustion (green: immediate start-up, orange: delayed start-up, red: no start-up)

			CO / vol.%	CO2 / vol.%	O2 / vol.%	H2 / vol.%
well ventilated	Pt	RF-A-02	0.01	1.01	19.23	1.00
			0.02	1.21	18.94	0.67
		RF-A-07	0.01	1.15	19.32	1.00
			0.02	0.75	19.93	0.68
	Pd	RF-B-01	0.09	2.05	18.15	1.00
			0.07	2.31	17.83	0.50
			0.03	2.43	17.63	0.25
		RF-B-04	0.11	2.04	18.11	1.00
			0.09	2.07	18.10	0.50
			0.03	2.89	16.97	0.25

6.2. Under-ventilated regime

Figure 68 and Figure 69 illustrate the experimental results of the tests with under-ventilated cable fire for both Pt and Pd-based catalysts. Under-ventilated combustion conditions are obtained with a reduced primary air flow. Characteristic for these tests is the significant lower CO_2/CO ratio compared to well-ventilated combustion.

Figure 68 shows the experiment RF-A-08 performed with a Pt catalyst. Before exposing the catalyst to the cable fire products, a brief hydrogen injection is performed in order to confirm that the catalyst sample is active (~14,350 s). Switching from bypass to reaction tube operation at about 16,200 s leads to an increase of both CO_2 and CO concentrations, which both reach steady-state values at approx. 17,600 s (~1.0 vol.% CO_2 and ~0.2 vol.% CO). When hydrogen injection starts at about 19,200 s at a level of ~1.0 vol.%, no increase of the gas temperature above the catalyst sample is observed. Obviously, the present cable fire products inhibit the catalytic hydrogen recombination. In subsequent steps, the hydrogen volumetric fraction is increased to ~1.5 and ~2.0 vol.%, but the catalyst remains inactive.

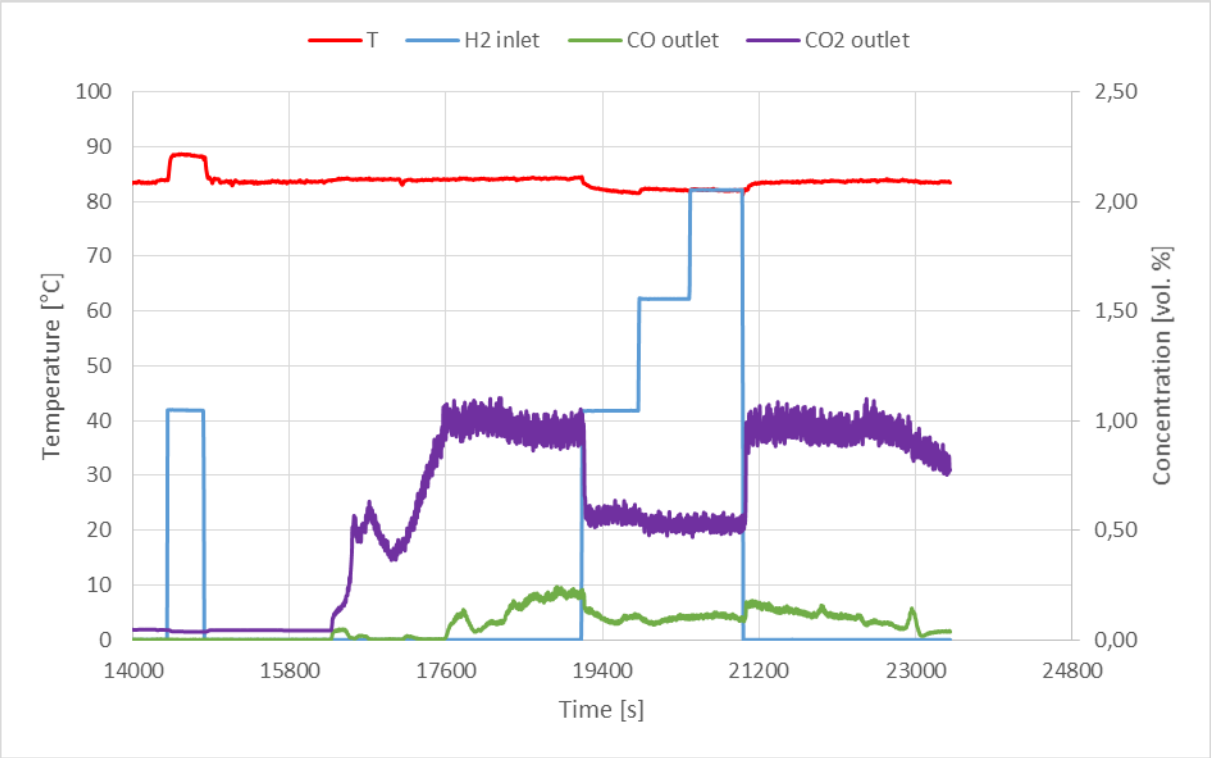

Figure 68: Pt catalyst behavior during under-ventilated combustion (RF-A-08)

Figure 69 shows experiment RF-B-05 performed with a palladium catalyst under the same combustion conditions and similar experimental procedure. As in all experiments with Pd-based catalysts, the secondary air flow is reduced during H_2 injection, in order to keep the combustion gas concentrations at constant level. After the catalyst foil is exposed to the combustion products, two hydrogen injection phases are performed from ~14,400 s and ~15,250 s at 1 vol.%. In both cases, catalyst start-up occurs immediately after start of the hydrogen injection as indicated by the temperature measurement. However, when a third hydrogen injection is performed at a reduced hydrogen concentration of 0.5 vol.% (~16,200s), the catalyst remains inactive.

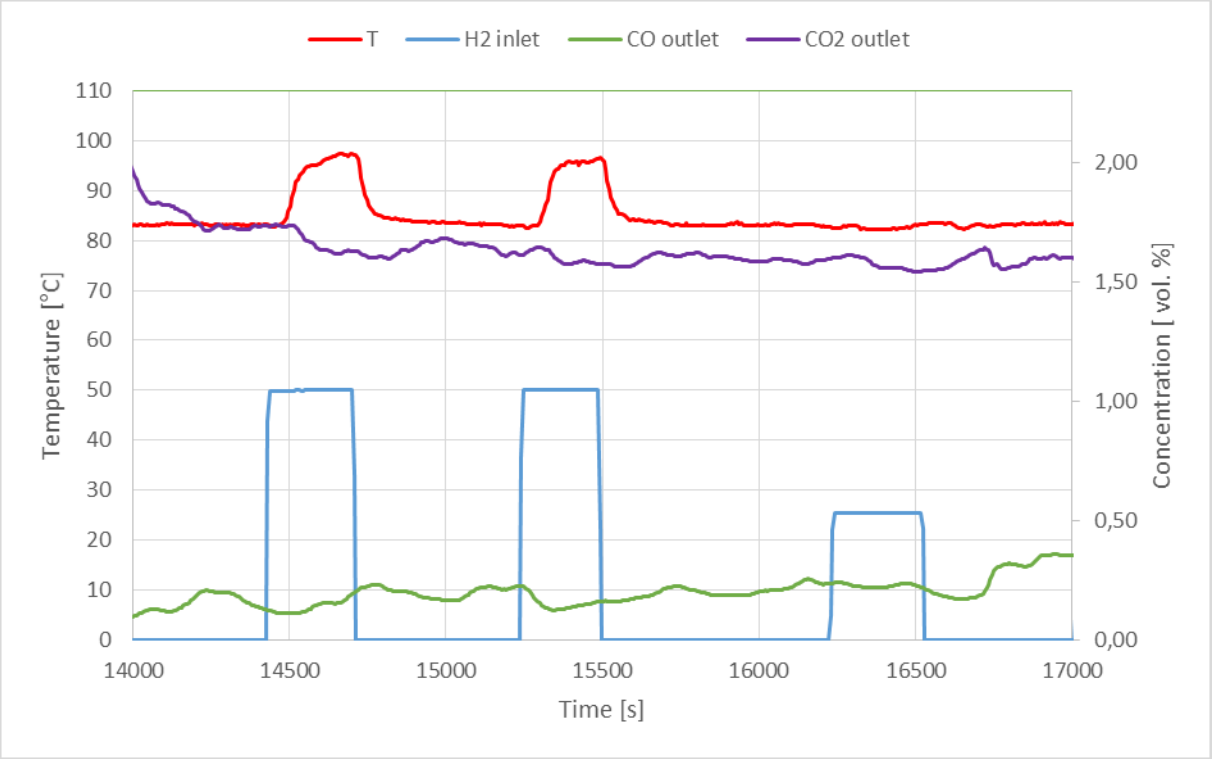

Figure 69: Pd catalyst behavior during under-ventilated combustion (RF-B-05).

The results of all tests performed with under-ventilated cable fire are summarized in Table 14. The given concentration values for CO, CO_2 and O_2 are average values measured during the corresponding hydrogen injection phase. While the Pt-based catalyst is significantly affected by the cable fire products, only minor impairment of the Pd-based catalyst is observed. As CO_2 can be ruled out as possible deactivating agent (see results under well-ventilated fire conditions), CO could be responsible for the deactivation of the Pt-based catalyst. Only in test RF-A-05, the catalyst managed to start with significant delay after increasing the hydrogen

concentration to 2 vol.%. Although the conditions for Pd-based catalyst were similar, the only impairment could be observed when the hydrogen concentration had a very low value (0.5 vol.%). The insensitivity of the Pd catalyst to the conditions of an under-ventilated cable fire compared to the Pt-based catalyst is an interesting observation.

Table 14: Summary of catalyst start-up behavior in under-ventilated combustion (green: immediate start-up, orange: delayed start-up, red: no start-up)

			CO / vol.%	CO2 / vol.%	O2 / vol.%	H2 / vol.%
under ventilated	Pt	RF-A-05	0.11	0.60	19.94	1.00
			0.08	0.45	20.19	1.28
			0.06	0.39	20.29	1.44
			0.05	0.45	20.22	1.69
			0.03	0.50	20.19	2.00
		RF-A-08	0.11	0.58	20.08	1.00
			0.09	0.53	20.16	1.56
			0.11	0.53	20.14	2.05
	Pd	RF-B-02	0.13	0.64	20.37	1.00
			0.09	0.63	20.40	1.00
		RF-B-05	0.14	1.68	18.45	1.00
			0.15	1.60	18.51	1.00
			0.23	1.58	18.46	0.50

6.3. Oxidative pyrolysis

Experimental results of tests with oxidative pyrolysis conditions are given in Figure 70 and Figure 71 for both Pt and Pd-based catalysts. The conditions inside the furnace yield low concentrations of CO and CO_2.

Figure 70 shows the experiment RF-A-06 performed with a Pt catalyst. Before exposing the catalyst to the cable fire products, a brief hydrogen injection is performed in order to confirm that the catalyst sample is active (~8,000 s). Switching from bypass to reaction tube operation at about 12,400 s leads to only minor increase of both CO_2 and CO concentrations.

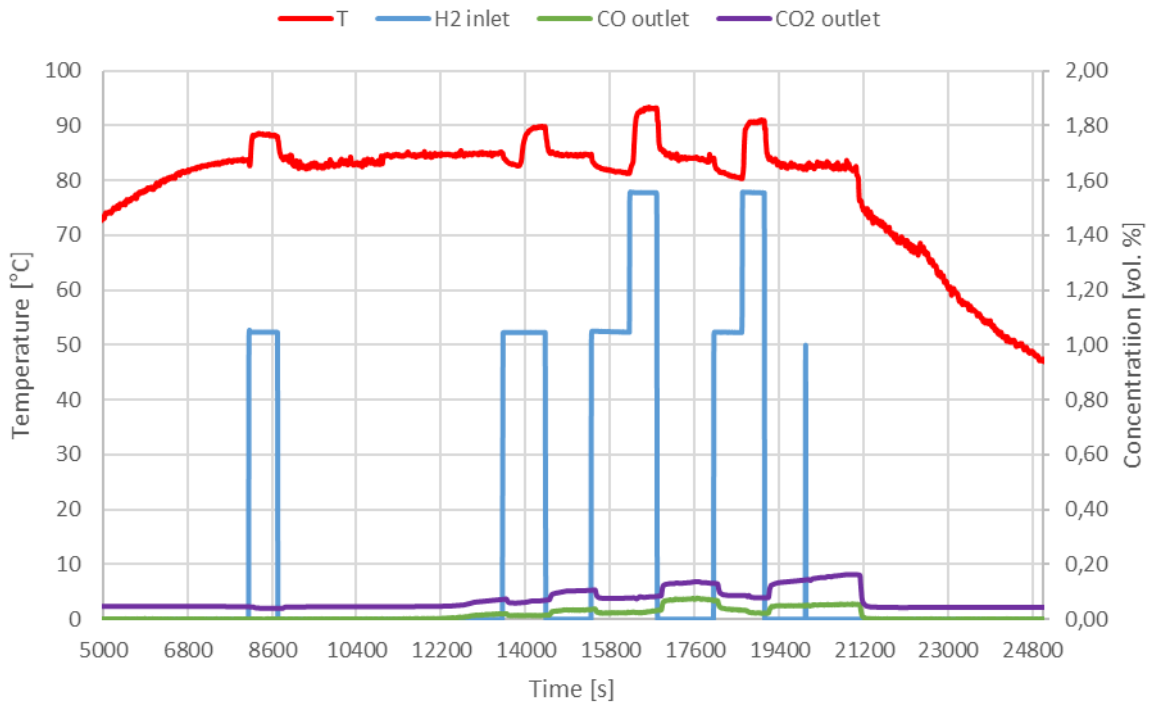

Figure 70: Pt catalyst behavior during oxidative pyrolysis (RF-A-06).

After the first hydrogen injection (1 vol.%, ~13,500 s), the catalyst starts with a delay of ~6 min. After the second injection (1 vol.%, ~15,400 s), no start-up is observed for 15 min. When the concentration is increased to 2 vol.%, the catalyst is immediately activated (~16,200 s). This procedure is repeated a second time with similar outcome (~18,000 – 19,100 s).

Similar observations are made in experiment RF-B-06 under oxidative pyrolysis conditions with a Pd-based catalyst (Figure 71). Several times, start-up delay is observed, e.g. in the first injection phase (~12,600 – 13,800 s) when the inlet hydrogen concentration needs to be increased to 2 vol.% to activate the catalyst. In a second injection series (~17,400 – 19,000 s), no start-up is observed at all. However, in-between injections of 1 vol.% hydrogen exhibit immediate or at least slightly delayed start-up of the catalyst.

Figure 71: Pd catalyst behavior during oxidative pyrolysis (RF-B-06).

Table 15 gives an overview of the results obtained in all tests performed under oxidative pyrolysis. As we expect particulate deposition on the surface to be the origin for possible catalyst deactivation, the time of exposure before the corresponding hydrogen injection has started is given. However, the overall picture remains unclear. Indeed, it is obvious that deactivation and start-up delay occur for both types of catalysts. There is also indication that the deactivation is more severe if the catalyst is exposed to the CFPs during a longer time. However, no distinct conclusion can be taken from the experimental data.

Table 15: Summary of catalyst start-up behavior under oxidative pyrolysis (green: immediate start-up, orange: delayed start-up, red: no start-up)

			time / min	CO / vol.%	CO2 / vol.%	O2 / vol.%	H2 / vol.%
oxidative pyrolysis	Pt	RF-A-06	15	0.01	0.06	20.94	1.00
			16	0.02	0.08	20.92	1.00
			24	0.03	0.08	20.91	1.55
			20	0.04	0.09	20.86	1.00
			28	0.03	0.08	20.90	1.55
		RF-A-09	5	0.02	0.06	20.95	1.00
			13	0.02	0.08	20.89	1.00
			15	0.03	0.09	20.86	1.00
			18	0.03	0.09	20.84	1.55
			15	0.04	0.09	20.81	1.00
			43	0.05	0.13	20.74	1.00
			46	0.04	0.13	20.75	1.55
		RF-A-10	20	0.04	0.10	20.74	1.00
			15	0.05	0.13	20.66	1.00
			40	0.08	0.14	20.49	1.00
	Pd	RF-B-03	15	0.04	0.11	20.89	1.00
			22	0.08	0.14	20.73	1.00
		RF-B-06	15	0.09	0.13	20.69	1.00
			20	0.09	0.13	20.78	1.00
			28	0.07	0.11	20.80	1.50
			33	0.06	0.11	20.66	2.00
			5	0.06	0.15	20.52	1.00
			15	0.08	0.21	20.52	1.00
			30	0.10	0.27	20.58	1.00
			35	0.09	0.26	20.61	1.50
			40	0.09	0.26	20.56	2.00
			25	0.07	0.30	20.68	1.00
			30	0.05	0.24	20.37	1.00
		RF-B-07	15	0.05	0.12	20.85	1.00
			30	0.07	0.13	20.80	1.00
			38	0.05	0.10	20.85	1.50
			44	0.05	0.11	20.86	2.00
			20	0.08	0.21	20.71	1.00
			28	0.08	0.21	20.73	1.50
			39	0.09	0.22	20.73	2.00

6.4. Conclusion

Three different fire conditions have been considered. For well-vented cable fire, neither gaseous (CO_2 in relatively large amounts and very little CO) nor particulate (mainly soot) CFPs seem to affect the onset of the catalytic H_2 conversion for both Pt and Pd-based catalysts. In under-ventilated fire conditions, different effects on both types of catalysts can be observed. The Pt-based catalyst is significantly deactivated, while the only impairment for the Pd-based catalyst is observed at a hydrogen concentration as low as 0.5 vol.%. Higher CO levels when compared with well-ventilated cable fires are suspected to be the reason for the observed deactivations. For products generated from oxidative pyrolysis, deactivation and start-up delay can occur for both catalyst types due to the physical blockage of the catalytic surface.

As a preliminary conclusion, the presence of carbon monoxide in the atmosphere as well as particulate depositions from cable pyrolysis seem to be two relevant mechanisms for catalyst deactivation. As cable fires could act as initiating event, the catalysts might be affected by corresponding CFPs before the actual severe accident occurs. As a consequence, hydrogen mitigation by PARs might be significantly delayed.

7. IMPACT OF OIL ON THE RECOMBINATION START-UP

Projections of oil coming from primary pumps have been found on catalytic plates in French nuclear power plants during PARs periodic controls. The oil partially covered the plates, with up to 85% of coverage of the catalytic surface. It is not known if the oil could just cause start-up delay, permanently damage the catalyst sheets leading to their deactivation and loss of efficiency, or if it is just a harmless deposit that could be handled with the heating of the catalyst. In this context, tests regarding the presence of oil on the catalyst sheets have been carried out in the REKO-4 facility and the results are presented in this chapter.

7.1. Results

The reference test, in which all the catalysts are without oil deposition, is shown in Figure 72. The dotted green line represents the value registered by the hydrogen sensor placed at the inlet while the full green line represents the sensor placed at the outlet of the recombiner. The dark green line is the temperature measured by the thermocouple at the outlet of the recombiner. The vessel atmosphere is at ambient temperature when the hydrogen is first injected until 4 vol.% at a flow rate of 0.2 m^3/h. The temperature starts increasing at the same time as the hydrogen concentration at the outlet of the recombiner decreases, indicating that the recombination of hydrogen into steam has started. After the hydrogen concentration inside the vessel reaches 4 vol.%, the injection automatically stops. The decrease in the hydrogen fraction at the inlet indicates the recombination rate. This procedure has been repeated three times for reproducibility. The results allow to identify possible start-up delay for the upcoming tests.

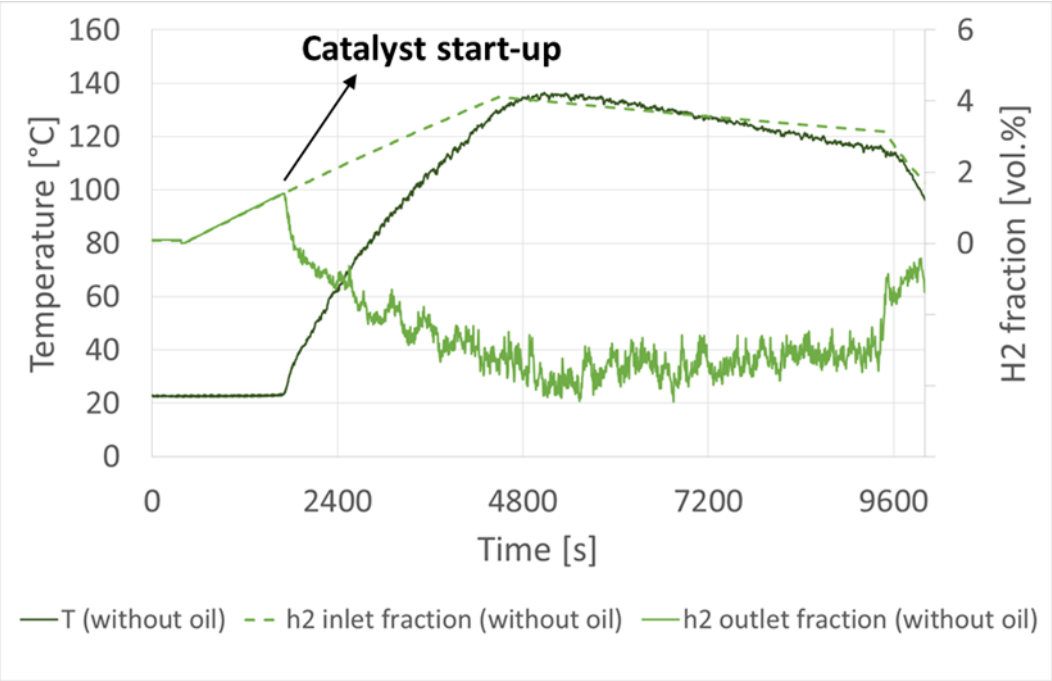

Figure 72: Behavior of catalyst without oil deposition under natural flow conditions (Reference test)

The behavior of the catalyst completely covered with oil is shown in Figure 73. The dotted red line shows the hydrogen fraction at the inlet while the full red line represents the content of H_2 at the outlet of the recombiner. The temperature is represented by the dark red line. The hydrogen is injected until it reaches the fraction of 4 vol.% inside the vessel. The measurements indicate that hydrogen is not recombined. Since the reaction did not started, around 5000 s the temperature of the vessel was increased to 80°C. After temperature increase, there was still no start-up. The temperature was not further increased due to facility limitations. The results indicate that if the entire catalytic surface is blocked by the oil, hydrogen and oxygen will not reach the active sites, therefore will not be converted.

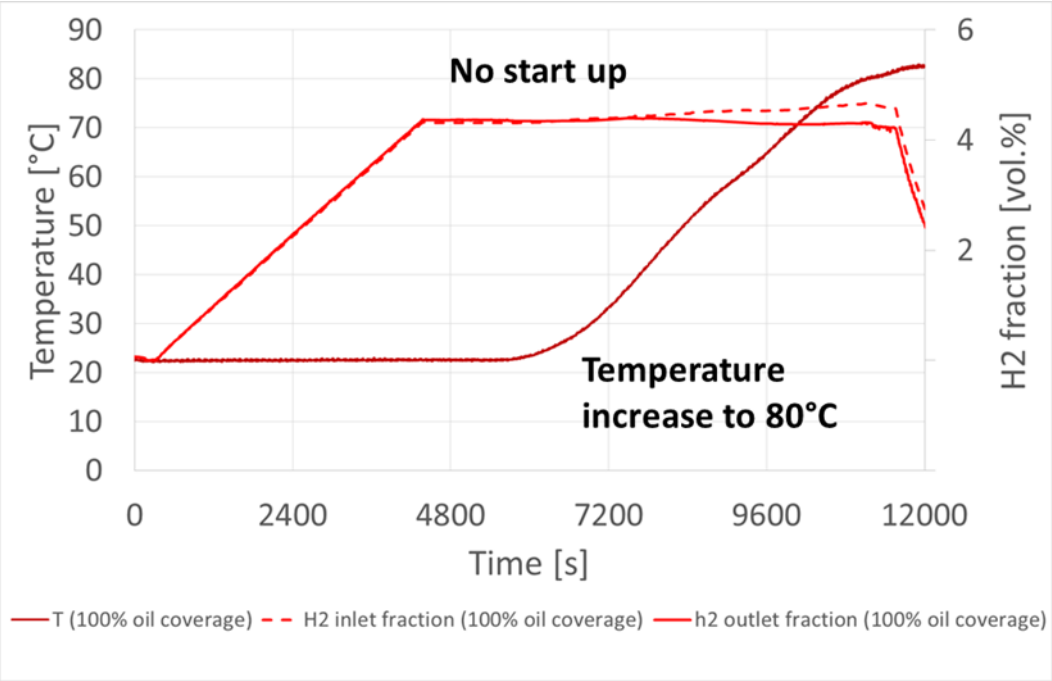

Figure 73: Behavior of catalyst with oil deposition on the entire surface.

In a next step, oil was applied to the two catalyst samples placed on the edge of the holder, while the middle one was unpolluted. Figure 74 exemplifies the behavior of the recombiner. The blue dotted line represents the hydrogen fraction at the inlet and the blue full line the value of the hydrogen sensor at the outlet of the small recombiner. The dark blue line corresponds to the temperature at the outside the recombiner along the time. Hydrogen is injected until the concentration reaches 4 vol.% inside the vessel. One can see an increase in temperature and decrease of the hydrogen fraction at the outlet of the recombiner around 2000 s, meaning that a reaction occurs. Later, there is a second increase of temperature and further reduction of the hydrogen fraction. This behavior indicates that the clean catalyst started the conversion of hydrogen around 2000 s and the heat released by the reaction was enough to heat the other two polluted catalyst, evaporating the oil. Once the oil was no longer blocking the active sites of the catalyst, the hydrogen could be recombined by those initially contaminated catalyst samples. After the hydrogen fraction of 4 vol.% was achieved, the injection stopped and the decrease of the hydrogen content at the inlet indicates the recombination rate.

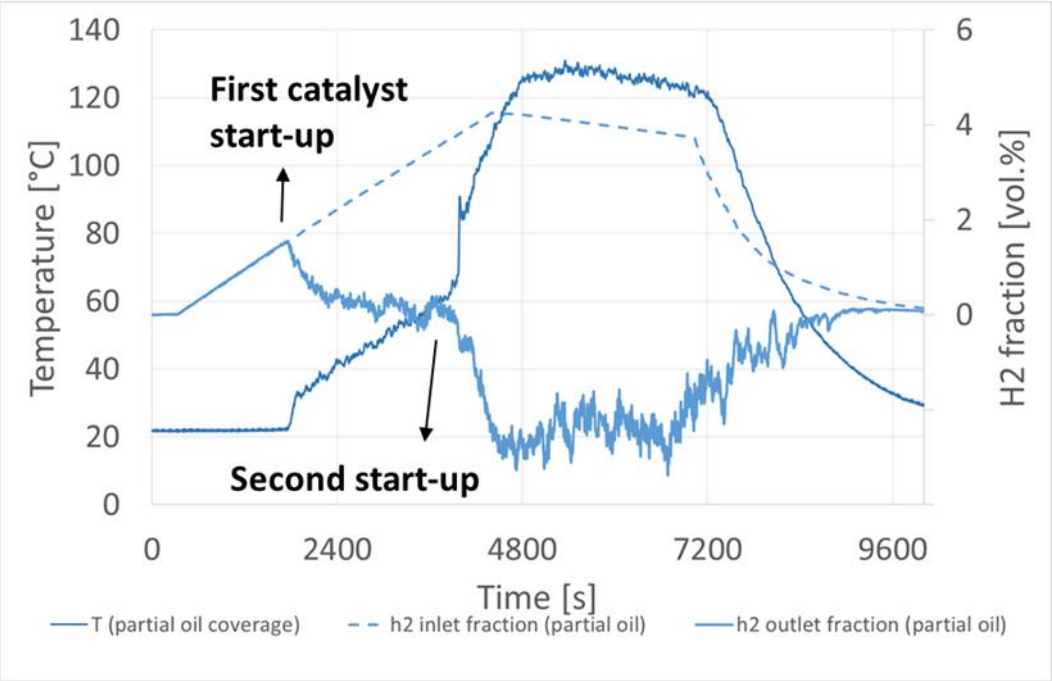

Figure 74: Behavior of recombiner with one catalyst without oil deposition in the middle and two polluted catalysts

Figure 75 compares the results obtained in the reference test and the experiment with two polluted catalysts. It can be noted that after the injection of hydrogen was stopped, both fractions of hydrogen in the inlet decrease at the same rate, indicating the same reaction rate.

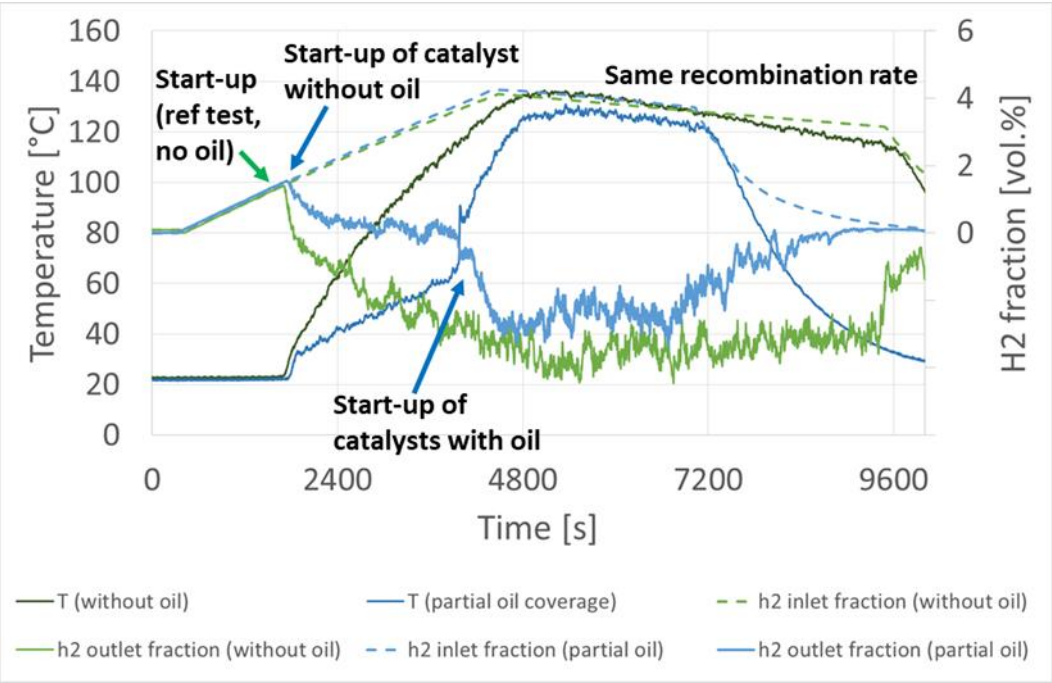

Figure 75: Comparison of reference test and test with partial oil coverage

7.2. Conclusion

Oil has been applied on platinum-based catalyst in order to investigate its impact on the behaviour of the recombiner. The results show that the catalyst is not able to convert hydrogen when the surface is entirely covered with oil and the temperature is not high enough to evaporate and/or burn off the oil. However, when only one catalyst was not covered with oil, the heat from the reaction of the hydrogen recombination on this sample was enough to evaporate and burn the oil off the surface of the other catalyst plates. Once the oil was no longer blocking the surface, the catalyst would start-up immediately.

Based on the results, it seems that the oil would not permanently deactivate the catalyst sheets in recombiners. Since the oil projections found in PARs were partially covering the catalytic surface, it is likely that the active sites without oil could be enough to start the hydrogen recombination, leading to the burning of the oil due to the heat released by the reaction.

8. CONCLUSION AND OUTLOOK

In case of a severe accident, a large amount of combustible gases (hydrogen and carbon monoxide) can be produced and form an explosive mixture in the reactor building. The induced combustion may threaten the reactor containment integrity, as well as safety-relevant systems. In order to prevent the hydrogen risk, passive autocatalytic recombiners have been installed in many nuclear power plants, notably in France and Germany. Recombiners are passive devices that were initially aiming at recombining hydrogen through an exothermic catalytic reaction. During normal operation and accidental scenarios, these devices can be exposed to various volatile compounds, gases and aerosols present in the atmosphere of the containment. Some of those products may cause partial or total catalyst deactivation inducing then delay in recombination start-up and reduction of the recombiner efficiency. Indeed, during the late phase (ex-vessel) of the accident, carbon monoxide can be produced with hydrogen. However, carbon monoxide may induce a poisoning of the catalyst leading to a halt to the recombination by the PARs.

For an efficient analysis of the mitigation roles of the passive autocatalytic recombiners, it is paramount to gain knowledge from experimental and analytical investigations aimed at characterizing catalyst deactivation. This thesis focuses on characterizing the conditions of deactivation of catalyst in recombiners by different products including gas, particles, and oil. It also aims to improve the models implemented in numerical tools used for safety analysis. To better understand the behaviour of PARs installed in NPPs and the deactivation mechanisms, experiments were performed at the REKO facilities at the Institute of Energy and Climate Research (IEK-6) at Forschungszentrum Juelich, Germany. The experiments focused on three potential poisoning products: carbon monoxide, combustion products from cable fires and oil used in the primary pumps in NPPs. Both scoping and post analysis were performed using the SPARK (Simulation for Passive Autocatalytic Recombiners' risK) code, a CFD code dedicated to the numerical simulations of catalytic recombiners developed at IRSN, for carbon monoxide poisoning tests.

Carbon monoxide is a known potential poisoning product due to its adsorption properties. The impact of carbon monoxide was investigated in the REKO-1 and REKO-3 facilities with H_2/CO/air mixtures, and two types of catalyst (platinum and palladium). In a first scoping test series, the deactivation conditions of a single catalyst sample have been investigated in the

REKO-1 facility. For this purpose, platinum- and palladium-based catalyst samples have been exposed to mixtures of hydrogen, carbon monoxide, air, nitrogen and steam at different temperatures and flow velocities. The results indicate that the poisoning process seems to be independent from the hydrogen molar fraction and it can be predicted by the carbon monoxide molar fraction, oxygen molar fraction and the catalyst temperature, which is influenced directly by the oxygen fraction under oxygen-lean conditions. Furthermore, the palladium catalyst is deactivated at lower catalyst temperatures than the platinum catalyst. The results show that the catalyst temperature in which the platinum is poisoned is independent from the gas temperature, while for the palladium catalyst the gas temperature seems to influence the poisoning temperature. The different behaviour between platinum-based and palladium-based catalysts can be attributed to the different adsorption rate of CO on the surface of the catalyst. The overall heat of the reaction lead to a different catalyst temperature. In a second step, the REKO-3 facility was used to study the effect of carbon monoxide on a section of a recombiner with four full scale catalyst sheets arranged vertically inside a rectangular channel. The results from this experimental campaign confirmed what was observed at REKO-1. These experiments provide data for the further enhancement of numerical codes in the framework of the AMHYCO project, a European project with the objective to improve the experimental knowledge and simulation capabilities in combustion risk management of hydrogen and carbon monoxide mixtures in severe accidents in nuclear power plants.

SPARK simulations for H_2/CO/air mixtures were performed and the impact of different parameters was analyzed. The comparison of the simulations with the numerical results reveals that SPARK code is able to reproduce catalyst deactivation by CO, and notably to capture the transition from partial to complete deactivation. However, the code predicts higher poisoning temperature than the ones observed in the experiments. The discrepancy between experiments and simulation can stem from different parts: (i) a need for more accurate chemistry, (ii) better consideration of heat losses that take place in the experiments, (iii) the density of active sites homogeneity along the catalyst sheets.

Even though a new reaction mechanism for H_2/CO on palladium was presented, the calculations could not be finished, and more experimental data are necessary for validation. This will be addressed in future work.

The present work objectives were mainly to produce a large database on the poisoning of the catalyst by carbon monoxide based on well-known boundary conditions. The heterogeneous chemical kinetics were addressed based on the available knowledge. In the future, an effort should be made on understanding what are the sensitivity of the elementary reactions and to identify the missing steps if any. This detailed kinetic analysis is a study in itself as we need to assess not only H2 and CO, but also the presence of unburnt hydrocarbons stemming from cable fires and oil deposition. This detailed study should rely on ab-initio calculations of heterogeneous reactions rates and identifying the important steps of H2 and CO catalytic oxidation versus temperature.

Products of cable fires can also induce catalyst deactivation, leading to start-up delay. In order to further understand how the combustion products from cable fires influence the start of the recombination reaction, experiments have been performed at the REKO-Fire facility. Platinum and palladium catalysts have been exposed to three possible fire regimes. The behavior of both catalysts was similar during two fire regimes: (i) during the well-ventilated regime, the combustion products did not seem to affect the recombination process; (ii) for the oxidative pyrolysis regime, the products physically blocked the catalyst, leading to start-up delay for both catalyst types. On the contrary, for the third regime, the products of the under-ventilated regime presented different impact for the catalysts. The palladium catalyst was not affected by the low oxidation products in this regime while the platinum-based catalyst did not start. This regime presents higher concentration of carbon monoxide, reinforcing the idea that platinum catalyst is more likable to be poisoned by carbon monoxide. The experimental campaign lead to the conclusion that the presence of carbon monoxide and the particles deposition due to the cables' pyrolysis are the two main mechanisms of deactivation.

In order to investigate its impact on the behaviour of the recombiner, oil has been applied on platinum-based catalysts. The tests were carried out in the REKO-4 facility. The results show that the catalyst is not able to convert hydrogen when the surface is entirely covered with oil and the temperature is not high enough to evaporate and/or burn off the oil. However, when only one catalyst was not covered with oil, the heat from the reaction of the hydrogen recombination on this sample was enough to evaporate and burn the oil off the surface of the other catalyst plates. Once the oil was no longer blocking the surface, the catalyst would start-up immediately.

Based on the present findings, it seems that the studied oil would not permanently deactivate the catalyst sheets in recombiners. Since the oil projections found in PARs were partially covering the catalytic surface, it is likely that the active sites without oil could be sufficiently active to start the hydrogen recombination, leading to the evaporation of the oil due to the heat released by the reaction. The presence of a film of oil blocks the active sites of the catalyst, but the recombination capacity can be restored by evaporation of the oil if a recombination reaction is initiated by a neighboring plate not covered with oil. On this topic, the future work should address the behavior of the PARs deactivation when either the oil type is varied, or the ageing of the oil. Indeed, during the ageing process, the composition of the oil is modified leading to different physical and chemical properties such as a modification of the vapor pressure, boiling point, pyrolysis and oxidation tendency.

REFERENCES

[1] D. Jacquemain et al., "Nuclear Power Reactor Core Melt Accidents - Current State of Knowledge", edp sciences, 2015.

[2] A. Bentaib, N. Meynet and A. Bleyer, "Overview on hydrogen risk research and development activities: Methodology and open issues" *Nuclear Engineering and Technology*, vol. 47, pp. 26-32, 2015.

[3] IAEA report TECDOC-1661, "Mitigation of Hydrogen Hazards in Severe Accidents in Nuclear Power Plants" 2011.

[4] A. Bentaib, A. Bleyer, N. Meynet, N. Chaumeix, B. Schramm, M. Höhne, P. Kostka, M. Movahed, S. Worapittayaporn, T. Brähler, H. Seok-Kang, M. Povilaitis, I. Kljenak und P. Sathiah, „SARNET hydrogen deflagration benchmarks: Main outcomes and conclusions," *Annals of Nuclear Energy*, Bd. 74, pp. 143-152, 2014.

[5] M. Hussaini, A. Kumar and R. Voigt., "*Major research topics in combustion"* 1991.

[6] IRSN technical information note, "Le risque associé à l'hydrogène dans les enceintes de confinement des réacteurs du parc nucléaire français", July 2011.

[7] F. Arnould, E. Bachellerie, M. Auglaire, B. D. Boeck, O. Braillard, B. Eckardt, F. Ferroni, R. Moffett and G. V. Goethem, "State of the art on hydrogen passive autocatalytic recombiner" *European union parsoar project, INIS FR0200284, 2005.* .

[8] J. A. Moulijn, A. E. Van Diepen und F. Kapteijn, "Catalyst deactivation: is it predictable? What to do?," Applied Catalysis A: General, Volume 212, Issues 1–2, Pages 3-16, 2001.

[9] A. Chakraborty, "Optimization of Passive Autocatalytic Recombiners (PARs) with respect to Gas-phase Ignition", PhD thesis, RWTH Aachen University 2017.

[10] S. Engelhardt and N. Meynet, "Analyse de l'impact de la pression et de la température sur l'inflammation d'hydrogène par les recombineurs », IPSN, rapport DSR/SAGR 2010 N°166 2010

[11] IRSN report DSR-2006-34 "Dimensionnement des système de recombineurs catalytiques d'hydrogène pour les paliers CPY et CP0*",* 2006.

[12] A. INC., « www.us.areva.com » 2011. [Online]. Available: http://us.areva.com/home/liblocal/docs/Solutions/literature/PAR%20Passive%20Autocatalyic%20Recombiner.pdf.

[13] I. Chorkendorff and J. Niemantsverdriet, "Concepts of Modern Catalysis and Kinetics" 2003.

[14] J. A. Moulijn, "Chemical kinetics of catalysed reaction" in *An Integrated Approach to Homogeneous, Heterogeneous and Industrial Catalysis*, Volume 79, Pages 69-86, 1993.

[15] D. Heidelberg, E.-A. Reinecke and H.-J. Allelein, "Systematic compilation of the present state of knowledge on the reduction of the efficiency of passive auto-catalytic recombiners caused by catalyst deactivation" 2013.

[16] E. Bachellerie, F. Arnould, M. Auglaire, B. De Boeck, O. Braillard, B. Eckardt, F. Ferroni und R. Moffett, "Generic approach for designing and implementing a passive autocatalytic recombiner PAR-system in nuclear power plant containments", 2003.

[17] F. Payot, E. A. Reinecke, F. Morfin, J. C. Sabroux, N. Meynet, A. Bentaib, P. March und R. Zeyen, "Understanding of the operation behaviour of a Passive Autocatalytic Recombiner (PAR) for hydrogen mitigation in realistic containment conditions during a severe Light Water nuclear Reactor (LWR) accident" *Nuclear Engineering and Design*, Bd. 248, pp. 178-196, 7 2012.

[18] N. Meynet, E.-A. Reinecke, S. Kelm und A. Bentaib, "Detailed experimental and numerical study of passive auto-catalytic recombiners" Proc. Second International Meeting of the Safety and Technology of Nuclear Hydrogen Production, Control and Management, American Nuclear Society, 2010

[19] F. Funke, G. Langrock, T. Kanzleiter, G. Poss, K. Fischer, A. Kühnel, G. Weber and H.-J. Allelein, "Iodine oxides in large-scale THAI tests" *Nuclear Engineering and Design 245* , vol. 245, p. 206– 222, 2012.

[20] T. Kanzleiter, "Quick Look Report Hydrogen Recombiner Tests HR-1 to HR-5, HR-27 and HR-28 Tests without steam , using an Areva PAR" 2009.

[21] AREVA NP Inc., "Qualification and Testing of the U.S. EPR Passive Autocatalytic Recombiner" 2012.

[22] S. Kelm, L. Schoppe, J. Dornseiffer, D. Hofmann, E.-A. Reinecke, F. Leistner and S. Jühe,poison "Ensuring the long-term functionality of passive auto-catalytic recombiners under operational containment atmosphere conditions—An interdisciplinary investigation" *Nuclear Engineering and Design,* vol. 239, p. 274–280, 2009.

[23] F. Morfin, J.-C. Sabroux and A. Renouprez, "Catalytic combustion of hydrogen for mitigating hydrogen risk in case of a severe accident in a nuclear power plant: study of catalysts poisoning in a representative atmosphere" *Applied Catalysis B: Environmental,* vol. 47, p. 47–58, 2004.

[24] M. Klauck, E. A. Reinecke, S. Kelm, N. Meynet, A. Bentaib and H. J. Allelein, "Passive auto-catalytic recombiners operation in the presence of hydrogen and carbon monoxide: Experimental study and model development", *Nuclear Engineering and Design,* Bd. 266, pp. 137-147, 1 2014.

[25] C. Kubelt, "Occupational health and safety when handling cable fire aerosols. Concept of cable fire aerosol generation", 2014.

[26] E.-A. Reinecke, A. Bentaïb, J. Dornseiffer, D. Heidelberg, F. Morfin, P. Zavaleta and H.-J. Allelein, "A first orienting investigation of the interaction of cable fire products with passive auto-catalytic recombiners (PARs)", *NURETH,* vol. 16, 2015.

[27] N. Meynet, "SPARK - Logiciel de calcul pour les recombineurs catalytiques", IRSN report PSN-RES/SAG/2015-00036, 2015.

[28] O. Deutschmann, R. Schmidt, F. Behrendt and J. Warnatz, "Numerical modeling of catalytic ignition," *Twenty-Sixth Symposium International on Combustion/The Combustion Institute,* p. 1747–1754, 1996.

[29] M. Rinnemo, O. Deutschmann, F. Behrendt und B. Kasemo, "Experimental and Numerical Investigation of the Catalytic Ignition of Mixtures of Hydrogen and Oxygen on Platinum" Combustion and Flame, Volume 111, Issue 4, Pages 312-326, 1997.

[30] C. H. Bartholomew, "Mechanisms of catalyst deactivation", Applied Catalysis A: General, 212, 17-60, 2001.

[31] A. Chakraborty, E. A. Reinecke, N. Meynet, A. Bentaib, N. Chaumeix und H. J. Allelein, "Investigation of ignition characteristics of passive autocatalytic recombiners" in *2017*

International Congress on Advances in Nuclear Power Plants, ICAPP 2017 - A New Paradigm in Nuclear Power Safety, Proceedings, 2017.

[32] R. Warnatz, M. D. Allendorf, R. J. Kee und M. E. Coltrin, "A Model of Elementary Chemistry and Fluid Mechanics in the Combustion of Hydrogen on Platinum Surfaces" 1994.

[33] L. Trimm, "Catalytic combustion (review)", Applied Catalysis, Volume 7, Issue 3, Pages 249-282, 1983.

[34] M. Rinnemo, M. Fassihi und B. Kasemo, "Volume 2 I 1, number 1 Chemical physics letters", 1993.

[35] M. Rinnemo, D. Kulginov, S. Johansson, K. L. Wong, V. P. Zhdanov und B. Kasemo, "Catalytic ignition in the CO-O 2 reaction on platinum: experiment and simulations", Surface Science, volume 376, Issues 1-3, Pages 297-309, 1997.

[36] U. Maas und J. Warnatz, "Ignition Processes in Hydrogen-Oxygen Mixtures", Combustion and flame 74: 53-69, 1988.

[37] S. Kelm, W. Jahn und E.-A. Reinecke, "Operational behaviour of catalytic recombiners-experimental results and modelling approaches", Proceedings of the OECD/NEA & IAEA Workshop on Experiments and CFD Codes Application to Nuclear Reactor Safety, 2008

[38] W. C. Jr. Gardiner, "Combustion Chemistry", Springer New York, 1984.

[39] O. Deutschmann, R. Schmidt, F. Behrendt und J. Warnatz, "Numerical modeling of catalytic ignition", Proc. Combust. Inst.. 26, 1996.

[40] M. Zwinkels, S. Järås und P. Menon, "Catalytic Fuel Combustion in Honeycomb Monolith Reactors", in *Structured Catalytic Reactors*, New York, 1998, p. 149

[41] E.-A. Reinecke, A. Bentaib, N. Chaumeix, A. Chakraborty, D. Heidelberg, S. Kelm, L. Maas, P.-M. Steffen, "Operating behavior of passive auto-catalytic recombiners under severe accident conditions", International Severe Accident Management Conference (ISAMC), 2018.

[42] M. Klauck, “Effects of carbon monoxide on the operation of catalytic hydrogen recombiners in light water reactor containments”, PhD Thesis, RWTH Aachen University, 2019.

[43] X. Zheng, M. Schultze, J. Mantzaras, R. Bombach, “Effects of hydrogen addition on the catalytic oxidation of carbon monoxide over platinum at power generation relevant temperatures”, Proceedings of the Combustion Institute, Volume 34, Issue 2, Pages 3343-3350, 2013.